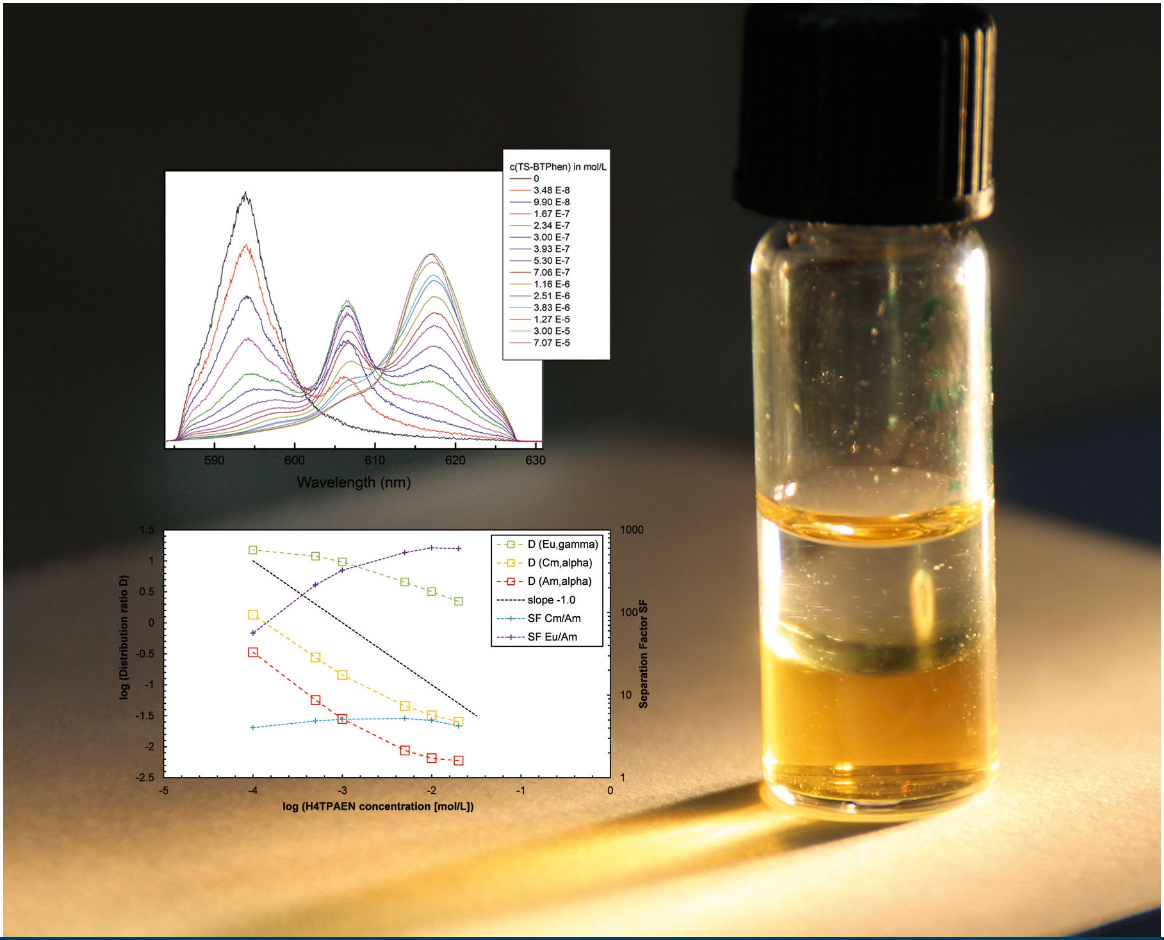

The Selective Separation of Am(III) from Highly Radioactive PUREX Raffinate

Peter Kaufholz

Energie & Umwelt / Energy & Environment
Band / Volume 402
ISBN 978-3-95806-284-9

Mitglied der Helmholtz-Gemeinschaft

JÜLICH
Forschungszentrum

Schriften des Forschungszentrums Jülich
Reihe Energie & Umwelt / Energy & Environment Band / Volume 402

Forschungszentrum Jülich GmbH
Institut für Energie- und Klimaforschung
Nukleare Entsorgung und Reaktorsicherheit (IEK-6)

The Selective Separation of Am(III) from Highly Radioactive PUREX Raffinate

Peter Kaufholz

Schriften des Forschungszentrums Jülich
Reihe Energie & Umwelt / Energy & Environment Band / Volume 402

ISSN 1866-1777 ISBN 978-3-95806-284-9

Bibliografische Information der Deutschen Nationalbibliothek.
Die Deutsche Nationalbibliothek verzeichnet diese Publikation in der
Deutschen Nationalbibliografie; detaillierte Bibliografische Daten
sind im Internet über http://dnb.d-nb.de abrufbar.

Herausgeber und Vertrieb: Forschungszentrum Jülich GmbH
Zentralbibliothek, Verlag
52425 Jülich
Tel.: +49 2461 61-5368
Fax: +49 2461 61-6103
zb-publikation@fz-juelich.de
www.fz-juelich.de/zb

Umschlaggestaltung: Grafische Medien, Forschungszentrum Jülich GmbH

Druck: Grafische Medien, Forschungszentrum Jülich GmbH

Schriften des Forschungszentrums Jülich
Reihe Energie & Umwelt / Energy & Environment, Band / Volume 402

D 82 (Diss., RWTH Aachen University, 2017)

ISSN 1866-1777
ISBN 978-3-95806-284-9

Table of Content

1. Abstract

The long-term heat load and radiotoxicity of spent nuclear fuel depicts a major challenge for its disposal as the size and cost of a deep geological repository is governed by the heat generation of the waste. A major reduction of the long-term heat load of radioactive waste is currently achieved by the separation and recycling of uranium and plutonium using the PUREX (plutonium and uranium reduction extraction) process. The remaining trivalent minor actinides americium and curium dominate the heat load after decay of the fission products. However, due to the short half-life of curium and its high neutron emission, any handling involving curium requires extensive neutron shielding. Therefore, the selective separation of americium from curium and the fission products is considered an advantageous option to further reduce cost and size of a final repository, although the separation of americium from curium is one of the most challenging tasks in separation chemistry.

A novel process for the separation of trivalent actinides from PUREX raffinate, the innovative selective actinide extraction process (i-SANEX), was developed previously and is taken as the basis of this work. The counter current laboratory-scale demonstration of the i-SANEX process in centrifugal contactors was carried out in context of this work. In this process, the co-extraction of trivalent actinides and lanthanides is carried out using a diglycolamide solvent followed by the selective back-extraction of trivalent actinides using a highly selective hydrophilic complexant.

Several combinations of lipophilic extractants and hydrophilic complexants were tested for their selectivity for americium over curium with the aim to increase the selectivity for americium in solvent extraction processes. Two hydrophilic complexants were found to provide promising selectivity towards americium in combination with a diglycolamide based lipophilic extractant.

Time-Resolved Laser Fluorescence Spectroscopy (TRLFS) investigations of selected actinide and lanthanide complexes with the hydrophilic complexing agents were carried out to better understand the fundamental mechanisms of complexation of the metal ions with these complexants. Conditional complex stability constants were derived for different media to analyze the influence of acidity and nitrate anions. Additionally, biphasic TRLFS-experiments were carried out to analyze the interaction between lipophilic and hydrophilic complexants. The data generated from solvent extraction and fluorescence-spectroscopic investigations enable for the development of a process for the selective separation of americium from PUREX-raffinate.

Kurzzusammenfassung

Der Langzeitsicherheitsnachweis eines tiefengeologischen Endlagers ist die primäre Herausforderung für die sichere Entsorgung ausgedienter Kernbrennstoffe. Dabei werden Größe und Kosten eines Endlagers von der Wärmeleistung der radioaktiven Abfälle bestimmt. Eine signifikante Reduktion der Langzeitwärmeleistung wird heute durch die Abtrennung von Uran und Plutonium im PUREX-Prozess (plutonium and uranium reduction extraktion) erreicht. Die verbleibenden dreiwertigen Minoren Actiniden Americium und Curium dominieren den Verlauf der Wärmeleistung nach dem Zerfall der Spaltprodukte. Die geringe Halbwertszeit von Curium in Verbindung mit seiner ausgeprägten Neutronenemission bedingt jedoch aufwändige Neutronenabschirmung für jeglichen Umgang mit Curium. Die Trennung von Americium und Curium gilt in der Separationschemie als eine der schwierigsten Herausforderung. Jedoch stellt die Abtrennung des Americium von Curium und den Spaltprodukten eine vorteilhafte Option dar, die Größe und Kosten eines Endlagers zu reduzieren.

Ein kürzlich entwickelter neuartiger Prozess, der Innovative Selective Actinide Extraction (i-SANEX) Prozess, wird als Basis für diese Arbeit dienen. Die Demonstration des i-SANEX-Prozess im kontinuierlichen Gegenstromverfahren mit Zentrifugalkontaktoren wurde im Rahmen dieser Arbeit im Labormaßstab durchgeführt. Der i-SANEX-Prozess basiert auf der Co-extraktion dreiwertiger Actiniden und Lanthaniden mittels einer Diglycolamid-basierten organischen Phase, gefolgt von einer Rückextraktion der dreiwertigen Actiniden mittels eines selektiven hydrophilen Komplexierungsmittels.

Verschiedene Kombinationen lipophiler Liganden und hydrophiler Komplexierungsmittel wurden mit dem Ziel getestet, die Selektivität für Americium in Extraktionsprozessen zu erhöhen. Zwei hydrophile Komplexierungsmittel wiesen dabei eine aussichtsreiche Selektivität für Americium in Verbindung mit Diglycolamid-basierten lipophilen Liganden auf.

Zeitauflösende Laserfluoreszenz-Untersuchungen (TRLFS) wurden an ausgewählten Actiniden- und Lanthanidenkomplexen mit hydrophilen Komplexierungsmitteln wurden durchgeführt, um die grundlegenden Mechanismen der Komplexierung von Metallionen mit diesen Komplexierungsmitteln zu untersuchen. Konditionale Stabilitätskonstanten wurden für verschiedene Medien ermittelt, um den Einfluss der Säurestärke sowie der Nitrat- Anionen zu untersuchen. Zusätzlich wurden zweiphasige TRLFS-Experimente durchgeführt, um die

Wechselwirkung zwischen lipophilen und hydrophilen Komplexierungsmitteln zu untersuchen. Die im Rahmen der Extraktions- und Fluoreszenzspektrometrischen Untersuchungen ermittelten Daten ermöglichen die Entwicklung eines Prozesses zur selektiven Abtrennung von Americium aus PUREX-Raffinaten.

List of abbreviations

ACSEPT	Actinide recycling by separation and transmutation
AmSel	Americium Selective
ASTRID	Advanced sodium technological reactor for industrial demonstration
ATALANTE	Alpha facility and laboratory for transuranium elements and reprocessing studies
AtG	Atomgesetz
BWR	Boiling water reactor
CEA	Commissariat a l' energie atomique et aux energies alternatives
CEA-DEN	Departement energie nucleaire
COEX	Coextraction
DGA	Diglycolamide
DIAMEX	Diamide extraction
FI	Fluorescence intensity
FP	Fission products
GANEX	Group actinide extraction
HAW	High active waste
HSAB	Hard soft acid base
ICP-AES	Inductive coupled plasma atomic emission spectrometry
ICP-MS	Inductive coupled plasma mass spectrometry
IEA	International energy agency
IEK	Institute for energy and climate research
INET	Institute of nuclear and new energy technology
i-SANEX	innovative SANEX
ITU	Institute for transuranium elements
Ln	Lanthanides
LOC	Limiting organic concentration
LUCA	Lanthaniden und Curium Americium Trennung
LWR	Light water reactor
MA	Minor actinides
MAGNOX	Magnesium non oxidized

MOX	Mixed oxide
MYRRHA	Multi-purpose hybrid research reactor for high-tech applications
NEA	Nuclear energy agency
NMR	Nucleon magnetic resonance
OECD	Organization for economic co-ordination and development
P&T	Partitioning and transmutation
PUREX	Plutonium uranium recovery by extraction
PWR	Pressurized water reactor
SACSESS	Safety of actinide separation processes
SANEX	Selective actinide extraction
StandAG	Standortauswahlgesetz
TPH	Hydrogenated tetrapropene
TRLFS	Time-resolved laser fluorescence spectroscopy

2. Introduction

A constant and stable supply of electrical power is a major basis for economic and civil wealth. For 2040, the OECD-IEA predicts an increase of 70 % of electricity demand within the OECD countries compared to 2015.[1] However, the reduction of greenhouse gas emissions is the primary goal to limit the effect of global warming. Within the 31 OECD member countries, 353 nuclear reactors were under operation at the end of 2015 resulting in an installed net capacity of 323.9 GW_e and 19.3 % share of nuclear power on electricity production in OECD countries in 2015.[2] The total number of operational nuclear power reactors in the world at the end of 2015 was 441 while emerging nations like China and India are planning to extend their nuclear programs.[3] However, to fuel the reactors under operation, 46,070 tons of natural uranium were required in 2015 which have to be treated in a way to prevent hazards to humans and the environment after its usage.[4] A major drawback of nuclear power is the spent fuel generated. Different strategies are developed related to the disposal and recycling of spent nuclear fuels. The recycling of U and Pu from spent nuclear fuel was implemented in industrial scale e.g. in France (La Hague) and the United Kingdom (Sellafield) with the PUREX process. Recent developments focus on closing the fuel cycle by reusing long-lived minor actinides and solely disposing of short-lived isotopes. The novel concepts base either on PUREX downstream processes starting with the PUREX raffinate or focus on a substitution of the PUREX process by an advanced process strategy to separate the minor actinides. One of the major contributors to current spent fuel management issues is americium. The development of inherently safe generation IV reactors enables for the recycling of minor actinides like americium.[5] A recycling of uranium and plutonium in combination with the separation and recycling of americium would therefore be an advantageous fuel management option.

This work contributes to the chemical separation (partitioning) of the long-lived transuranium element americium from highly active raffinate in a single PUREX downstream process.

2.1. Nuclear fission and fission products

The fuel loaded to LWR is usually utilized for 3-4 years. The transformation of fissile nuclides e.g. ^{235}U and ^{239}Pu to fission products by irradiation with neutrons is the heat generating process in a nuclear power plant. Assuming one initial ton of heavy metal pure UOX fuel with an enrichment of 3.3 % ^{235}U and a burn-up of 34 GWd/t_{HM}, 36 kg of fission products are generated during irradiation.[6] The mass of the initial uranium in the fuel decreases due to fission and neutron activation of the uranium isotopes resulting in a share of 95.4 % U in the spent fuel with a burn-up of 34 Gwd/t_{HM}.[6] The nuclides forming the fission products are generated by asymmetric fission of the fissile nuclei. The distribution of those fission products shows a characteristic pattern having two maxima around A=100 and A=134 mass numbers for ^{235}U fission. Because of the neutron excess of the heavy fissile material, the fission fragments are all strongly proton deficient and many of them have a very short half-life. After 1 year of cooling, 30 kg of the 36 kg fission products given in the sample above decayed to stable isotopes.[6] The residuals depict intermediate or long-lived nuclides. The relative abundance (thermal fission yield) of an isobaric line determines the chemical composition of the spent fuel. Spent nuclear fuel generates decay heat after irradiation, requiring cooling in wet storage for some years after unloading from the reactor. After several years of cooling, the fission products observed during consecutive spent fuel handling are stable or rather long-lived isotopes

Chemically, the fission products in spent nuclear fuel consist of stable and long-lived isotopes of elements between numbers A = 34 and A = 64 (with A = atomic number). This range covers a large number of elements from different element groups, resulting in a complex mixture of solid and gaseous elements which is contained in the ceramic fuel matrix.

Figure 1 shows the elements of the fission products in blue and the transuranium (TRU) elements in different shades of red. The TRU elements are referred to in chapter 2.2. As a result of the wide spread of the fission products over the periodic table, the chemistry of spent nuclear fuel is very complex.

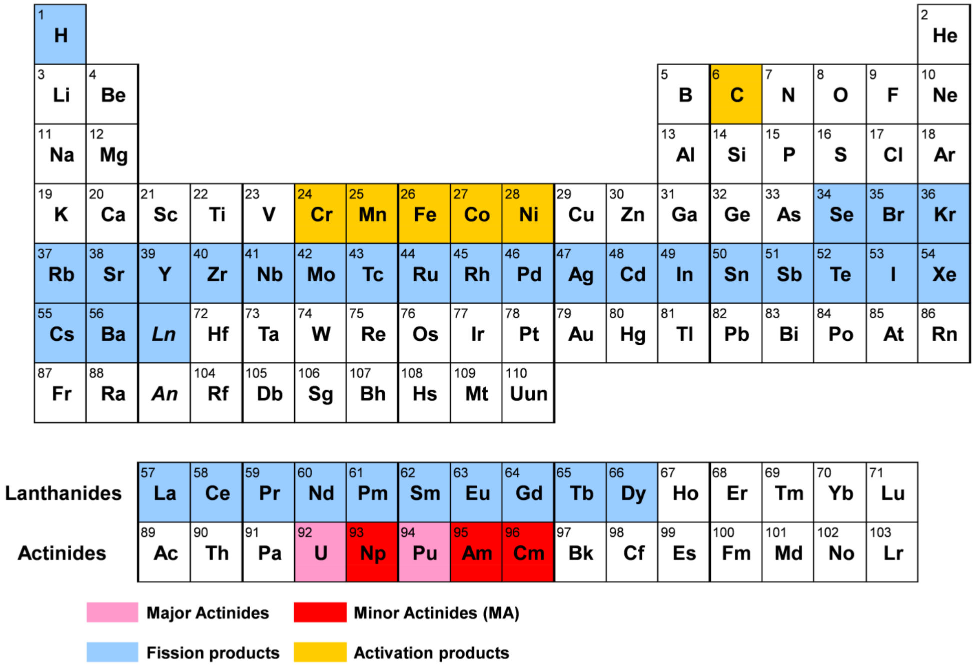

Figure 1: Elements abound in spent nuclear fuel apportioned by their origin.[6]

For a comprehensive view on the composition of spent fuel it is important to know its quantitative composition. Due to the high number of elements, the fission product elements are combined to the group of lanthanides and light fission products. Table 1 shows the quantitative composition of LWR UOX spent nuclear fuel.

Table 1: Composition of typical LWR spent fuel after 1 year of cooling (UOX; ^{235}U: 3.3 %; 34 GWd/T_{HM}) [6]

Component:	U	Np	Pu	Am	Cm	Ln	light FP
Share [%]	94.5	0.05	0.9	0.015	0.004	1.1	2.4

The fission products consist to reasonable amounts of lanthanide f-elements being similar to the trivalent actinide f-elements Am and Cm. Within the lanthanide group the electrons are distributed in the shielded 4 f-orbital, leading to a very similar chemistry of the different lanthanide elements. The similarity of the elements provides the possibility to address the elements in the group as a grouped separation. However, the similarity hinders the mutual separation of the elements within the group. The preferred oxidation states of all Ln in aqueous solutions is +III. Due to the shielded f orbital, the atomic radii of the lanthanides follow an inverse trend with increasing atomic number. The effect is known as lanthanide contraction.[7] In spent nuclear fuel, the lanthanides La-Gd are contained in reasonable amounts (in sum approx. 1.1 %).[6] Due to the large neutron capture cross sections of some Ln, a contamination of separated actinides with lanthanides would have negative consequences of the neutronic properties of recycled fuels. The lanthanides behave as a group in solvent extraction and show high similarity to the trivalent 5f-elements as explained in the following chapter.

2.2. Transuranium elements

The matrix of light water reactor fuels consists of the uranium isotope ^{238}U, which is non-fissile with thermal neutrons. Even if ^{238}U does not take part in the fission process, it is a fertile isotope. ^{238}U is able to form small amounts of ^{239}U by caption of a neutron. This uranium isotope ^{239}U generated by neutron capture decays via β^- decay to ^{239}Np which consecutively decays to the fissile ^{239}Pu (Figure 2). The plutonium generated by this reaction is either taking part in a fission process during irradiation in the reactor or is unloaded from the reactor with the spent fuel.

Comparable processes also take place with other nuclides during irradiation generating transuranium elements. The actinides in a nuclear reactor can be divided into major and minor actinides. Figure 1 shows the differentiation of the actinides present in SNF in different red shades. The major actinides uranium and plutonium are either initially introduced into the reactor (MOX fuels) or are generated in larger quantities during irradiation of the fuel. Major actinides have been in the focus of the nuclear science since the first reactor operations as well as for military purpose. Therefore, processes related to handling and recycling of major actinides U and Pu are quite optimized. The predominant buildup path of the minor actinide isotopes ^{241}Am, ^{244}Cm and ^{237}Np are given in Figure 2.[8] In typical spent UOX fuel with an initial ^{235}U enrichment of 3.3 % and a burn-up of 34 GWd/t$_{HM}$ only 0.05 % Np, 0.015 % Am and 0.007 % Cm are present.[6]

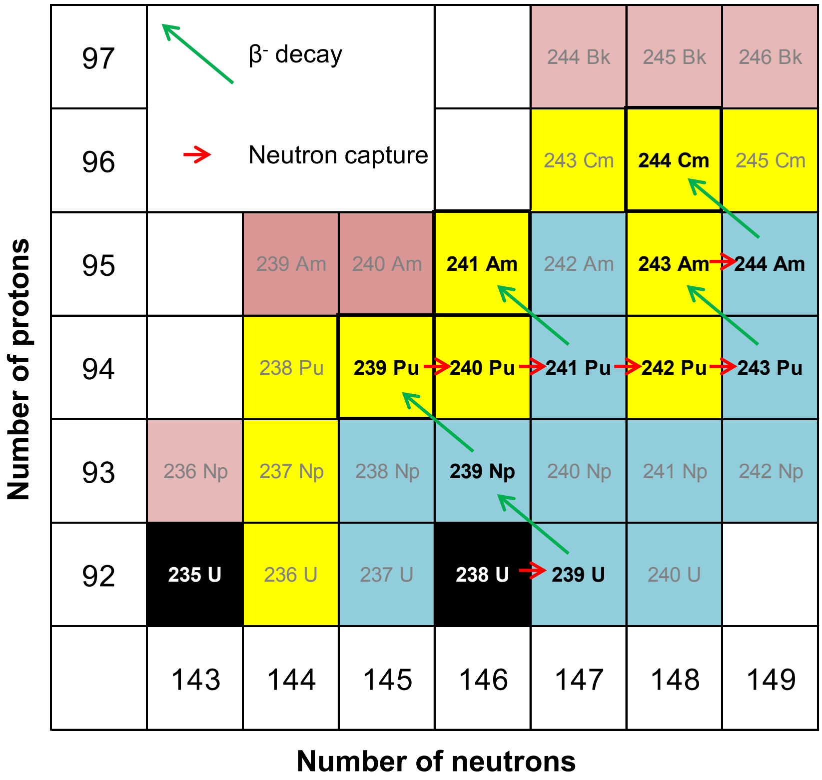

Figure 2: Pathway of the generation of minor actinides in a schematic nuclide chart.[9]

The chemistry of the 5f–elements shows some more deviation compared to the 4f–elements. Different oxidation states are stable under different conditions for some of the actinides. Table 2 shows the possible oxidation states, electron configurations and ionic radii of the most stable oxidation states of the actinides from U to Cm. Am and Cm are known to be trivalent actinides, having the most stable oxidation state of +III. Due to comparable radii and trivalent ionic state and the shielded 5f-orbitals Am and Cm react similar to trivalent 4f-elements. The intergroup separation between trivalent actinides and lanthanides requires advanced process chemistry and is still addressed by several current research projects. Additionally, the intragroup separation of the trivalent actinides Am and Cm is actually strived and depicts one of the most difficult tasks in spent fuel partitioning.[10]

Table 2: Properties of selected actinide elements. Oxidation states are related to chemistry in solution. Most stable oxidation states are written bold. Ionic radii in non-complexing acidic solution.[11]

Element	Most common ox. state	Electron configuration	Ionic radius (pm)
U	+III; +IV; +V; **+VI**	$[Rn]5f^36d^17s^2$	
Np	+III; +IV; **+V**; +VI; +VII	$[Rn]5f^46d^17s^2$	
Pu	+III; **+IV**; +V; +VI	$[Rn]5f^67s^2$	88.7 (Pu(IV)
Am	**+III**; +IV; +V; +VI	$[Rn]5f^77s^2$	98.2 (Am(III))
Cm	**+III**; +IV	$[Rn]5f^76d^17s^2$	97.0 (Cm(III))

2.3. Options of spent fuel management

Some of the properties of spent nuclear fuel make the disposal a challenging task. The radiotoxicity of spent nuclear fuels demands for a safe long-time storage mandatory to prevent harm to humans and environment. With the introduction of the atomic law ("Atomgesetz, AtG") into the German regulatory framework in 1960, the reimbursed utilization of spent nuclear fuel and recycling of U and Pu was given as the preferred option for the disposal of spent fuel. The vitrified high level wastes originating from reprocessing were planned to be disposed of in deep geological formations. In 1994 the German "Law on the peaceful use of atomic energy" was changed to allow both, direct disposal as well as reprocessing of spent nuclear fuel.[12] Since 2005 the only option for disposal of high level waste in Germany is the direct disposal of spent nuclear fuel in deep geological repositories.[13] On the European level the options for disposal of high level radioactive waste are coordinated in the EU directive Euratom 70/2011 and the closely related "joint convention on the safe management of radioactive wastes and spent nuclear fuel" in which every country has to evaluate options for the disposal of nuclear waste and present its national program to the commission in a three years interval.[14] In Germany, the "Kommission Lagerung hochradioakiver Abfälle" (Commission on the final storage of highly radioactive waste) has evaluated several options for the disposal of high level nuclear wastes. In the final report the commission states the deep geological disposal in clay, salt or crystalline host rock to be the preferential option.[15] The national program for Germany based on Euratom 70/2011 was reported to the European Commission in August 2015. It defines the safe disposal of spent nuclear fuels and high level vitrified wastes from reprocessing in deep geological formations.[16] Additionally, in the German regulatory framework a law was established to evaluate possible locations for a final disposal of high level radioactive wastes. Herein, the different options of host rock are included. The new law ("Standortauswahlgesetz, StandAG") focuses on a decision for the location of a final repository in 2031 expecting it to be ready for operation in 2050.[17] The Euratom 70/2011 opens the possibility to every country to define their own national program, resulting in different national policies for the countries, also including reprocessing or intermediate-term surface storage of high level waste (e.g. The Netherlands).[18] Underground final repositories for nuclear wastes are under consideration in different countries.

The size of such a repository is limited by the heat generated by the nuclear wastes. The costs of an underground repository are guided by the size of the repository. From this limitations one can assume that a spent nuclear fuel final storage can be optimized related to its long-term safety and costs by minimizing its size.[19] The fastest and technically most simple option would be a direct disposal of the spent nuclear fuel elements as unloaded from the reactor into the deep geological repository. Before disposal, cooling of the spent fuel is necessary to reduce its decay heat and afterwards the fuel has to be packed for transport and storage in combined dual purpose casks or individual casks for transport and for final disposal. Another positive aspect of a direct disposal of fuel assemblies is the fuel handling. There is no need for complicated processes to open the fuel cladding as its primary barrier. The form of the spent nuclear fuel unloaded from the reactor would already be the form for final storage. Criticality aspects for the direct disposal of spent LWR fuel are addressed in the design of the transport and storage casks. The biggest issue in this option of waste disposal is the huge size and with it also the immense costs of a repository necessary for the direct final storage of the spent fuel.[19] In 2013 a study was published evaluating an implementation of different partitioning and transmutation (P&T) concepts for the German national waste disposal policy.[19] The volume of high level waste arising from the civil use of nuclear power in Germany until the final phase out in 2022 is assumed to be approximately 28,100 m^3. It can be divided into spent fuel (21,000 m^3), vitrified high level waste from reprocessing (1,400 m^3), and wastes arising from research reactors and reactor concept demonstrations (5,700 m^3). Spent nuclear fuel consists to a share of about 95 % of the initial uranium. The removal of uranium would be a first step to an optimization of the nuclear waste volume.[19] Additionally, the plutonium generated in the fuel during irradiation can be separated and reused as fissionable reactor fuel. A complete recycling of the German spent fuel inventory generated until the phase out in 2022 would reduce the amount of resulting high level waste from this procedure to 2,200 m^3. However, the separated U and Pu have to be managed either by considering it as new fuel for light water reactors or for conditioning and final deposition. A consecutive partitioning of the transuranium elements Np, Am and Cm followed by transmutation of these elements in a European network of partitioning and transmutation systems would allow for a reduction of the long term thermal power of the high level wastes by 1 to 2 orders of magnitude. The transmutation of the German stock of transuranium elements reduces their amount by 97 % and could be implemented by using 7 to 8 transmutation systems over a period of 150 years. The partitioning and transmutation strategy significantly reduces the amount of high level waste on the one hand but generates low and intermediate level waste on the other hand. Medium and low level waste would rise by a factor of approximately 2 compared to the amount of medium and low active wastes in the direct disposal strategy.[19] Even if the strategy of partitioning and transmutation is in the focus of international developments, it does not depict a technically fully developed concept, making extensive scientific development mandatory to enable its application.[20] The development of the radiotoxicity of the different spent fuel management strategies is given in Figure 3. The heat generation of the high level wastes is proportional to its radiotoxicity. For the direct disposal option, the radiotoxicity decreases rather slowly, being the sum of the radiotoxicity of uranium, fission products and transuranium elements. The option of today's reprocessing reduces the radiotoxicity by separation and recycling of U and Pu. The development of the remaining radiotoxicity over time for the innovative waste disposal using partitioning and transmutation is close to the curve of the fission products as nearly all transuranium elements are separated and transmuted to fission products. In Figure 3 the increased amount of low and intermediate level wastes which have to be managed is not shown. However, the activity and hazard potential of the low and intermediate level waste is significantly lower compared to high level waste, giving a significant benefit related to the repository size and long term storage.

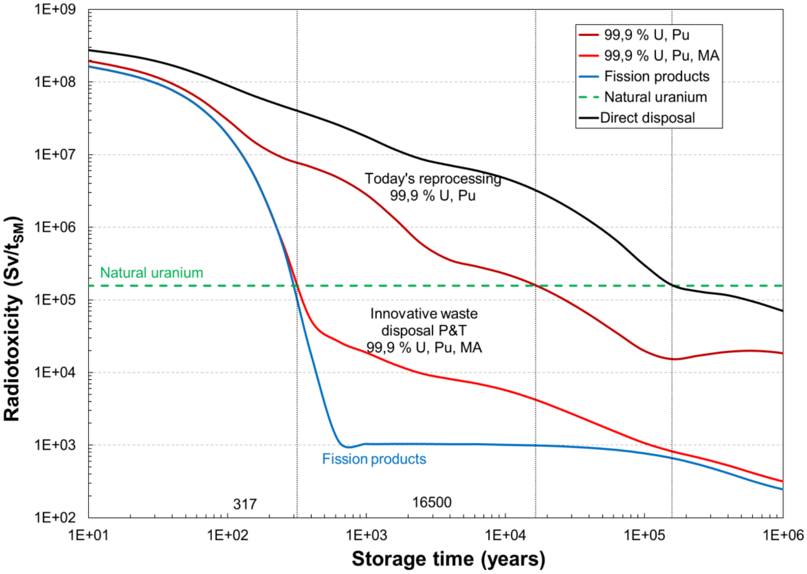

Figure 3: Effect of the separation of U, Pu and MA from spent fuel on the radiotoxicity vs. storage time.[21]

2.4. The nuclear fuel cycle

On the front end of the nuclear fuel cycle uranium is treated in several purification steps starting from uranium ore which is digested by sulfuric acid. From the solution, "Yellow cake", a mixture of ammonium uranates and uranium oxides and hydroxides is precipitated. This mixture is dissolved in nitric acid to be purified using liquid-liquid extraction to give pure uranyl nitrate. The uranyl nitrate is calcinated and treated with hydrofluoric acid and fluorine to form volatile UF_6 which can be used for the enrichment of ^{235}U for LWR fuel production. The most common method of uranium enrichment is ultracentrifugation of the gaseous UF_6. Two uranium streams are leaving the enrichment step. On the one hand there is the enriched uranium which can be used as reactor fuel and on the other hand there is depleted uranium which is stored or used in industry. The enriched uranium is converted to UO_2 powder used for the production of ceramic UO_2 pellets which is the form of nuclear fuel in LWR fuel assemblies.[22]

The fuel assemblies are irradiated in LWR reactors for a period of 3-4 years which depicts three to four operational cycles of the reactor. The position of the fuel element in the core is changed during every reactor revision in between the cycles to optimize the utilization of the fuel. Within the irradiation they gain a burn–up of 30 to 60 GWd/t_{HM}, depending on fuel type and reactor operation schedule.[23] The average burn–up of PWR fuel in present fuel development and reactor management is 55 GWd/t_{HM}.[24] After its irradiation spent fuel is unloaded from the reactor and cooled in the spent fuel pool until the residual heat criteria for transport and storage casks are met.

Spent nuclear fuel can be recycled to re-use uranium and plutonium generated during irradiation. A recycling of U and Pu from the spent nuclear fuel reduces the volume and long-term heat generation of the downstream nuclear wastes and allows for a recycling of U and Pu in light water reactors. The recycling of U and Pu has been realized by the "Plutonium and Uranium Recovery by Extraction" (PUREX)[25] process in an industrial scale since the 1950's.[26] In this process the long lived minor actinides are combined with the fission product stream and end up as vitrified high active waste. The low amount of minor actinides in the nuclear waste however guides the heat burden of a final repository after decay of the fission products. The PUREX process is described in detail in chapter 0. After the PUREX process, the recycled plutonium oxide is mixed with depleted or reprocessed uranium oxide to form MOX fuels. A number of LWRs in the world are using a share of MOX fuel elements in their cores and novel reactor designs focus on an extended use of plutonium-containing fuel.[23] The recycling of Pu and U can be considered as the basis for advanced nuclear fuel cycles. However, the PUREX process is optimized to recycle uranium oxide fuels. A recycling of MOX fuels with the PUREX process was tested in industrial scale but has to be improved with regards to fuel dissolution and higher Pu content in the process.[27] The main disadvantages of strategies including the PUREX process are the proliferation risk of a separated Pu stream and the lack of separating minor actinides from fission products within the PUREX process. Different approaches have been investigated to develop more sustainable and safer nuclear fuel cycles.

2.5. Solvent extraction

Solvent extraction is a common separation procedure applied in industry. The liquid state of all process media simplifies its application in a remote controlled, continuous system. Additionally, the formation of dust is prevented resulting in a relatively clean process which is important especially for the nuclear industry. Due to modular designs, liquid–liquid contactors can be used very flexibly. Different flow sheets can be realized by connecting pumps and contactors to an individual process facility.

Basically, solvent extraction describes the distribution of a substance between two immiscible, liquid phases. In classical liquid–liquid extraction the phases consist of a water-based aqueous phase and an organic phase based on a non-polar aromatic or aliphatic diluent. The exchange of substances between the two phases takes place at the contact surface between the phases. To achieve a fast exchange between the phases, the surface has to be maximized. The phases are therefore mixed, forming a mixture of small droplets with high surface. Figure 4 shows the basic operation procedure of liquid-liquid extraction in laboratory scale.

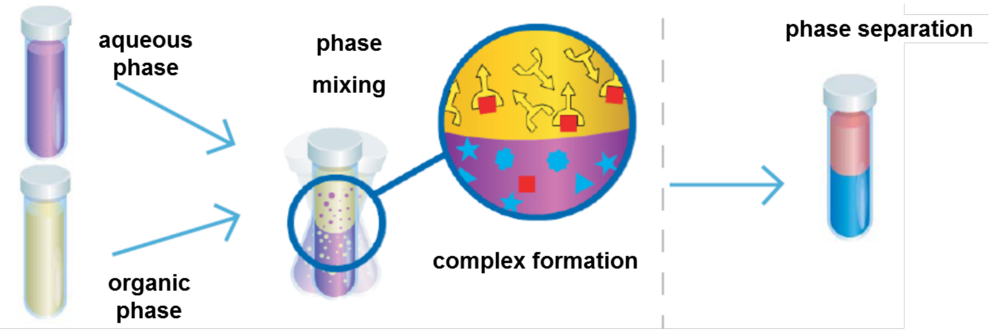

Figure 4: Basic procedure of liquid-liquid extraction.Taken from ref.[28]

The density difference of the phases has to be sufficiently high to provide a fast and complete separation after phase mixing is finished. The solubility of substances is often much higher in one of the phases compared to the solubility in the other phase. A separation of e.g. different ions using an aqueous phase (high solubility of the ions) and an organic solvent (very low solubility of the ions) would not be possible. There are two approaches to achieve a transfer into the organic phase: On the one hand an increasing polarity of the organic phase would lead to a higher stability of ions in the organic phase resulting in a higher equilibrium concentration of the ions in the organic phase. On the other hand it is possible to add a ligand to the organic phase, reacting with the ions to form a lipophilic complex which is soluble in the organic phase.

The choice of an appropriate ligand/solvent combination is the first step for effective solvent extraction. Two major types of ligands can be distinguished by their extraction mechanism. The simplest liquid-liquid extraction system consists of an organic phase and a non-complexing aqueous phase. A description of the system is shown in Equation 1 assuming a single complex to be formed in the organic phase by the solvation mechanism with negligible complexation in the aqueous phase.

Equation 1: Simplified equation for the extraction of plutonium into the organic phase by the solvation mechanism using TBP.

$$\mathbf{Pu^{IV+}_{aq} + 4\ NO_3{}^-_{aq} + 2\ TBP_{org} \rightarrow Pu(NO_3)_4{\cdot}2\ TBP_{org}}$$

The charge compensation of the extraction is fulfilled by the co-extraction of the counter ion of the extracted metal ion. The equilibrium in Equation 1 can be described by the law of mass action using the concentration of the ligand, metal and its counter ion. The second possible mechanism for the complexation of a metal ion is the ion exchange mechanism. Equation 2 shows the complexation of Am(III) with HDEHP following the ion exchange mechanism.

Equation 2: Simplified equation for the extraction of americium into the organic phase by the ion exchange mechanism using HDEHP $(C_8H_{17}O)_2$-POOH.

$$\mathbf{3\ (C_8H_{17}O)_2\text{-}POOH_{org} + Am^{III+}_{aq} + 3\ NO_3{}^-_{aq} \rightarrow ((C_8H_{17}O)_2\text{-}POO)_3{\cdot}Am_{org} + 3\ HNO_{3\ aq}}$$

The charge compensation in the ion exchange mechanism is fulfilled by exchanging the acidic hydrogen atoms of the ligand by the extracted metal-ion. The equilibrium in Equation 2 can be described by the law of mass action using the concentration of the ligand, metal and the acidity.

An ideal ligand has a very good solubility in the organic diluent while it is insoluble in the aqueous phase. Taking into account more than one lipophilic complexes and the formation of hydrophilic complexes makes the system much more complicated. The number of lipophilic complexes and the stability of these complexes guide the equilibrium concentration of the metal in the organic phase. To describe the distribution of an individual substance between two immiscible phases the distribution ratio D is introduced. D is defined as the concentration of a substance (X) in the organic phase divided by the concentration of the same substance in the aqueous phase ($D_x=[X_{org}]/[X_{aq}]$). A separation between two substances X and Y can be quantified using the separation factor $SF_{X/Y}$ which is defined as the quotient of the distribution ratios of two substances ($SF_{X/Y}=D_x/D_y$ with $D_x>D_y$). The distribution ratio of a substance in an extraction system can be seen as a comparison of the stability of the complexes formed in the organic phase and the stability of the complexes formed in the aqueous phase. The complexation equilibrium reaction is depending on thermodynamic values. Following the principle of le Chatelier, the temperature is an important factor in the reaction influencing the distribution ratio by changing the stability of the complexes.

Certain selectivity to the separation can be provided by adapting the electronic properties of the ligand to the electronic properties of the metal ion. A description of this phenomenon was given by R. G. Pearson with the HSAB classification of acids and bases using the definition of Lewis[29]. According to this, “harder” electron acceptors (for metals higher charge and smaller ionic radius resulting in high charge density) preferentially form complexes with “harder” electron-donating compounds (O-electron donating ligands) and soft acceptors (e.g. f-elements) preferentially with soft donors (N-electron donating ligands). The most important O- and N-donor ligands are discussed at the end of this chapter.

2.5.1. Effects influencing liquid-liquid extraction systems

Different effects influence the performance of a liquid-liquid extraction system. The most important parameters for the development of efficient liquid-liquid extraction systems are given below.[30]

- The affinity of the solvent towards the target ions needs to be high under extraction conditions and low under back-extraction conditions.
- The selectivity for the target ions over other ions present in the system should be sufficiently high to allowing efficient extraction.
- The kinetics of the system needs to be sufficiently fast to enable for a counter current application in short residence time contactors
- The hydraulic properties of the system need to be good to maintain a constant phase separation and prevent for the formation of stable emulsions or phase entrainment.

Diglycolamide ligands (DGA)

Diglycolamides were first described by Stephan *et al.*[31] They belong to the O-donor ligands and show selectivity for f-elements over d-elements but have a very limited ability to distinguish between An(III) and Ln(III). The basic structure for this ligand type is given in Figure 5. There are six positions in which the DGA molecule can be altered affecting extraction performance and solubility. The positions of highest importance with regards to solubility are R1, R2, R3 and R4 which have been extensively investigated within the last years.[32] Table 3 shows the solubility of symmetric, linear alkylated DGAs in water and *n*-dodecane respectively as a function of the alkyl chain length at R1,2,3,4. Additionally, the distribution ratio of Am(III) is given.

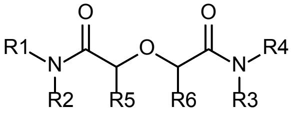

Figure 5: Functional backbone of DGA-type ligands.

Table 3: Extraction relevant properties of different DGA-derivatives[33]. D_{Am} for 1 mol/L nitric acid and 0.1 mol/L DGA. Data taken from ref.[33]

Alkyl chain length	Abbreviation	Solubility in H_2O (mmol/L)	Solubility in *n*-dodecane	D(Am)
3	TPDGA	57	Very poor	-
4	TBDGA	2.3	Poor	-
5	TADGA	0.27	Soluble	100
6	THDGA	0.11	Soluble	40
8	TODGA	0.042	Freely soluble	30
10	TDDGA	0.042	Freely soluble	18

Besides a good solubility of the ligand in the organic phase, also the extraction performance needs to be as good as possible. From Table 3 it is visible that the compromise of solubility and extraction performance is best fulfilled by the tetraoctyl-substituted diglycolamide TODGA (*N,N,N',N'*-tetraoctyl-diglycolamide). Due to millimolar concentrations of Ln(III) in spent fuel partitioning processes, third phase formation is an important issue in TODGA-based processes. The problem of third phase formation can be overcome in two ways. On the one hand, an increase of the ligand concentration increases the limiting concentration of metal ions in the organic phase where third phase formation starts (limiting organic concentration, LOC). However, with increased DGA concentration the distribution ratios increase making a back-extraction from the organic phase more difficult. On the other hand, phase modifiers e.g. TBP or 1–octanol can be used to significantly decrease the effect of third phase formation.[32, 34-36]

The positions R5 and R6 in the ligand backbone have an additional effect on the extraction efficiency and radiolysis stability. The effect of methylation at these positions was intensively studied during the ACSEPT project of the European Commission (Ref. No.: FP7-211267). The single (Me-TODGA, Figure 6), as well as the double methylation (Me_2-TODGA, Figure 6) at the R5 and R6 positions decrease the distribution ratios of An(III) and Ln(III) with increasing substitution.[37-39] Additionally, stereoisomeric species of R5 and R6 methylated TODGA derivatives were under investigation in the SACSESS project (Ref. No.: FP7-Fission-2012-323-282). Recent developments also focus on the use of DGA ligands in the aqueous phase.[40]

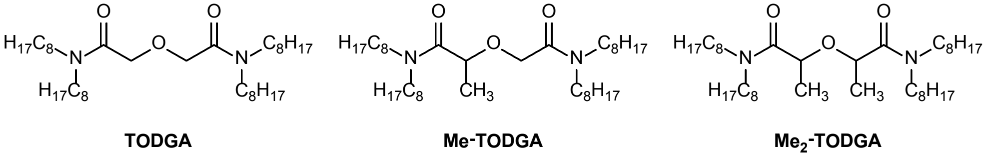

Figure 6: Structures of TODGA, Me-TODGA and Me_2-TODGA.

TODGA is known to provide high distribution ratios for An(III) and Ln(III) in combination with nitric acid based aqueous phases.[36, 41-43] The distribution ratios are above one already at nitric acid concentrations between 0.01 and 0.1 mol/L and reach very high values (> 500; D.L.) already at acidities around 1 mol/L. The preferences of TODGA to form complexes with trivalent f-elements can be ranked as Eu > Cm > Am showing a small selectivity for Cm over Am of $SF_{Cm/Am} \sim 1.6$ between 0.01 mol/L and 1 mol/L nitric acid. The separation between Eu(III) over Am(III) is $SF_{Eu/Am} = 8.0$.[33, 44]

The methylated TODGA derivative has an additional steric hindrance at its backbone. Additionally, the methyl group attached to the molecule changes the electronic properties of the molecule and destroys its symmetry. These effects result in less symmetric complexes and lower distribution ratios. In comparison to TODGA the distribution ratios of all analyzed An(III) and Eu(III) are significantly lower.[37, 39] An(III) and Eu(III) reach distribution ratios of > 1 at nitric acid concentrations of approx. 1 mol/L. The extraction in a process will be carried out directly from the raffinate feed providing acidities of 3 to 5 mol/L nitric acid. The separation factor of Cm over Am provided by Me-TODGA is $SF_{Cm/Am} = 1.4$ which is slightly decreased compared to TODGA (1.6). The separation between Eu(III) and Am(III) is $SF_{Eu/Am} = 4.5$. The preference pattern for the analyzed Ln(III) and An(III) stays the same in comparison to TODGA.[33, 39]

2.5.2. Diamide Ligands

Diamide ligands play an important role in the development of the DIAMEX-process and depict a liland class with high loading capacity.[45-46] The diamide type ligand DMDOHEMA is used in the EXAm process in combination with HDEHP to preferentially extract Am(III) together with some light Ln and fission products.[47] The distribution ratios of An(III) and Ln(III) using DMDOHEMA are significantly lower compared to TODGA and Me-TODGA at the same ligand concentration. D-values of $D > 1$ are reached only at nitric acid concentrations above 3 mol/L. DMDOHEMA shows an inversed extraction pattern compared to the DGA based ligands, extracting Am(III) more than Cm(III) and Eu(III). The separation factor of Am(III) over Cm(III) is $SF_{Am/Cm} = 1.7$, the separation of Am(III) over Eu(III) is $SF_{Am/Eu} = 1.9$.[48-49]

2.5.3. Heterocyclic N-donor ligands for actinide lanthanide separation

The development of highly selective soft-donor ligands lead to investigations on several heterocyclic, aromatic N-donor ligands.[50-52] A ligand type of special importance within the heterocyclic N-donor ligands were the bis-triazinyl-pyridine (BTP) type ligands (Figure 7). In 1999, Kolarik et al. reported a high selectivity for An(III) over Ln(III) ($SF_{Am(III)/Eu(III)} = 130$) using the alkylated *n*-Pr-BTP. BTP type molecules are able to extract An(III) direct from highly acidic nitric acid solutions.[53] However, *n*-Pr-BTP suffered from slow extraction kinetics and low hydrolytic as well as radiolytic stability. Different aliphatic substitutions were introduced at the triazinyl-moieties to improve solubility and stability of the ligand.[54-55] The cyclo-aliphaticly substituted $CyMe_4$-BTP showed a very high separation factor of $SF_{Am(III)/Eu(III)}$ of >1000 and improved radiolytic and hydrolytic stability.[56] However, the $CyMe_4$-BTP system suffers from very slow extraction kinetics making it unsuitable for the application in an industrial partitioning process. By adding a second pyridine to the center of the structure, the 6,6'-bis(1,2,4-triazin-3-yl)-2,2'-bipyridine (BTBP) type ligand family (Figure 7) was developed.[57-58] With respect to $CyMe_4BTP$, the BTBP analogue $CyMe_4BTBP$ synthesized at the University of Reading provides an excellent hydrolytic stability with a selectivity of $SF_{Am(III)/Eu(III)} = 150$.[58] However, the extraction kinetics of $CyMe_4$-BTBP is still quite slow. A pre-organization of the ligand by cis-locking the rotation axis between the two pyridine moieties was examined to achieve faster kinetics. These 2,9-bis(1,2,4-triazin-3-yl)-1,10-phenanthroline (BTPhen) (Figure 7) type ligands show faster kinetics with an increased selectivity towards the separation of trivalent actinides ($SF_{Am(III)/Eu(III)}$=250) compared to the BTBPs.[59-61] By introducing sulfonated phenyl groups to the structure of BTP and BTBP, hydrophilic BTP and BTBP derivatives have been synthesized and tested for their suitability as hydrophilic complexing agents in liquid-liquid extraction. Geist et al. reported a separation factor of $SF_{Eu/Am}$ = 1200 by using hydrophilic sulfonated phenyl- BTP in combination with TODGA in the organic phase.[62] Sulfonated Phenyl-BTBP was tested for its application as hydrophilic complexing agent by Wagner et al. providing a separation factor of $SF_{Eu/Am}$ of 600.[63]

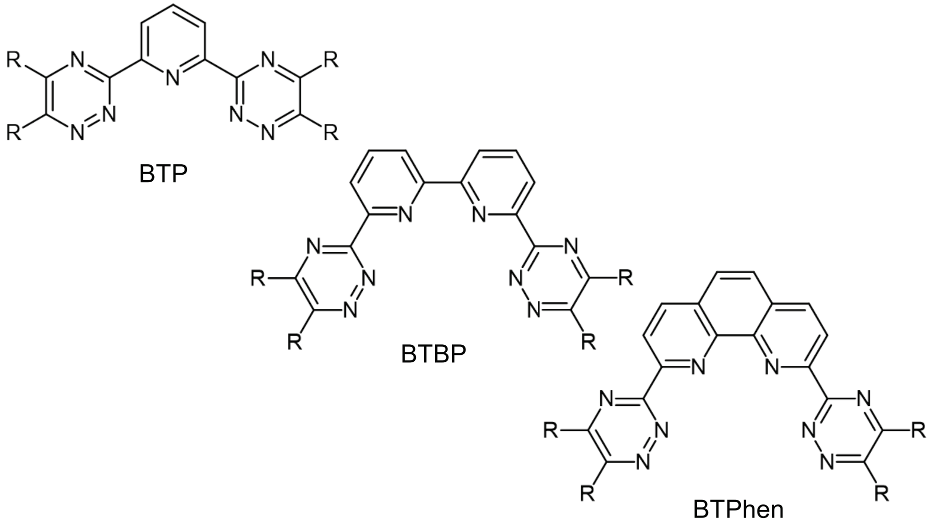

Figure 7: Basic structure of the BTP, BTBP and BTPhen ligands.

2.5.4. Hydrophilic complexants for masking of fission products.

To achieve a better separation within the process steps, hydrophilic masking agents can be used to selectively hold-back undesired elements within an extraction or to achieve better separations during back extraction steps. The first masking agents used were quite simple complexants e.g. oxalic acid. Further developments are based on the well-known ethylene-diaminotetraacetic acid (EDTA). Different polyaminocarboxylic acids were synthesized and tested for their application in partitioning processes.[41, 48, 64] The EDTA derivative HEDTA was found to prevent the extraction of Pd in TODGA-based extraction system[35, 65] With the development of novel partitioning processes, the demand for selectivity rose. However, the addition of oxalic acid causes a slow precipitation of plutonium. CDTA was found to be a novel masking agent to effectively prevent the extraction of Zr and Pd in TODGA based extraction system without the formation of precipitates.[66] Already small amounts of this polyaminocarboxylic acid significantly decrease the distribution ratios of some challenging fission products.[66] The use of hydrophilic masking agents enables for the reduction of process stages and a cleaner loaded organic phase making prosess management more effective.

2.6. The PUREX process for the separation of U and Pu from spent nuclear fuel.

The PUREX process is an industrially applied process and has been in the focus of science and development since its first application. It is applied at industrial scales in France (La Hague) and the UK (Sellafield) and also Japan (Rokkasho-mura) started a PUREX plant.[67] The resource for the PUREX process is irradiated UOX LWR fuel. A treatment of graphite-moderated reactor fuels (e.g. MAGNOX) and fast reactor fuels (e.g. sodium fast reactor fuel) using PUREX is generally possible but not described in detail.[25] To prepare the spent fuel for the extraction processes, the head and foot elements of the fuel bundles are removed and the fuel pins are chopped into smaller pieces. The chopped fuel and cladding is afterwards treated in boiling concentrated nitric acid to dissolve the fuel, leaving the non-dissolved cladding behind. Cladding and fuel bundle structures are allowed to be treated as intermediate level wastes due to their low activation in the reactor.[11] The suspension emerging from the dissolution procedure is filtered to give a spent fuel solution. The solution consists mainly of uranium and plutonium but also of minor actinides and the non-volatile fission products as well as corrosion products from cladding and fuel treatment. The resulting solution is adjusted to a nitric acid concentrations of 2 to 4 mol/L to provide plutonium in the Pu(IV) oxidation state.[67] Any treatment of this solution as well as the initial dissolution has to be performed “criticality safe” requiring limitations to the size of vessels, concentrations and structure materials to prevent the formation of a self-sustaining, neutron multiplying “critical” volume in the system. The solution is contacted with an organic phase containing tri-*n*-butyl phosphate (TBP) dissolved in odorless kerosene (c.f. Figure 8). In a first step, the spent fuel solution is contacted with the organic phase where U(VI) and Pu(IV) are co–extracted as $UO_2(NO_3)_2$ and $Pu(NO_3)_4$, respectively, before the aqueous and organic phases are separated from each other. The extracted Pu(IV) is then reduced to non-extractable Pu(III) using hydroxylamine (NH_3OH) or U(IV) and is consecutively separated from the uranium by selective back-extraction (stripping). After separating plutonium as Pu(III) from the organic phase, uranium is stripped in a final step using an aqueous phase of low acidity to give the uranium product.[67] The spent organic phase is recycled after regeneration using a basic scrubbing step to remove acidic radiolysis products of TBP. The Pu and U products are finally purified by using solvent extraction cleaning processes based on the same organic phase as in the separation process. Uranium is precipitated by addition of ammonia and the precipitate is calcinated to form U_3O_8. The separated plutonium is precipitated as oxalate and calcinated to form PuO_2.[67]

Different variations of the PUREX process are published and applied for different fuel types and burn-up. Besides the desired products uranium and plutonium, which are recycled into the fuel cycle, there is a waste stream consisting of fission and corrosion products as well as the minor actinides. An advanced PUREX process has been developed being able to stabilize Np in the Np(VI) oxidation state as which it can be extracted.[68] Np can therefore be recovered as a separate stream opening the possibility to reduce the amount of actinides in the PUREX raffinate to mainly Am and Cm. Any optimization of the fuel cycle regarding fission product treatment and minor actinide separation can be implemented as downstream processes of the PUREX or PUREX-analogous process (e.g. COEX).[27]

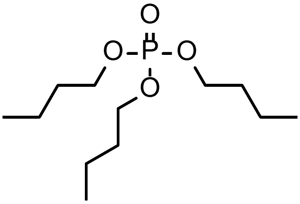

Figure 8: Chemical structure of tri-*n*-butyl-phosphate (TBP)

2.7. Advanced partitioning concepts for actinide recycling.

Due to the experience gained in the application of the PUREX process, liquid-liquid extraction is an ideal method for the selective separation of elements in spent fuel management. Different strategies of minor actinide handling have been developed. Neptunium as the most abundant minor actinide can be separated in an advanced PUREX process.[68] For the trivalent minor actinides Am(III) and Cm(III), different strategies of homogenous and heterogeneous recycling are under consideration and an integral part of current research and development projects.[10, 27, 69-70] The most abundant americium isotope ^{241}Am has a half-life of 432.2 years and decays via alpha decay.[9] In a final repository, americium is guiding the heat generation after decay of the fission products.[19] The major Cm isotope ^{244}Cm has a relatively short half-life (18.1 a) and shows a high neutron dose as a result of the high share of spontaneous fission in its decay pattern.[9] Any handling of Cm containing material therefore requires special shielding and remote handling. Due to the low abundance and its low half-life it is considered to be disposed of together with the fission products. The decay product of ^{244}Cm is ^{240}Pu which has a half-life of 6563 years resulting in a significantly lower activity (factor $\approx$ 360). In combination with the low abundance of ^{240}Pu generated from Cm decay the potential risk arising from Cm and its decay daughter ^{240}Pu in a final repository is rather limited with regards to chemical and radiotoxicity. Therefore, it would be beneficial to separate Am from high level waste and leave Cm in the fission product fraction for decay.[71] This approach would simplify the further treatment of minor actinides having less neutron emission without significantly influencing the final storage of the high level waste in a negative way. Figure 9 shows an overview of advanced partitioning processes which are under development in Europe.

The concept can be divided into the mutual separation of all transuranium elements called homogenous recycling, and the consecutive separation of major actinides and Np followed by a minor actinide separation process in the heterogeneous recycling.

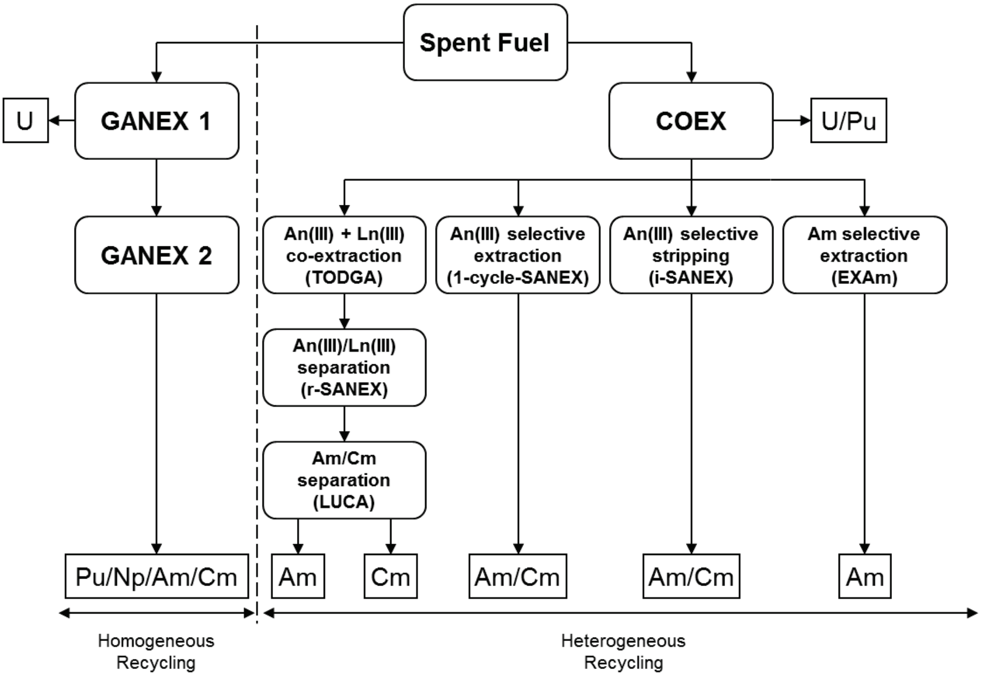

Figure 9: Overview of advanced partitioning processes. Taken from ref.[72]

2.7.1. Homogenous recycling: The Euro-GANEX process

The concept of homogenous recycling starts directly from the spent fuel solution after fuel dissolution. Its objective is the mutual separation of the transuranium elements without a necessity of handling a pure plutonium stream, significantly reducing the risk of proliferation.[73] In the European Commission project ACSEPT, the EURO-GANEX (Group Actinide Extraction) process was developed and tested.[74-76] The GANEX process is divided into two cycles. Bulk uranium has to be removed in a first step to allow for an effective separation of the transuranium elements. Separation of U is achieved using the monoamide DEHiBA (*N*,*N*-di-(2ethylhexyl)-isobutyramide) extracting uranium and leaving transuranium elements and fission products in the raffinate.[77] The second GANEX cycle focuses on the separation of Pu and the MA from the fission products. A co-extraction is carried out using TODGA and DMDOHEMA (*N,N'*-dimethyl-*N,N'*-dioctylhexylethoxymalonamide) in odorless kerosene.[78] Subsequently, Pu and the MA are back-extracted using a combination of the hydrophilic SO_3-Ph-BTP and AHA (acetohydroxamic acid). Remaining Ln are finally removed using a glycolate buffer solution.[77]

2.7.2. Heterogeneous recycling

The alternative approach to homogenous spent fuel recycling is the heterogeneous recycling concept starting from the raffinate of a U and Pu selective recycling process (PUREX or COEX). In the heterogeneous option, the elements are separated in individual product streams for each element or group of elements. Due to its industrial application, the raffinate of the PUREX process is taken as a reference for the heterogeneous recycling option. With an advanced PUREX process Np will be separated together with U and Pu and only trivalent Am and Cm have to be separated. The COEX process shown in Figure 9 depicts a more proliferation resistant evolution of the PUREX process. The different multi-cycle or single cycle options for heterogeneous recycling are described in detail below. The focus of the separation processes is the separation of Am and Cm from fission and corrosion products. The separation of americium alone from curium and fission- and corrosion products is the preferred option in the modern minor actinide management strategies. However, this separation assumed considered to be the most difficult task in hydro-chemical spent fuel partitioning.

2.7.2.1. The COEX process as an optimized PUREX alternative.

The COEX process was developed by the French CEA in cooperation with Areva.[67] It can be seen as a proliferation resistant, evolutionary development of the PUREX process. In analogy to the PUREX process, U and Pu are co-extracted from the spent fuel solution using TBP in kerosene, leaving the fission products and minor actinides in the raffinate. In a consecutive plutonium- stripping step, some uranium is allowed to follow the plutonium. The resulting U and Pu mixed fraction is reduced to U(IV) and Pu(III) to allow for a co–precipitation using oxalic acid. The resulting (U(IV),Pu(III)) mixed oxalate can be transferred to a (U,Pu) mixed oxide by thermal treatment, depicting the MOX master-blend for mixed oxide fuel production. The route prevents for a pure Pu stream, as U and Pu are mixed on the molecular scale. The residual U left in the organic phase is stripped by diluted nitric acid. The aqueous raffinate solution originating from the COEX-process containing the minor actinides and fission- and corrosion products and is compareable to the PUREX-raffinate.[79]

2.7.2.2. Multi cycle Processes: DIAMEX, r-SANEX, TODGA

One of the most elaborated options of heterogeneous recycling is the French DIAMEX + SANEX concept where a separation of trivalent An and Ln from lighter fission and corrosion products is carried out by an An(III)+Ln(III) co-extraction.

In the DIAMide-EXtraction process, a separation of An(III) and Ln(III) together from the lighter fission and corrosion products is achieved. First process developments were carried out using the diamide DMDBTDMA.[80] The system was tested in spiked and a hot test with genuine PUREX raffinate consecutively and confirmed its feasibility as an An(III) + Ln(III) selective partitioning process.[81-82] Further developments focused on the organic phase. Using DMDOHEMA in the non-polar aliphatic diluent TPH, an extraction of Ln(III) and An(III) directly from the highly acidic PUREX raffinate became possible. To prevent the extraction of some undesired fission products, oxalic acid and HEDTA (*N*-(2-hydroxyethyl)-ethylendiaminetriacetic acid) were added. After scrubbing of the loaded organic phase with oxalic acid and HEDTA in diluted nitric acid, An(III) and Ln(III) were back-extracted using diluted nitric acid.[48]

The TODGA-process can be seen as an alternative process to the DIAMEX-Process. The diglycolamide-based TODGA provides high distribution ratios of Ln(III) and An(III) in combination with the high acidic PUREX-raffinate.[33] However, TODGA is prone to third phase formation and only provides limited loading capacity. Therefore, TBP was added as phase modifier, increasing the loading capacity of TODGA and minimizing the risk of third phase formation. However, to limit the co-extraction of the light fission products zirconium, molybdenum, ruthenium, and strontium, HEDTA and oxalic acid had to be added to the feed and scrubbing section.[35] The resulting solvent contains only the co-extracted An(III) and Ln(III) elements, which are stripped consecutively using diluted nitric acid solution. Decontamination factors >10000 for the actinides in combination with very good recovery of >99.9 % for An(III) and Ln(III) were found in a laboratory scale counter current test.[41] The TODGA-process was successfully tested using a genuine spent fuel solution in a counter current process setup. The flowsheet for the hot test was slightly modified enabling for a recovey of >99.99 % of the MA with minor impurities of Y and Ru in the An(III) product. The advantages of the TODGA process over the DIAMEX-Process are the more efficient extraction section and the increased product quality.[65]

The received An(III) + Ln(III) product fraction of the DIAMEX or TODGA process can be used as feed for the An(III)/Ln(III) separation in the consecutive SANEX (Selective ActiNide EXtraction) process.[83] To distinguish between the Ln(III) and An(III), the selectivity of soft N-donor ligands is necessary. For selective extraction of the trivalent actinides, either alkylated tripyridyl-triazine (TPTZ) or alkylated *bis*-triazinylpyridine (BTP) ligands diluted in TPH were first used.[53] Due to investigations regarding radiolytic stability, the final ligand for the SANEX process was chosen to be $CyMe_4BTBP$ in combination with DMDOHEMA or TODGA as phase transfer catalyst.[84-85] After selective extraction of the An(III), the loaded organic phase was scrubbed and the actinides were back-extracted using a glycolic acid solution.[42, 83]

Different countries developed similar multi step processes e.g. the TRUEX + TALSPEAK concept (USA), or the TRPO + CYANEX process (China).[69, 86]

2.7.2.3. The LUCA process for Am(III)/Cm(III) separation.

In 1999 Modolo et al. published the selective extraction of An(III) over Ln(III) from acidic solutions up to 1 mol/L HNO_3 using synergistic mixtures of diorganyl-dithiophosphinic acids in combination with TBP and TOPO.[87] It was shown that (*bis*-(chlorophenyl)dithiophosphinic acid, BCDTP (Figure 10) revealed the most promising separation factors of An(III) over Ln(III).[88] Further investigations of BCDTP showed high separation factors for Am(III) over Cm(III) using a synergetic mixture of the dithiophosphinic acid in combination with tris(2-ethylhexyl)phosphate (TEHP). The selective separation of Am(III) from Cm(III) after applying the SANEX process would provide the opportunity of solely recycling Am while Cm is left for decay storage. The LUCA process for the selective separation of Am(III) was developed based on the synergistic mixture of BCDTP and TEHP in *tert*–butylbenzene and isooctane. It was successfully demonstrated in a laboratory-scale spiked counter-current test.[87] After extraction, a scrubbing step is introduced to remove co-extracted Eu and Cm. The Am is consecutively stripped using a diluted nitric acid solution. The LUCA process can be carried out either after an An(III) + Ln(III) co-extraction process (e.g. DIAMEX) or for the mutual separation of Am and Cm after a SANEX process.[89] Am/Cm separation factors of up to $SF_{Am/Cm} = 8$ were achieved in the LUCA system, but unfortunately it shows low hydrolytic stability in contact with nitric acid solutions.[88, 90]

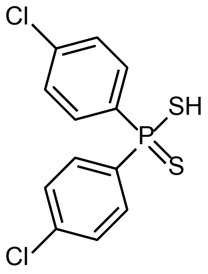

Figure 10: Structure of bis- chlorphenyl- dithiophosphinic acid (BCDTP).

2.7.2.4. Single cycle process options for optimized process management

Recent investigations focus on the development of single cycle processes opening the possibility to simultaneously separate An(III) from the light fission and corrosion products and Ln(III) in a single process.[85] Single cycle process options eliminate the need for raffinate treatment and transport between the different processes probably resulting in a reduced overall effort. The 1-cycle SANEX process is based on an organic phase containing CyMe$_4$BTBP and TODGA as a phase transfer reagent. After the extraction of An(III) and some co-extracted light fission products scrubbing steps with oxalic acid and L-cysteine are carried out followed by the stripping step yielding the actinide product.[91-93] Another one-cycle option for Ln(III)/An(III) separation from PUREX raffinate is the innovative SANEX process.[43, 94] The concept is based on the co-extraction of An(III) and Ln(III) by TODGA in TPH + 5 vol.-% 1-octanol.[36, 62, 72] After scrubbing of the organic phase, the An(III) are selectively stripped using the hydrophilic complexant SO$_3$-Ph-BTP.[62] The Ln(III) remain in the organic phase and are removed consecutively. Numerical simulations have been carried out to find the optimal process flow-sheet with respect to the 16 stage centrifugal contactor rig available at IEK-6, Forschungszentrum Jülich GmbH, Germany.[95] The demonstration of the innovative SANEX process is part of this work. The i-SANEX process will be described in detail in chapter 5.1 and is published in ref.[43, 72, 96]

2.7.2.5. Direct selective separation of Am(III)

The direct selective separation of Am(III) from PUREX provides the most straight-forward option of the different minor actinide handling strategies. Ideally, Am is separated in a single PUREX downstream process preventing the application of different consecutive processes, reducing the potential dose to employees and reducing the amount of secondary wastes. However, the direct selective separation of Am(III) is also one of the most challenging tasks in spent fuel partitioning.

2.7.2.6. The EXAm process for Am separation from PUREX raffinate

The concept of solely separating Am(III) from fission products and Cm(III) in a single process was first realized by the French CEA in the EXAm process.[97] The principle of the process is based on increasing separation factors by using a combination of lipophilic extractant and hydrophilic complexing agents with inverse selectivity.[40] A separation factor of Am(III) over Cm(III) of $SF_{(Cm/Am)} = 2.5$ is reached within this process. As organic phase, a mixture of DMDOHEMA and HDEHP (di(2-ethylhexyl)phosphoric acid) diluted in TPH is used to co-extract Am(III) together with some Ln(III) and light fission products, while Cm(III) is complexed in the aqueous phase by TEDGA (*N,N,N',N'*-tetraethyl-diglycolamide) as hydrophilic complexant.[40] The co-extracted metal ions Pd, Ru, and Mo are removed by a temperature and pH controlled step before americium is stripped from the organic phase. The remaining lanthanides are finally scrubbed resulting in a very complex 68-stage process.[97] The EXAm process was the first Am selective single cycle process to be tested using genuine spent fuel solution in a counter current setup. The hot test of the EXAm process showed a recovery of >99 % for Americium and a decontamination factor of Am versus Cm of 500.

2.7.2.7. AmSel process for the selective separation of trivalent americium

The AmSel process was proposed to enable the selective separation of americium(III) using TODGA in combination with the hydrophilic complexant SO_3–Ph–BTBP.[63, 98] The combination of TODGA and SO_3–Ph–BTBP leads to an increased selectivity for Cm(III) over Am(III) with a separation factor of $SF_{Cm/Am} = 2.5$. First, an extraction is carried out using TODGA to extract the f-elements into the organic phase, followed by the selective stripping of americium using SO_3–Ph–BTBP. A separation factor of $SF_{Eu/Am} = 600$ is reached with this combination. The separation factor of the least extracted lanthanide La is still higher compared to the $SF_{Cm/Am.}$ This enables for an effective separation of Am(III) from Cm(III) together with the lanthanides. The process is currently under development and has not yet been tested in a counter current process setup.[63]

2.7.2.8. Am oxidation for a selective extraction of the oxidized species

The most stable oxidation state of americium and curium in aqueous solutions is +III. However, there is a difference in the oxidation potential of Am(III) and Cm(III). The selective oxidation of americium to Am(V) and Am(VI) followed by a stabilization and extraction of the oxidized species are investigated as an alternative approach to the liquid-liquid extraction of trivalent americium.[69, 99] . An important process based on the oxidation of americium is the SESAME process.[100] The Am(III) is oxidized to Am(VI) using an electrochemical process and stabilized by polyanionic ligands.[101] After the oxidation, Am(VI) can be extracted using TBP (tributyl-phosphate). The major challenges of this procedure are the oxidation step and the stabilization of the higher Am oxidation state, as well as interfering elements in the process feed. The application of the SESAME process therefore requires an upstream purification process like DIAMEX after PUREX.[100]

2.8. Fluorescence-spectrometric investigations on Eu(III) and Cm(III) complexes.

Time resolved laser spectrometry is the preferred method for the spectroscopic analysis of f-element metal ions. Its advantage is a very low detection limit which is in the range of 5x10^{-13} mol/L for Cm(III) and 5x10^{-12} mol/L for Eu(III). The low detection limit of the method allows for an analysis of complexes of f-elements in sub-micro-molar concentration without the necessity for enhances shielding in case of actinide elements. The method bases on the time-resolved delayed measurement of the fluorescence light of the f-element which was previously excited by a laser-pulse. Due to the delay of the measurement, which is typically about 1 µs it is possible to discriminate short lived fluorescence and observe solely the fluorescence light of the metallic species.

The TRLFS-setup can be used in three different modes. In the emission-spectrometry mode, the fluorescence light emitted by the metal species is detected with in a constant time-frame after the excitation, giving a spectrum of fluorescence intensity as a function of the wavelength. The method allows for analysis of the position, splitting and form of the emission bands. The data of this method enables for a precise analysis of the different species of the f-element ions in the observed solution. Due to the delay between the laser pulse and the fluorescence light detection it is possible to analyze solely the metal fluorescence light without any interferences from the matrix. In the excitation-spectrometry mode, the fluorescence light of the metallic species is detected as a function of the excitation laser wavelength. The method allows for the analysis of the excitation energies of the metal ions in the solution. In the fluorescence lifetime mode, the intensity of the fluorescence of a fixed wavelength is measured with increasing delay time. The lifetime spectrum gives the evolution of the emission intensity at a wavelength or a wavelength area as a function of the delay. It can be used to analyze the properties of the inner coordination sphere of the observed metal ion. Due to a radiation free energy transfer of the metal to coordinating hydroxyl- anions the fluorescence is quenched by coordinating hydroxy-ions in the first coordination sphere. This effect was analyzed by Horrocks et al. and Kimura et al. to give a numerical relation between the fluorescence lifetime and the amount of water in the inner coordination shell for Eu(III) and Cm(III), respectively.

2.8.1. Luminescence of the Cm(III) ion

The trivalent curium ion depicts the electron configuration of [Rn]5f^7 which would result in a ground state of $^8S_{7/2}$. However, due to mixing with higher states and spin-orbit coupling the real ground state is depicted as $^8S'_{7/2}$. Figure 11 shows the electronic properties of the Cm(III) ion.[102] The trivalent curium ion shows different absorption maxima for its excitation. Figure 12 shows the absorption spectrum of Cm(III) in 1 mol/L perchloric acid.

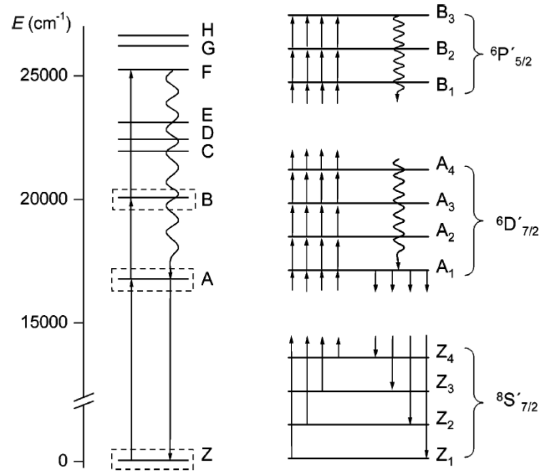

Figure 11: Electronic properties of the Cm(III) ion (left side) including an enlarged view on the ground state Z and the excited states A and B with their splitting (right side). Taken from ref.[102]

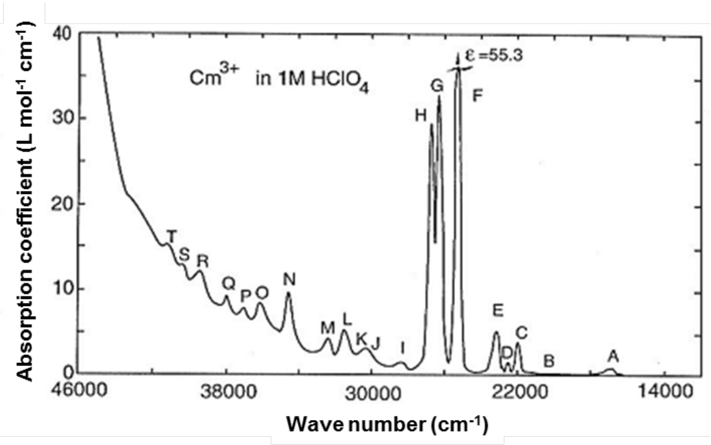

Figure 12: Absorption spectrum of the Cm(III) ion with the F band used for laser excitation of the Cm(III) ion at 396.6 nm (25214 cm^{-1}) having a molar extinction coefficient of 55.3 L mol^{-1} cm^{-1}.Taken from ref.[103]

Commonly, the absortption band with the highest molar extinction factor, namely band F with an excitation wavelength of 396.6 nm is used for the excitation of the Cm(III) ion. After excitation a radiation free relaxation leads to the $^6D'_{7/2}$ A_1 state which consecutively stabilizes by the fluorescence photon emission to the ground state.[103] The relatively low energy of the electrons at room temperature results in a favored population of mainly the A_1 state. With increasing temperature the higher states are populated following the Boltzmann distribution. Ligands which coordinate to the Cm(III) ion result in a splitting of the A_1 to A_4 energy levels due to changes of the symmetry. This results in a lowering of the A_1 state which can be observed as batochromic shift in the fluorescence spectrum.[103] The change in the emission wavelength of Cm(III) is used to analyze the distribution of the Cm(III) species in the solution.

2.8.2. Luminescence of the Eu(III) ion

Eu(III) has the electron configuration of [Xe]f^6 which results in a $^7F_0$ ground state. Figure 13 shows the electronic properties of the trivalent europium ion. The excitation of Eu takes place at a wavelength of 394.0 nm to excite the Eu(III) ion to the $^5L_6$ state. Figure 14 shows the excitation scheme of the trivalent europium ion.[105]

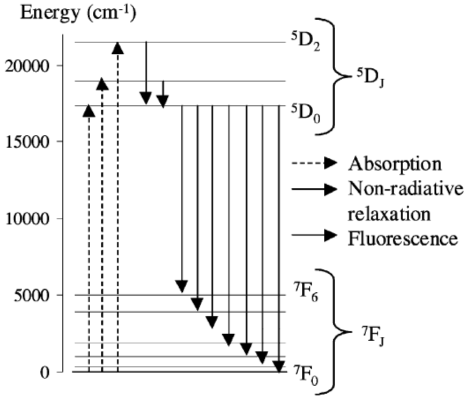

Figure 13: Electronic properties of the Eu(III) ion with splitting of the ^5D_J excited state and ^7F_J ground state.Taken from ref.[104]

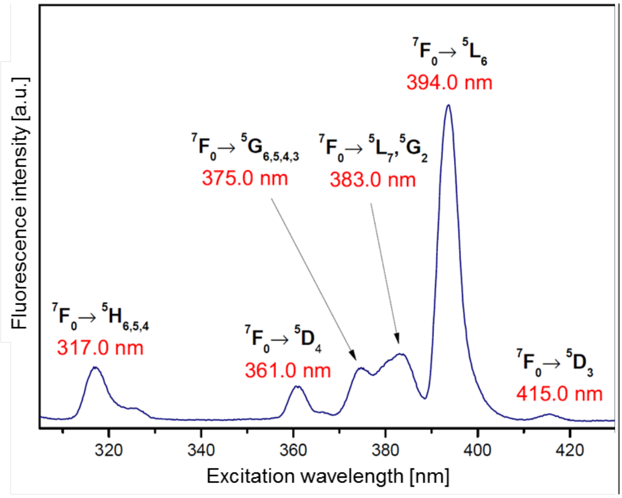

Figure 14: Excitation spectrum of the Eu(III) ion with the $^7F_0$ to $^5L_6$ transition used for laser excitation at 394.0 nm.Taken from ref.[106]

The excitation is followed by a radiation free de-excitation to the ^5D_J state. Due to the low energy of the electrons at room temperature the preferably populated state is the lowest $^5D_0$ state. The fluorescence emission takes place from the $^5D_0$ to one of the ^7F_J states with J=0-6. The fluorescence emissions of the $^5D_0$ to $^7F_0$, $^7F_1$, $^7F_2$ and $^7F_4$ can be used for the identification of the Eu(III) complexes in the solution.[107-108] However, due to the stong shielding of the 4f-electrons, the emission bands do not significantly change their position in the spectra. The dipol-transition of the $^5D_0$ to the $^7F_0$ can be used for a direct analysis of the number of different Eu(III) species in the solution. The emission intensity is herein sensitive to symmetry effects, increasing with decreasing symmetry. The $^5D_0$ to $^7F_4$ dipol-transition emission shows a splitting into maximal 9 different maxima with changing ligand fiels and can therefore be taken to analyze the Eu(III) species distribution in the solution.[107-108]

3. Scope of work

The mutual separation of minor actinides from the fission products was demonstrated in multi process as well as in single process approaches. The innovative selective actinide extraction (i-SANEX) process is a recently developed single process approach for the separation of trivalent actinides from PUREX-raffinate. The process is based on a co-extraction of trivalent actinides and lanthanides followed by a selective back-extraction of the actinides using a hydrophilic complexing agent. However, this process has not yet been demonstrated in a laboratory scale counter current contactor setup. The demonstration of the i-SANEX process using spiked simulated PUREX raffinate will be a key element of this work and will furthermore provide a basis for the development of an americium selective process.

Keeping in mind that the separation of trivalent americium from curium is a challenging task, there are three major questions arising:

- Is there a possibility for a modification of the innovative-SANEX process to enable for a separation of americium from the fission products?

- Are there combinations of lipophilic ligands and hydrophilic complexants that increase the selectivity for americium(III), necessary for its separation from curium(III)?

- Are there conditions which enable for the selective separation of americium from curium and the lanthanides in a continuous counter current process?

The concept of the innovative SANEX process is based on the co-extraction of trivalent actinides (An(III)) and lanthanides (Ln(III)) using a diglycolamide based organic solvent. The separation of the trivalent actinides from the lanthanides is carried out by increasing the selectivity for trivalent actinides by using an aqueous complexing agent. The adaption of the An(III) selective innovative SANEX process to an americium selective process would need for increased selectivity of trivalent americium.

The challenging task of the mutual separation of the trivalent actinides americium and curium calls for increased selectivity in an americium selective stripping section. To achieve this increased selectivity, novel hydrophilic complexing agents have to be tested. Different hydrophilic complexing agents based on polyaminocarboxylic acids or hydro-soluble substituted lipophilic ligands were developed in the past. A smart combination of lipophilic ligands and hydrophilic complexants may lead to an increased separation between americium and curium.

Besides the separation between americium and curium, other process relevant variables like the behaviour of the lanthanide elements, the optimal nitric acid concentration for the separation, or the optimal ligand and complexant concentration play an important role in the development towards am americium selective process. Fluorescence spectroscopic investigations on lanthanide and actinide complexes of the hydrophilic complexing agents using time resolved laser fluorescence spectrometry (TRLFS) conditional stability constants of the complexes, support understanding of complexation mechanisms and support process development.

4. Experimental Part

4.1. Materials

A combined aqueous tracer containing 300 kBq/mL ^{152}Eu and 150 kBq/mL of ^{241}Am and ^{244}Cm each was used for batch extraction studies if not stated differently. The radiotracers were delivered by Isotopendienst M. Blaseg GmbH, Waldburg, Germany, Eckert & Ziegler Nuclitec GmbH, Braunschweig, Germany and Oak Ridge National Laboratory, Oak Ridge, TN, USA. A lanthanide solution containing all lanthanides except promethium in a concentration of 10^{-5} mol/L of each was used for the lanthanide experiments. High active waste (HAW) simulate solutions were prepared according to the literature.[109] DMDOHEMA and TODGA were purchased from TechnoComm, UK. The TODGA derivative Me-TODGA was synthesized at the University of Twente, The Netherlands. The diluent TPH (Hydrogenated Tetrapropene) was received from CEA Marcoule, France. Exxsol D80 was purchased from ExxonMobil. Nitric acid (analytical grade, > 96 %) and 1-octanol (analytical grade, > 99 %) were purchased from Merck, Germany. Cyclohexanediaminetetraacetic acid monohydrate (CDTA, purity ≥ 98 %) was purchased from Fluka. TS-BTPhen was received from University of Reading, UK. The synthesis is described in Ref.[110]. Pytri-diol and H_4TPAEN were both synthesized by the University of Parma according to the literature.[111]

4.2. Methods

4.2.1. Batch solvent extraction experiments

Extraction experiments were carried out either as forward extraction or as stripping (back-extraction). Batch liquid-liquid extraction experiments were conducted using equal volumes of 500 µL of each organic and aqueous phase. The shaking experiments were carried out in a temperature-controlled aluminum block shaker. After shaking, 5 minutes of centrifugation (2,500 rpm) were applied to maintain a complete separation of the phases, and the phases were separated using pipettes. In the forward extraction experiments, the aqueous phase contained the desired metal ions as well as the radiotracers and was contacted with an equal volume of the pure organic phase. During the extraction process, the metal ions were extracted into the organic phase according to their distribution ratio. For back-extraction experiments, the organic phase was pre-loaded and analyzed according to the forward extraction method. Afterwards, the loaded organic phase was used as basis for the stripping experiment in analogy to the forward extraction experiments. Batch kinetic experiments were carried out using the forward or back-extraction method and applying different mixing time intervals to the individual batches. The uncertainties of the data is < 5 % for 0.01 < D < 100. Below and above these limits the uncertainties are lower than 20 % for all data shown.

4.2.2. Actinide loading experiments

Actinide loading experiments were carried out at L28, ATALANTE facility at CEA Marcoule, France. The experiments were carried out in de-pressurized glove boxes. The organic phase was loaded using an aqueous solution prepared from stock solutions of Am(III) (10 mmol/L) ^{241}Am and Cm(III) (15 GBq/L) ^{244}Cm. Tracers of Eu(III) ^{152}Eu and Ce(III) ^{139}Ce were added and the acidity was set using 5 mol/L nitric acid solution. The resulting solution was contacted with the organic phase, and afterwards phases were separated and analyzed. The loaded organic phase was subsequently used for stripping experiments according to the general procedure for batch back-extraction experiments.

4.2.3. Composition of the i-SANEX process demonstration feed solution.

A simulated high active raffinate solution was used as the feed for the i-SANEX process demonstration. It was prepared according to the literature by dissolving the appropriate nitrate salts, metals or oxides of the elements, respectively, in water or nitric acid. The resulting seven individual mixtures were combined according to the literature procedure to give the simulated high active raffinate.[109] Subsequently, ICP-MS analysis was carried out to verify the concentrations of the individual components of this complex mixture. Table 4 shows the composition of the high active raffinate used for solvent extraction tests.

Table 4: Composition of the simulated high active raffinate analyzed by ICP-MS.

Element	Concentration [mg/L]	Element	Concentration [mg/L]	Element	Concentration [mg/L]
Y	79	Ag	11	Re	59
La	214	Al	2	Rh	72
Ce	482	Ba	259	Ru	355
Pr	189	Cd	22	Sb	3
Nd	860	Cr	94	Se	35
Sm	144	Cs	499	Sn	0.1
Eu	29	Cu	19	Sr	161
Gd	41	Fe	1900	Te	116
Na	1600	Mo	658	Zr	382
Ni	45	Pd	204		

4.2.4. Continuous counter-current extraction in centrifugal contactors

Chinese type centrifugal contactors with 1 cm rotor diameter were used for counter current experiments. The contactors were manufactured at Institute of Nuclear Energy Technology (INET), Tsinghua University, Beijing, China. They consist of a rotor and a stator. Figure 15 shows a simplified cross section of a typical centrifugal contactor with the rotor parts (red lines) and stator parts (black lines) and the mixed (green), aqueous (blue) and organic (yellow) phases. The separation efficiency in the contactor depends on a number of kinetic variables making an analytical approach of a process flow-sheet very complex. Therefore, tests using a single centrifugal contactor at different flow rates are used to solve the problem in a numerical approach.

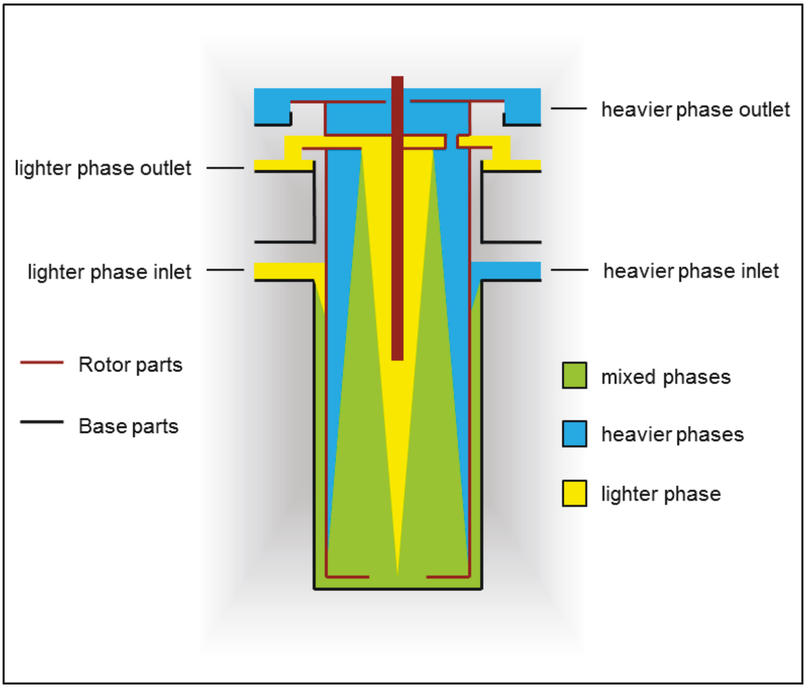

Figure 15: Overview of the parts of a centrifugal contactor in cross section and their function.[112]

The rotor is fully introduced into the housing containing phase inlets and collection rings for the separated phase outlets. The spacing between the rotor and the housing depict the mixing chamber. Mixing is facilitated by adhesion forces between the liquids, the stationary housing and the fast rotating rotor. The mixed phases flow through a hole in the bottom of the rotor. The centrifugal forces inside the rotor separate the phases before they pass an organic or aqueous phase weir, respectively. The separated phases are collected in the rings of the contactor housing and are transferred to the next stage of the contactor battery in a counter current flow. Figure 16 shows the counter current flow connection of the centrifugal contactors within a battery.

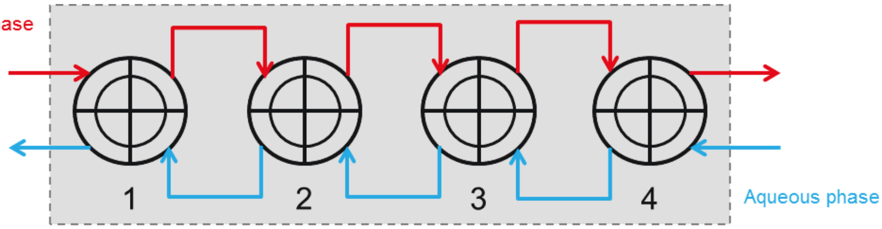

Figure 16: Interconnection scheme of a centrifugal contactor battery used at IEK-6. The black circles depict the centrifugal contactor stages.[112]

The setup used at IEK-6 is a 4 x 4 centrifugal contactor setup consisting of 16 contactors being combined to 4 batteries with 4 contactors each. The technical details of the contactors are given in Table 5.

Table 5: Specifications of the centrifugal contactors used at IEK-6.[112]

Tsinghua University Chemical Contactor	
Rotor Diameter	10 mm
Rotor Material	Titanium
Housing Material	Stainless steel
Rotor speed (typical)	3000-5000 rpm (4500 rpm)
Suggested capacity (at o/a=1)	60-250 mL/h
Hold up volume including tubing	Approx. 6 mL

The contactor itself is surrounded by structure and supply material. Figure 17 shows a centrifugal contactor as used at IEK-6. The complete setup of the 4 x 4 centrifugal contactor rig is shown in Figure 18.

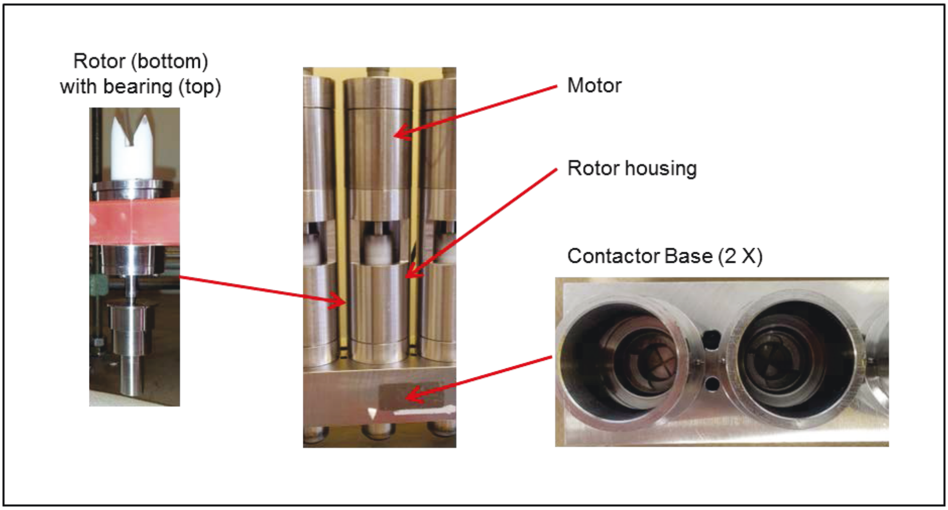

Figure 17: Pictures of the main contactor parts and a complete contactor used at Jülich IEK-6.

Figure 18: The 4 x 4 contactor batteries for process development and testing at IEK-6.

The modular design of the contactors allows for flexibility. A complete change of the phases can be realized at the interconnection of each battery. Additionally, reagents can be introduced to the system between the individual contactors. To realize flow-sheets with a higher stage number than 16, the flow-sheet has to be split in two parts where the equilibrium phases of the first part are collected to be used as feed for the second part. This strategy allows for running flow-sheets with high stage numbers in the 16 stage system with minimal deviations in comparison to a system with a higher number of stages.

For process demonstration, the rig was set up according to the desired flowsheet and the pumps were calibrated. The rig was started with an identic inactive aqueous phase, followed by the organic phase after the first aqueous phase left the system. The system was switched to the active feed when the first organic phase left the system, depicting the start of the process demonstration. Samples were taken from all process effluents in adequate intervals. On-line γ-spectrometric measurements of the effluent samples were used for monitoring of the process. Once the system reached steady state, the contactors were switched off and the content of each stage was removed and analyzed to give the data for stage by stage process profiles.

4.2.5. Radiolysis experiments

Radiolysis experiments were carried out at Chalmers University in Gothenburg, Sweden using a Gammacell 220 irradiator purchased from Atomic Energy of Canada Ltd. A weighed amount of H_4TPAEN was dissolved in the appropriate solvent and irradiated in sealed 2 mL glass flasks using the ^{60}Co based, shielded gamma irradiation source with a dose rate of 9.4 kGy/h (decay corrected for the time of irradiation) for different time intervals. The samples were removed from the irradiation apparatus, visually inspected and shipped to Jülich for solvent extraction experiments according to chapter 4.2.1.

4.2.6. Time resolved laser-fluorescence spectrometry (TRLFS)

TRLFS experiments were carried out at the Institut für Nukleare Entsorgung (INE) of the Karlsruher Institut für Technologie (KIT) in cooperation with Christoph Wagner, Dr. Andreas Geist and Prof. Dr. Petra Panak from the University of Heidelberg. The measurements were carried out using a setup consisting of a Continuum SURELITE Nd:YAG laser with a repetition rate of 10 Hz in combination with a NARROWscan D-R dye laser containing an Exalite 398 dye.[113] For the excitation of Cm(III), a wavelength of 396.6 nm was used. The fluorescence was detected at a 90° angle to the exciting laser pulse using a Shamrock 303i spectrographic analyzer with an ANDOR iStar generation III ICCD camera.[113] Short-lived fluorescence of organic compounds and Raman scattering was discriminated by starting the measurement at a time delay of 1 µs after laser excitation. Samples for single-phase titration experiments were prepared by adding 30 µl of a $3.34 \cdot 10^{-6}$ mol/L Cm(III) stock solution to 970 µl of the respective aqueous medium. The Cm(III) stock solution had an isotopic mass distribution of 89.7 % Cm-248, 9.4 % Cm-246, ≤ 1 % Cm-243, Cm-244, Cm-245 and Cm-247. Cm(III) shows a single fluorescence emission band of the $^6D'_{7/2}$ to $^8S'_{7/2}$ transition within the observed range of wavelengths (580 nm – 630 nm). A stronger ligand field of the Cm(III) ion resulting from complexation of a strong complexing ligand results in a bathochromic shift of the emission wavelength. The Cm(III) emission spectra obtained in the presence of a complexing ligand are composed of a linear combination of the spectra of the individual complex species. They can be analyzed by peak de-convolution using the spectra of the individual species as base data. For the excitation of Eu(III), a wavelength of 394 nm was used in an analogous setup to the Cm(III) TRLFS-system. Samples for single-phase titration experiments were prepared by adding 4.7 µl of a 1.065 mol/L Eu(III) stock solution to 995 µl of the respective medium. The Eu(III) stock solution had natural isotopic mass distribution. Eu(III) is excited to its $^5L_6$ state followed by a radiation free de-excitation to its $^5D_0$ state. The fluorescence of the Eu(III) $^5D_0$ state shows a maximum of 7 theoretical fluorescence emission spectra ($^5D_0$ to $^7F_0$-$^7F_6$). For the analysis of complex species the Eu(III) F_1/F_2 and F_4 emission bands are optimal due to their high emission probability. The F_0 emission band can be used for a direct observation of the Eu(III) species but its emission probability is very symmetry dependent. TRLFS spectra of the Eu(III) F_1/F_2 and F_4 emission bands do not show large bathochromic shifts like the Cm(III)-system. However, an analysis of the different complex species is still possible applying peak de-convolution. The distinction between the different species is possible due to changes in the splitting of the observed emission bands resulting from changes in the symmetry around the Eu(III) ion caused by the complexation of Eu(III). TRLFS experiments were carried out as single or bi-phasic experiments. Single phase titration experiments were carried out by stepwise addition of ligand to a metal-ion solution. With each step, a defined amount of complexant was added to the solution, increasing the total ligand concentration in the solution. Before starting the measurements, mixtures were allowed to equilibrate. In the bi-phasic TRLFS experiments an extraction is carried out prior to the TRLFS measurement. After separation of the phases, both phases were analyzed using TRLFS.

4.2.7. Gamma spectrometry

Gamma measurements of ^{152}Eu (121.9 keV) and ^{241}Am (59.6 keV) were carried out using a Eurisys EGC35-195-R germanium coaxial N-type detector. Organic and aqueous phases of the batch extraction experiments were measured directly taking a sample volume of 300 µL each maintaining constant measurement geometry. Due to relatively low count rates achieved with the standard tracers, a dead time correction was not necessary for batch extraction experiments. Gamma spectrometry of counter current tests was carried out by direct measurement of the phases using volume and dead time correction.

4.2.8. Alpha spectrometry

Alpha measurements were carried out after thin layer sample preparation for ^{241}Am (5486 keV) and ^{244}Cm (5805 keV) using an Ortec Octête-pc eight chamber alpha measurement system equipped with PIPS detectors. An aliquot of the organic or aqueous sample (10 µL), respectively, was diluted in an acetone/zapon lacquer 100:1 mixture. The solution was transferred to the stainless steel sample holder and dried under infrared warming. Subsequently, organic components were removed using an open butane flame. The samples were measured in vacuum.[43]

4.2.9. Inductive coupled Plasma (ICP) based stable element analysis

For stable elements, inductively coupled plasma mass spectrometry (ICP-MS) and atomic emission spectrometry (ICP-AES) were applied using a Perkin Elmer SCIEX Elan 6100 DRC at Jülich and a Perkin Elmer OPTIMA 8300DV at CEA Marcoule. In Jülich, aqueous samples were measured after dilution in 1 % v/v nitric acid solution without further treatment. Organic samples were measured directly in a surfactant matrix (Triton-X-100) in 1 % v/v nitric acid after dilution. At Laboratoire 28 of the ATALANTE facility of the CEA Marcoule ICP-AES analysis was only applicable for aqueous, non-radioactive solutions. The aqueous phase was analyzed directly after dilution using 3 vol. % nitric acid. Analysis of the organic phase was carried out by stripping all metal ions from the organic phase using a solution containing TEDGA (0.2 mol/L), HEDTA (0.05 mol/L) and oxalic acid (0.5 mol/L) in distilled water. The stripping solution was analyzed after dilution using 3 vol. % nitric acid.

4.2.10. Mixer-cell experiments for TPAEN extraction kinetics.

Mixer cell experiments were carried out at L28, ATALANTE-facility at CEA Marcoule using a genuine mixer–settler blade at 2,500 rpm in combination with a 10 mm test tube made from PMMA in tempered glass housing. 3.0 ml of the pre-tempered organic phase were provided in the tube with rotating mixer blade. The time was started when 3.0 ml of the pre-tempered aqueous phase were added. Samples were taken from the emulsion above the mixer blade, centrifuged for 3 minutes and the phases were separated for analysis.

4.2.11. Acidity and pH measurement

Acidities of aqueous phases were determined by potentiometric titration using a Methrom Titrino automatic titration system with a Methrom pH-meter. Acidities of organic phases were determined using a mixture of water and Triton-X-100 as titration medium for the appropriate organic phase. The pH values depict direct measurements of the appropriate solution using a Methrom pH-meter.

5. Results and Discussion

The results and discussions presented in the following chapter are divided into four parts. First, the demonstration and results of the innovative SANEX (i-SANEX) laboratory scale counter current process test are presented. The results of the test were part of different publications.[43, 72, 95-96] The innovative SANEX process depicts the basis for further investigations carried out in this work. Subsequently, screening tests of four hydrophilic complexants were carried out to analyze their ability of separating americium from curium in a selective back-extraction step in analogy to the procedure demonstrated in the i-SANEX process (chapter 5.2). The two hydrophilic complexing agents TS-BTPhen and H_4TPAEN showed promising results for selective Am(III) back-extraction in the screening tests and were investigated in detail for their potential use as Am(III)-selective complexing agents as described in chapter 5.3 and 5.4.

5.1. Innovative SANEX Process for the separation of An(III) from RUREX raffinate

The latest developments in advanced partitioning processes focus on single cycle adaptions of the DIAMEX-SANEX process. In this chapter a novel innovative-SANEX process is presented, making use of the latest developments regarding lipophilic and hydrophilic complexants. The demonstration of the process on the laboratory scale in annular centrifugal contactors using a spiked simulate solution is described. The results of the i-SANEX process demonstration were published in ref.[43] The TODGA (Figure 19) extractant is known to co-extract An(III) and Ln(III) efficiently from highly concentrated nitric acid solutions.[32] The co-extraction of Zr and Pd was overcome using the polyaminocarboxylic acid CDTA (trans-1,2-diaminocyclohexane-*N*,*N*,*N'*,*N'*-tetraacetic acid, Figure 19) as masking agent.[66] Third phase formation was suppressed by addition of 5 vol-% 1-octanol.[36] For the selective recovery of An(III) the hydrophilic complexing agent SO_3-Ph-BTP (Figure 19) was used, instead of a buffered polyaminocarboxylic acid based solution.[62] The composition of the synthetic PUREX raffinate used as the feed solution for the innovative-SANEX process was described in the materials and methods section and is shown in Table 4. 0.05 mol/L of the novel masking agent CDTA (Figure 19) was to the feed to prevent the extraction of Zr and Pd.[66]

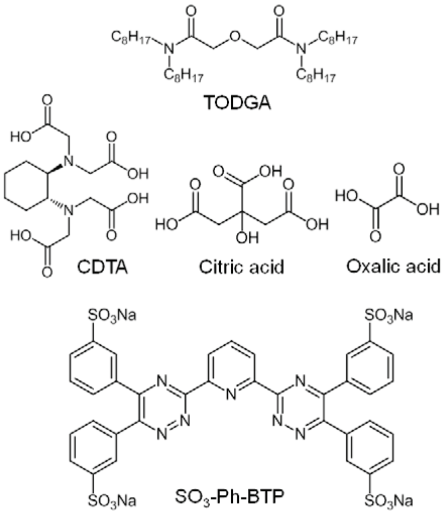

Figure 19: Structure of the ligand TODGA and different masking and complexing agents used for the innovative SANEX process demonstration.

5.1.1. Flow-Sheet Design, Computer Code Calculations

The main goals of the flow-sheet design were to achieve a high recovery yield of actinides (> 99.9 %) and to obtain decontamination factors for fission products (FP) that were as high as possible. The constraints taken into account for the calculations were the number of stages available (16). Important parameters to be optimized were the total number and distribution of contactors between the extraction, scrubbing and stripping sections, concentrations (acidity, complexing agents, etc.) and flow rates. The flow-sheets were optimized using batch data, single-stage centrifugal contactor experiments, and data from previous TODGA processes.[35, 41, 65, 114] The kinetics of the system is a very important parameter for the flow-sheet design with centrifugal contactors due to the short residence time in the contactors.[115] The average residence times for both phases in the mixing chambers (approx. 6 mL volume) of the centrifugal contactors are given in Table 6. Calculations were carried out using the "SX Process" program, described in reference [116-117], which is designed for centrifugal contactors with an emphasis on a simple model for the system's kinetics. Details of the flow-sheet design for this process are described in reference.[95]

Table 6: Average residence time of the phases in the mixing chambers of the centrifugal contactors (approx. 6 mL volume) for each part of the i-SANEX flow-sheet (see Figure 20).

	Extraction	Scrub 1	Scrub 2	Ln Re-extr.	An Strip	Ln Strip
Flow rate (org + aq) [ml/h]	263	202	116	80	120	120
Residence time [min]	1.37	1.78	3.10	4.50	3.00	3.00

5.1.2. Description of the Flow-Sheet

The innovative SANEX process was designed using an organic phase comprising 0.2 mol/L TODGA in TPH + 5 vol.-% 1-octanol and an aqueous phase containing 18 mmol/L SO_3-Ph-BTP in 0.35 mol/L HNO_3 for the An(III) selective stripping. This process consists of 4 main steps (cf. Figure 20):

Step 1: Co-extraction of An(III) and Ln(III): 4 stages.

Step 2: Back-extraction of co-extracted Mo, Sr and HNO_3 using two scrubbing solutions: 8 stages of Scrub 1 (0.05 mol/L CDTA+ 0.2 mol/L oxalic acid in 3 mol/L HNO_3) and 4 stages of Scrub 2 (0.5 mol/L HNO_3).

Step 3: 6 stages for the selective back-extraction of An(III) using the selective aqueous complexing agent SO_3-Ph-BTP at moderate acidity (0.35 mol/L HNO_3) and additional 6 stages for Ln(III) re-extraction.

Step 4: Stripping of lanthanides and residual elements remaining in the solvent using a citric-acid-buffered solution at pH 3: 4 stages.

Similar versions of the first part of the flow-sheet (extraction, Scrub 1, Scrub 2, see Figure 20) have been tested successfully in a spiked TODGA/TBP demonstration process in Jülich[41] and in a hot TODGA/TBP demonstration process at the Institute for Transuranium Elements in Karlsruhe.[65] It was shown that TBP can be replaced by 1-octanol (5 vol.-%), which also reduces the nitric acid extraction and suppresses 3rd phase formation.[36] Therefore, a solvent comprising 0.2 mol/L TODGA in TPH + 5 vol.-% 1-octanol was chosen, as TODGA extracts An(III) and

Ln(III) with the desired high efficiency and with good kinetics. In addition, oxalic acid and HEDTA used in previous processes (e.g., DIAMEX and TODGA/TBP) for masking Zr and Pd were replaced by the hydrophilic complexing agent CDTA (Figure 19) in the feed.[66] The problem of co-extraction of fission and corrosion products, such as Zr, Mo, Sr, Ru, Fe, or Pd, is well known and occurs in several innovative partitioning processes. Recently, it was found that CDTA can be used to efficiently mask Zr and Pd in the feed under GANEX, DIAMEX, and innovative-SANEX solvent extraction conditions, preventing those metal ions from being extracted from High Active Raffinate (HAR) simulate solutions.[66] In batch extraction studies, it was demonstrated that a relatively small concentration of CDTA (0.05 mol/L) was sufficient to complex Zr and Pd and to keep them in the aqueous phase, while the lanthanides and TRU were efficiently extracted. Hence, the challenge was to prove the efficiency of CDTA under realistic process conditions in a counter-current test. The process decontamination factors $DF_{feed/raffinate}$ were calculated according to Equation 3.

Equation 3: Calculation of the feed/raffinate decontamination factors.

$$\mathrm{DF}_{\mathrm{feed/raffinate}} = \frac{\mathrm{Q}_{\mathrm{feed}} \cdot \mathrm{C}_{\mathrm{feed}}}{\mathrm{Q}_{\mathrm{raffinate}} \cdot \mathrm{C}_{\mathrm{raffinate}}}$$

With: Q=flow rate (ml/h); C=concentration (weight-ppm or Bq/L)

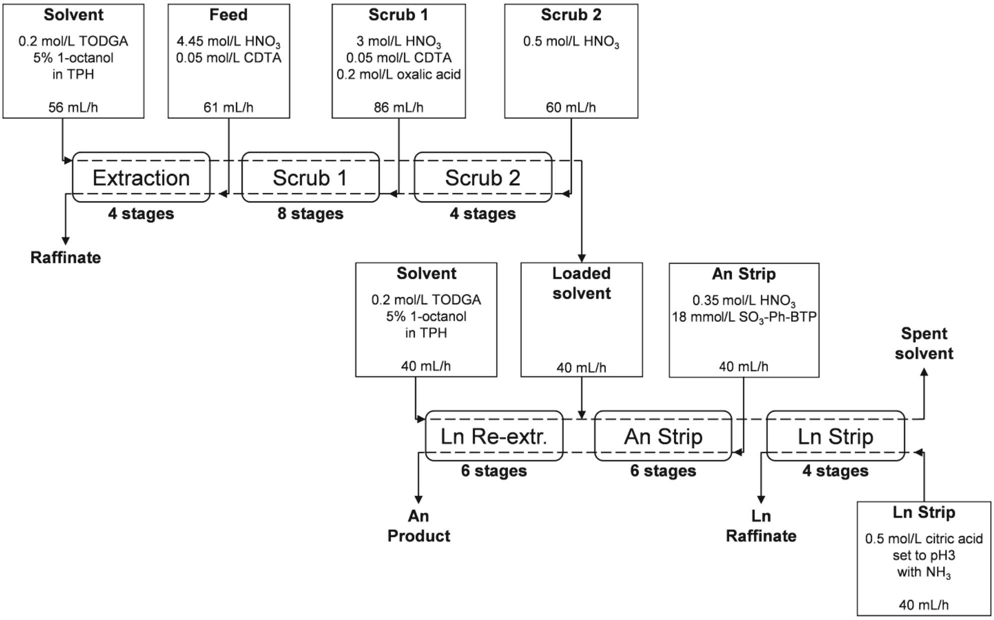

Figure 20: Flow-sheet of the i-SANEX counter current centrifugal contactor test with the average individual flow rates achieved during the test.[93, 95]

5.1.3. Batch Studies and Single-Stage Experiments

Solvent extraction batch studies were performed in a wide range of conditions (e.g. variable nitric acid concentrations, variable ligand concentrations) to construct a database of experimental equilibrium distribution ratios of actinides and all important fission products contained in a typical PUREX raffinate. Optimization studies were then carried out under different experimental conditions related to the flow-sheet (extraction, scrubbing, and stripping) presented in Figure 20 using different selective masking and stripping agents to optimize the system formulation. Important solvent extraction data collected for the development of the innovative SANEX process are reported elsewhere.[62] Single-stage experiments were carried out in a centrifugal contactor setup described previously.[115] The single-stage experiments were run while varying the organic/aqueous flow rates to determine the distribution ratios for some key elements as well as the stage efficiency. Results from the single-stage experiments for the innovative SANEX process were reported recently.[95] The experiments showed that the kinetics of the TODGA-based system for An(III)+ Ln(III) co-extraction and the SO_3-Ph-BTP system for selective An(III) stripping is fast, which is in agreement with earlier batch studies.[62]

5.1.4. Results of the Process Demonstration Test: First Part, Extraction and Scrubbing

Following the flow-sheet in Figure 20, the centrifugal contactor rig was first filled with the Scrub 1 and Scrub 2 solutions at stage 12 and 16, respectively. Then, the organic solvent was fed into the rig. The demonstration test was started by introducing the active feed at stage 4 into the rig. After two hours, the steady-state was reached and the collecting bottle of the organic phase outlet (stage 16) was changed and the test was continued to collect enough loaded solvent for the second part of the test. Thereby, two fractions of loaded solvent were collected; one fraction of the solvent in transient state, and one fraction of the solvent in steady-state. After 5 hours 30 minutes, the experiment was stopped and the content of the mixing chambers of the centrifugal contactors were analyzed as described above to determine the profiles shown in Figure 21 and Figure 22. Figure 21 shows the americium and Eu profiles, and Figure 22 shows the americium and curium profiles. Am(III), Cm(III), Y(III), and Ln(III) were quantitatively extracted (> 99.9 %, cf. Table 7) and high feed/raffinate decontamination factors (Equation 3) were achieved with $DF_{feed/raffinate}$ generally >1000 (Table 7). Only for Cm a slightly lower $DF_{feed/raffinate}$ was observed (750), and the value for Eu determined by ICP-MS, seems to be unusually low (380). In contrast, the gamma-spectroscopic result for ^{152}Eu showed a value of 1100. Four stages were found to be sufficient to reach the high feed/raffinate decontamination. The trivalent actinides and lanthanides stayed in the organic phase during the two scrubbing sections with high distribution ratios (Table 8). The distribution ratios decreased slightly in the last four stages (increased aqueous concentrations, cf. Figure 21. and Table 8), due to the lower nitric acid concentration in those stages. The acidity profile of the first part of the test is shown in Figure 23. The acidity in the different sections reflects the dilution of the feed with the two scrubbing solutions. Therefore, a maximum HNO_3 concentration of 3 mol/L was reached in the extraction section, while 2.5 mol/L was reached in the first scrubbing section. In the second scrubbing section, the acidity was 0.5 mol/L, as this aqueous phase was not diluted by other aqueous streams. The organic nitric acid concentration reflected a nitric acid distribution ratio of ~0.1-0.15.

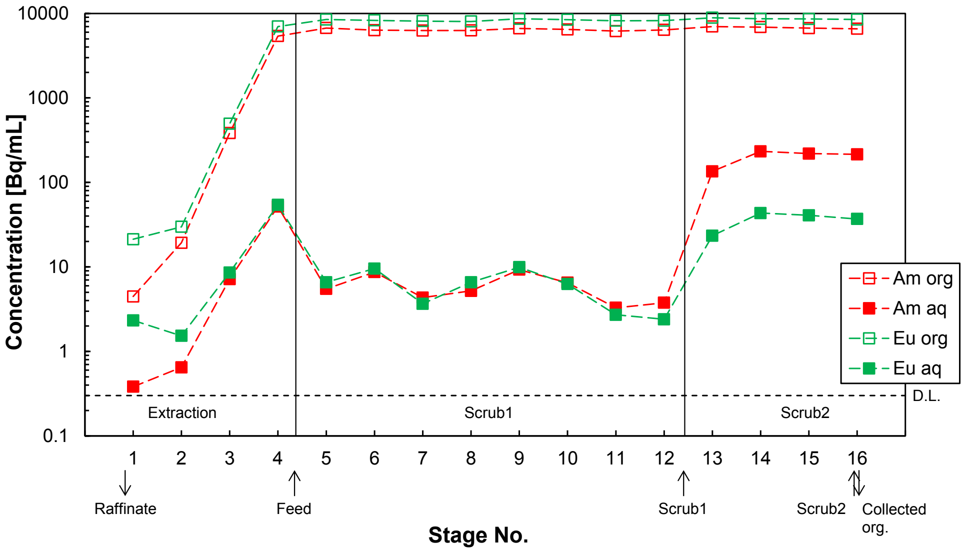

Figure 21: Experimental aqueous and organic concentration profiles of ^{241}Am and ^{152}Eu during the first part of the innovative SANEX test.

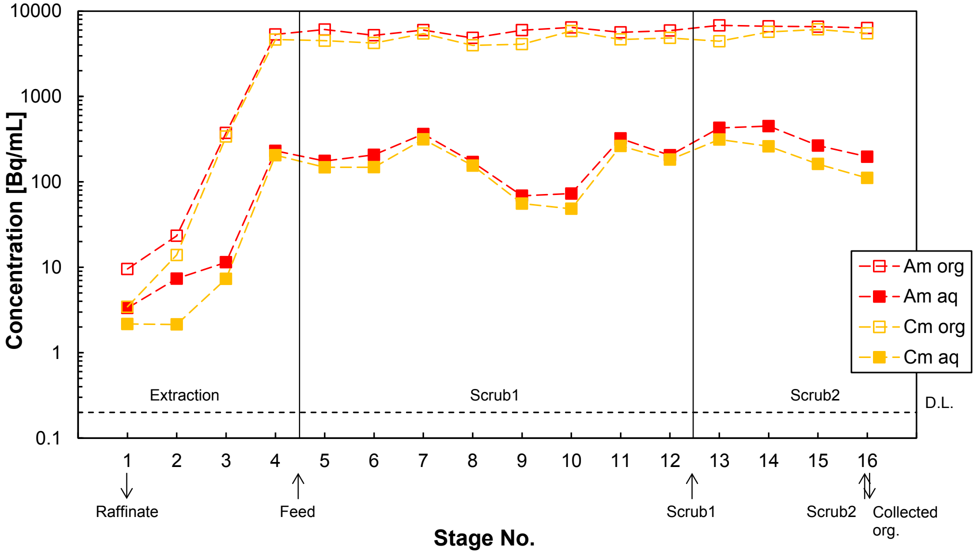

Figure 22: Comparison of the ^{241}Am and ^{244}Cm concentration profiles measured by alpha-spectroscopy during the first part of the innovative SANEX test. Note that alpha-spectroscopy is less precise than gamma-spectroscopy, especially in the samples with high salt content.

The addition of 0.05 mol/L CDTA to the feed efficiently limited the co-extraction of Zr and Pd. Distribution ratios of 0.01 and 0.09 were observed for Zr and Pd, respectively. The Scrub 1 and Scrub 2 steps turned out to be less effective for the back-extraction of Mo, Pd, and Zr, as reflected by distribution ratios >1 in those sections (Table 8). This finding was quite surprising, as oxalic acid was used additionally for scrubbing in the Scrub 1 solution, which had been used in several demonstration tests before. The slow kinetics of Zr extraction and poor back-extraction of Zr from loaded TODGA solvent by CDTA has been described previously.[64] However, the masking of Mo, Pd, and Zr in the feed was quite efficient, since the collected organic solvent (stage 16) contained only 0.1 % Mo, 0.1 % Zr, and 2.8 % Pd of the initial amounts (Table 7). The lower acidity Scrub 2 solution proved to be very efficient for scrubbing Sr, as distribution ratios of 0.21 were observed and only 0.3 % Sr of the initial amount (Table 7) was found in the collected organic solvent (stage 16). The lower nitric acid concentration of 0.5 mol/L in the Scrub 2 section was essential for scrubbing Sr. Figure 24 shows the Sr and Ru concentration profiles and it shows that Sr was extracted very well and went through the Scrub 1 section. Only in the Scrub 2 section a back-extraction was observed. This in turn lead to an accumulation of Sr in the Extraction and Scrub 1 sections of the test, observable by the high steady-state concentrations in stages 1-12 compared to the initial feed concentration and a peak in the org. and aq. Sr concentration in stages three (org.) and four (aq.). However, a steady state was reached for Sr (constant effluent concentrations at the aqueous and organic outlets) and the maximum concentration of Sr in the solvent accounted for only ~10 % loading of TODGA (an 1:2 Sr:TODGA complex was assumed[118]). The behavior of Ru was very similar to that observed in earlier tests using TODGA based solvents, since 16 % of the initial Ru amount was co-extracted (see also Figure 24). A fundamental understanding of the Ru behavior in TODGA-based solvents is still lacking and needs to be further investigated.

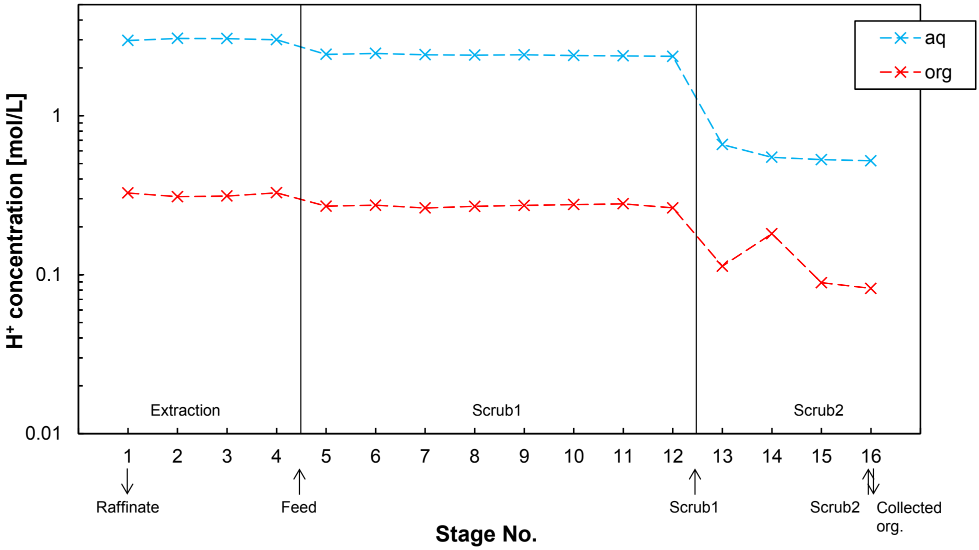

Figure 23: Acidity profile over the first 16 stages of the i-SANEX process demonstration.

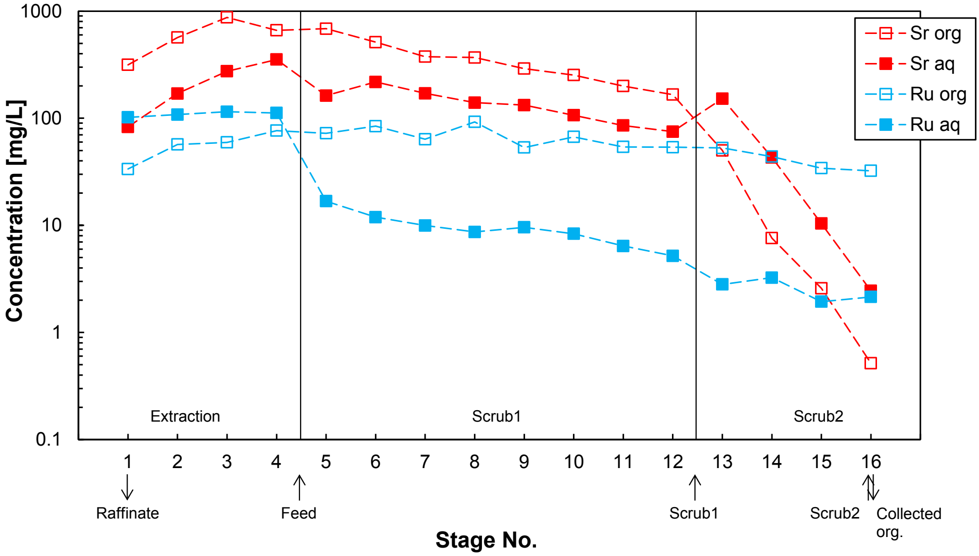

Figure 24: Profiles of Ru and Sr over the extraction and scrubbing section analyzed by ICP-MS

5.1.5. Results of the Process Demonstration Test: Second Part, An(III) and Ln(III) Stripping

On the second day of the continuous test, the centrifugal contactor rig was first filled with the An-Strip and Ln-Strip solutions, as given in Figure 20. Then the loaded organic solvent collected in the transient state was fed into the rig, together with fresh solvent (Figure 20). After the first organic phase left the organic outlet (stage 32), the organic feed was changed to the loaded solvent collected in the steady-state. After 2 hours 38 minutes, the new steady state was reached, the experiment was stopped, and the content of the mixing chambers of the centrifugal contactors was analyzed as described above to determine the An(III) and Eu(III) profiles shown in Figure 25 and Figure 26. Figure 25 shows the Am/Eu profiles, and Figure 26 shows the Am/Cm profiles. Table 7 shows the mass balances, recoveries, and feed/raffinate decontamination factors of all metal ions and Table 8 shows their distribution ratios in the different process steps. Selective back-extraction of An(III) with SO_3-Ph-BTP was very efficient with distribution ratios ≤ 0.06 (Table 8). The An(III) were efficiently stripped within six stages and > 99.8 % Am(III) and Cm(III) were recovered in the An product fraction. Good separation from the Ln(III) was achieved in the Ln Re-extraction section, the Am(III) + Cm(III) product was fairly clean and only contaminated with 0.3 % Sr, 0.4 % Ru and < 0.1 % Ln(III). The Ln(III) were very efficiently stripped in the last four stages using a citric acid based stripping solution (distribution ratios $\leq$ 0.07, Table 8). Only four stages were needed for complete Ln(III) stripping. In this section, also the remaining Pd (2.8 %) was stripped together with the lanthanides. Interestingly, Pd was not stripped in the trivalent actinide stripping section with SO_3-Ph-BTP. As the lipophilic BTPs and BTBPs are known to extract Pd very well, a complexation with SO_3-Ph-BTP would also have been possible. In the An stripping section no CDTA was present to mask the Pd extraction, so the well-known TODGA extraction of Pd competes with the complexation with the BTP. In this case, the TODGA extraction seems to be stronger than the complexation by the BTP in the aqueous phase. Figure 27 shows the acidity profile of the second part of the test. In the Ln re-extraction and An Strip sections an aqueous acidity of 0.44 mol/L was observed; slightly higher than the 0.35 mol/L HNO_3 introduced by the An Strip solution. The higher acidity resulted from co-extracted nitric acid present in the loaded solvent (0.08 mol/L HNO_3). The co-extraction of nitric acid in the extraction section of the process had been accounted for in the flow-sheet calculations and the nitric acid concentrations in the Scrub 2 and An Strip sections had been adjusted accordingly.[95] The acidity in the organic phase was very low over all stages in the second part of the test. The aqueous H^+ concentrations of stages 29-32 (Ln strip) were calculated from the measured pH. A pH measurement of the organic samples was not possible and the H^+ concentrations were below the detection limit of the potentiometric titration. Therefore, the organic concentrations in the Ln strip section are omitted in Figure 27. The spent solvent after stripping contained < 0.1 % of Am(III), Cm(III), and Eu(III). A maximum spent solvent contamination of light lanthanides was observed for La(III) with 0.4 %, although La(III) shows the lowest distribution ratios in TODGA extraction.

Table 7: Mass recovery and process decontamination factors obtained during the i-SANEX demonstration

Element	% in raffinate	% in loaded solvent	% in An(III) product	% in Ln(III) product	% in spent solvent	$DF_{feed/raffinate}$
^{241}Am	< 0.1	99.9	99.9	0.1	< 0.1	2.6E+3
^{244}Cm	0.1	99.9	99.7	0.1	0.1	750
^{152}Eu	0.1	99.9	0.1	99.8	0.1	1.1E+3
La	< 0.1	99.9	D.L.	99.5	0.4	2.3E+4
Ce	< 0.1	99.9	D.L.	99.7	0.3	5.7E+5
Pr	< 0.1	99.9	D.L.	99.7	0.3	2.2E+5
Nd	< 0.1	99.9	D.L.	99.8	0.2	3.9E+4
Sm	< 0.1	99.9	D.L.	99.9	0.1	3.4E+3
Eu	0.3	99.7	D.L.	99.7	0.1	380
Gd	< 0.1	99.9	D.L.	99.9	0.1	4.9E+4
Y	< 0.1	99.9	D.L.	99.9	D.L.	4.7E+4
Ru	84.0	16.0	0.4	0.9	14.7	1.2
Pd	97.2	2.8	< 0.1	2.8	< 0.1	1.0
Zr	99.9	0.1	0.1	< 0.1	< 0.1	1.0
Mo	99.9	0.1	0.1	< 0.1	< 0.1	1.0
Sr	99.7	0.3	0.3	< 0.1	D.L.	1.0
Rh	99.9	D.L.	D.L.	D.L.	D.L.	1.0
Rb	99.9	D.L.	D.L.	D.L.	D.L.	1.0
Ba	99.9	D.L.	D.L.	D.L.	D.L.	1.0
Cs	99.9	D.L.	D.L.	D.L.	D.L.	1.0
Te	99.9	D.L.	D.L.	D.L.	D.L.	1.0
Cd	99.9	D.L.	D.L.	D.L.	D.L.	1.0
Sn	99.9	D.L.	D.L.	D.L.	D.L.	1.0
Sb	99.9	D.L.	D.L.	D.L.	D.L.	1.0
Ag	52.1	D.L.	D.L.	D.L.	D.L.	1.0
Cu	99.9	D.L.	D.L.	D.L.	D.L.	1.0
Ni	99.9	D.L.	D.L.	D.L.	D.L.	1.0
Cr	99.9	D.L.	D.L.	D.L.	D.L.	1.0
Fe	99.9	D.L.	D.L.	D.L.	D.L.	1.0
Na	99.9	D.L.	D.L.	D.L.	D.L.	1.0

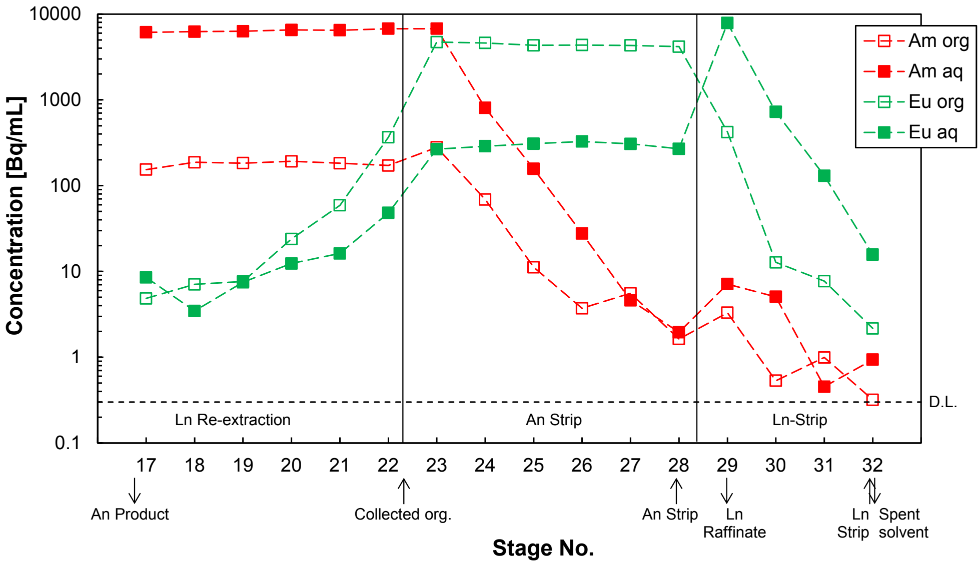

Figure 25: Am(III) and Eu(III) profiles over the stripping section of the flow-sheet measured by gamma spectrometry.

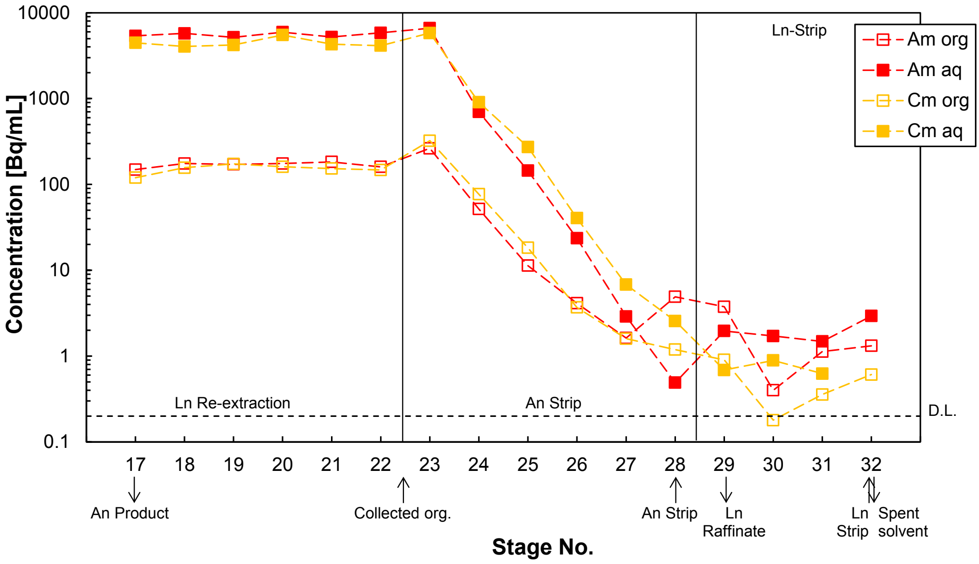

Figure 26: Am(III) and Cm(III) profiles over the stripping section of the flow-sheet analyzed by alpha spectrometry.

Table 8: Distribution ratios of the metal ions contained in the feed for selected stages of the process demonstration according to chapter 4.2.4. D.L. = detection limit.

	Extraction	Scrub 1	Scrub 2	An(III) Strip	Ln strip
Element	Stage 4	Stage 12	Stage 16	Stage 23	Stage 29
^{241}Am gamma	104	>1000	30.7	0.04	0.46
^{241}Am alpha	23.1	28.9	32.2	0.04	D.L.
^{244}Cm alpha	22.6	26.7	49.4	0.06	D.L.
^{152}Eu gamma	129	>1000	230	17.7	0.05
La	24.6	57.8	3.4	1.7	0.04
Ce	37.4	145	5.9	2.9	<0.01
Pr	53.1	270	10.1	4.9	0.05
Nd	60.3	409	20.4	9.4	0.04
Sm	69.3	536	95.0	22.5	0.06
Eu	66.9	543	137	19.3	0.06
Gd	68.1	446	36.3	12.9	0.05
Y	57.6	528	191	123	0.07
Ru	0.68	10.4	15.1	12.7	6.11
Pd	0.09	88.9	168	24	0.10
Zr	0.01	2.92	4.32	0.53	D.L.
Mo	0.21	2.62	4.43	1.47	0.22
Sr	2.28	2.22	0.21	0.14	D.L.
Rh	<0.1	D.L.	D.L.	D.L.	D.L.
Rb	<0.1	D.L.	D.L.	D.L.	D.L.
Ba	0.05	D.L.	D.L.	D.L.	D.L.
Cs	<0.1	D.L.	D.L.	D.L.	D.L.
Te	<0.1	D.L.	D.L.	D.L.	D.L.
Cd	0.11	D.L.	D.L.	D.L.	D.L.
Sn	<0.1	D.L.	D.L.	D.L.	D.L.
Sb	<0.1	D.L.	D.L.	D.L.	D.L.
Ag	0.01	D.L.	D.L.	D.L.	D.L.
Cu	<0.1	D.L.	D.L.	D.L.	D.L.
Ni	<0.1	D.L.	D.L.	D.L.	D.L.
Cr	<0.1	D.L.	D.L.	D.L.	D.L.
Fe	<0.1	D.L.	D.L.	D.L.	D.L.
Na	<0.1	D.L.	D.L.	D.L.	D.L.

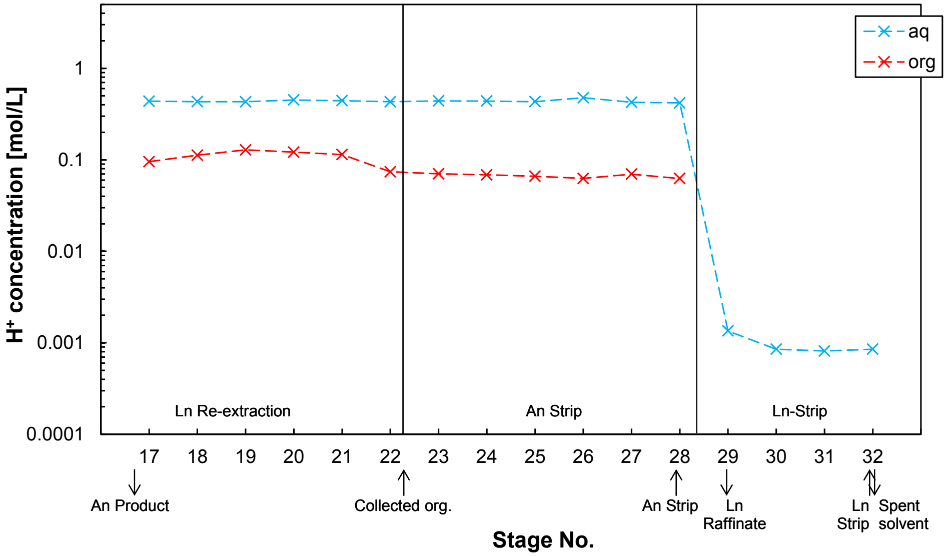

Figure 27: Acidity profile of the stages 17-32 of the i-SANEX process demonstration.

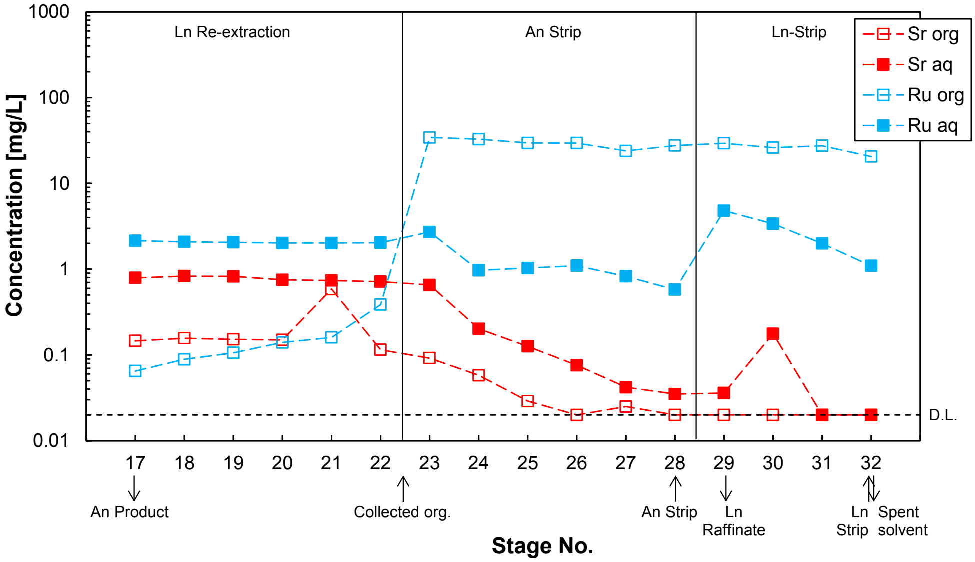

Figure 28: Sr and Ru profiles over the stripping sections of the flow-sheet analyzed by ICP-MS

The higher stripping efficiency towards heavier lanthanides is attributed to a stronger complexation of the heavier lanthanides with citrate. The only major contamination of the spent solvent was Ru. Figure 28 shows that Ru was not stripped by SO_3-Ph-BTP or the citric-acid based stripping solution and 14.7 % Ru were found in the spent solvent. A similar behavior was already described for other demonstration tests using the TODGA extractant.[41, 65] Further investigations are required either to avoid the extraction of Ru using special complexing agents or to regenerate the solvent by specific washing steps. The recoveries and mass balances shown in Table 7 were very good, except for Ag. Only 52% of the initial amount was recovered in the raffinate, but no Ag was found in any other effluent. Probably Ag precipitated in the feed, during the test, or in the raffinate before analysis. The hydrodynamic behavior of the solvent was excellent during the whole spiked test and no phase entrainment or 3rd phase formation was observed. Thanks to the promising results obtained in the spiked counter-current test, a hot demonstration is planned after re-calculation of the results to verify the computer-code models and further optimizations. Furthermore, recycling of solvent as well as recycling of SO_3-Ph-BTP and the long term stability of the organic molecules has to be further investigated.

5.1.6. Conclusion to the i-SANEX process demonstration

The innovative SANEX- process was demonstrated in a 32 stage counter current flow sheet which was split in two parts of each 16 stages. During the two day process test, no hydrodynamic issues were observed. The novel hydrophilic masking agent CDTA performed well, preventing the extraction of undesired fission products and enabling for an oxalic acid free feed. The loaded organic phase collected after the second scrubbing step showed no phase entrainment and provided a good quality loaded solvent for the consecutive part of the test. The actinide stripping section using the hydrophilic complexing agent SO_3-Ph-BTP enabled for an efficient back-extraction. Excellent product purities and a high recovery of the actinides were obtained due to the combination of the actinide stripping with a lanthanide re-extraction section. The residual lanthanides in the organic phase were finally removed from the organic solvent by a buffered citric acid solution. The co-extraction of ruthenium to the organic phase can be seen as a minor issue of the concept. However, ruthenium fortunately did not contaminate the actinide and lanthanide products. The i-SANEX process test showed a good overall performance with high decontamination factors and high product purities.

5.2. Ligand screening for selective separation of Am(III) from PUREX raffinate

A screening of different complexants related to high selectivity for Am(III) or Cm(III) in diglycolamide and diamide based lipophilic systems was conducted.

In case of the lipophilic ligand, there are two major ligand types to distinguish between with respect to Am/Cm selectivity. On the one hand there are ligands with a preference for Am and on the other hand there are ligands with a preference for Cm. To achieve the optimal separation of Am(III) from all other elements in high active raffinates (HAR), two major concepts can be followed.

1. The selective extraction of Am(III) leaving all other elements in the aqueous phase.

2. The co-extraction of An(III) followed by a selective back- extraction of the Am(III).

In this work the well-known TODGA (used in the i-SANEX process, chapter 5.1) and DMDOHEMA (used in the EXAm process, CEA, France) extractants were chosen to provide the extraction into the organic phase. Additionally, a methylated TODGA derivative (Me-TODGA) was analyzed providing lower distribution ratios compared to TODGA which can be an advantage for process robustness.

5.2.1. Screening of hydrophilic complexing agents.

Hydrophilic complexing agents are often used to decrease distribution ratios by a hydrophilic competitive complexation to the lipophilic complex in the organic phase. In analogy to their lipophilic complement, hydrophilic complexing agents are able to provide selectivity for several elements. A smart combination of lipophilic ligands and hydrophilic complexants is able to significantly increase the selectivity of a system.

DMDOHEMA favors the direct extraction of Am(III) and a consecutive selective stripping of co-extracted fission products or Am(III), respectively. The DGA-based ligands show a preference for Cm(III) over Am(III) providing a feasible base for a co-extraction of An(III) and Ln(III) followed by an Am(III) selective stripping which may be designed according to the An(III) selective stripping in the i-SANEX test described in chapter 5.1. Three hydrophilic complexing agents were tested for their selectivity for Am(III) over Cm(III) in combination with the appropriate lipophilic ligand. The structures of the complexants are shown in Figure 29.

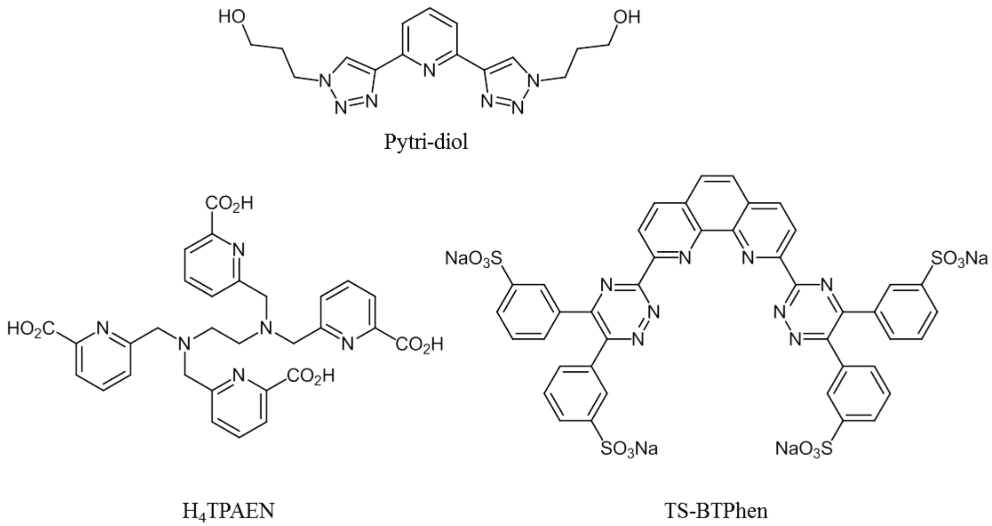

Pytri-diol

H$_4$TPAEN

TS-BTPhen

Figure 29: Structures of the novel hydrophilic complexants Pytri-diol, H$_4$TPAEN and TS-BTPhen.

TS-BTPhen and Pytri-diol are derived from lipophilic ligands which have been modified to provide a water-soluble complexant. TS-BTPhen is a hydrophilic derivative of CyMe$_4$-BTPhen, a lipophilic ligand used in the An/Ln separation.[61] The evolution from bis-triazinyl-based ligands to CyMe$_4$-BTPhen and finally TS-BTPhen is described in chapter 2.5.3. Pytri-diol was developed by the University of Parma together with the University of Milan as an An(III)/Ln(III) selective ligand for a CHON compatible stripping agent in an i-SANEX process.[119] H$_4$TPAEN was developed as hydro-soluble polyaminocarboxylic acid for an application in high luminescent Ln(III) complexes for medical imaging at the medical department of the CEA in France.[111, 120-121] It was identified as an Am(III) selective hydrophilic complexing agent at CEA Marcoule, France.

5.2.2. TS-BTPhen

TS-BTPhen (3,3',3'',3'''-[3-(1,10-phenanthroline-2,9-diyl)-1,2,4-triazine-5,5,6,6-tetrayl] tetrabenzenesulfonic acid) is a hydrophilic derivative of the lipophilic BTPhen ligand family.[59-60, 110] It was developed as a cis-locked ligand version of the BTBP ligands used e.g. in the 1-cycle SANEX process.[72, 91-93] The high selectivity of TS-BTPhen towards americium has been previously described in the literature for the chromatographic separation of Am(III) from Cm(III) using a TODGA-PAN based chromatographic column.[122] Figure 30 shows the distribution ratios of Am(III), Cm(III), and Eu(III) using TODGA without a hydrophilic complexant in the aqueous phase (open symbols) as well as TODGA in the organic phase and TS-BTPhen in the aqueous phase (closed symbols) as a function of the initial nitric acid concentration. Compared to TODGA alone the distribution ratios of Am(III) and Cm(III) are significantly decreased by the application of TS-BTPhen. Furthermore, the separation factor between Cm(III) and Am(III) is significantly increased. In the region where a mutual separation of Am from Cm is possible ($D_{(Am)}<1$; $D_{(Cm)}>1$) the separation factor increases from $SF_{(Cm/Am)} = 1.6$ for TODGA alone to $SF_{(Cm/Am)} = 3.6$ for the combination of TODGA with TS-BTPhen making it a promising combination for the selective separation of Am(III) from PUREX raffinate.

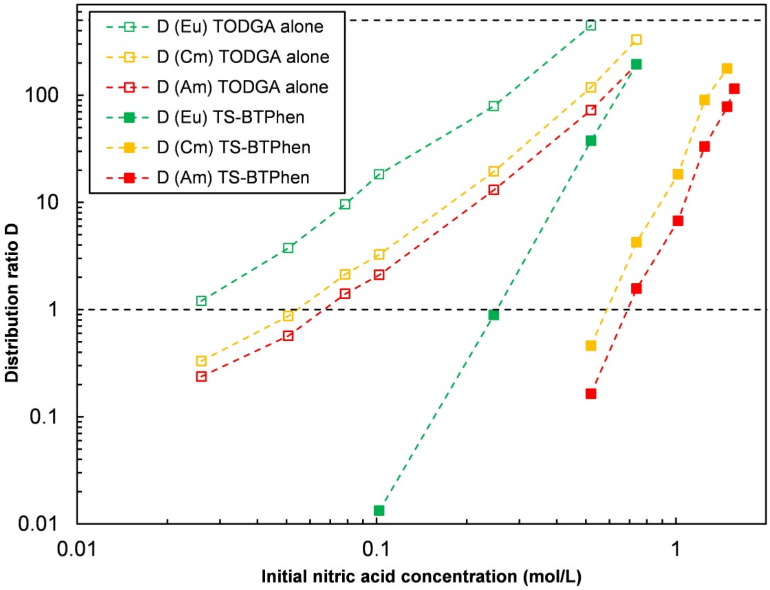

Figure 30: Distribution ratios of Am(III), Cm(III), and Eu(III) as a function of the initial nitric acid concentration. Org: 0.2 mol/L TODGA in TPH +5 vol.-% 1-octanol; aq: 10 mmol/L TS-BTPhen in different nitric acid concentrations. 30 min of contact time at 22 °C, 5 min of centrifugation.

Due to its high affinity for trivalent f-elements the use of TODGA leads to high distribution ratios of An(III) and Ln(III) (c.f. Figure 30) making stripping of these elements difficult. In order to find an extractant which extracts well at high nitric acid concentrations but does not reach as high distribution ratios at low HNO_3 concentrations, derivatives of TODGA were synthesized.[37] The methylated TODGA derivative Me-TODGA was found to provide extraction by reaching slightly lower An(III) and Ln(III) distribution ratios compared to TODGA. Me-TODGA was tested as an alternative ligand for the selective separation of Cm(III) over Am(III) in combination TS-BTPhen. Figure 31 shows the results of a comparison of the distribution ratios of Am(III), Cm(III) and Eu(III) using TODGA and Me-TODGA both with TS-BTPhen in the aqueous phase. The lower distribution ratios of Me-TODGA combined with TS-BTPhen resulted in an Am(III) selective strip using nitric acid concentrations greater than 1 mol/L. The application of Me-TODGA in combination with TS-BTPhen can thus reduce the difference in nitric acid concentration between the extraction and stripping step leading to a more robust system with respect to changes in the nitric acid concentration. In addition, stripping at high nitric acid concentrations opens the possibility of reducing the number of steps needed for the nitric acid scrubbing from the organic phase. The separation factor between Cm(III) and Am(III) is increased from $SF_{(Cm/Am)} = 1.4$ for the Me-TODGA alone to $SF_{(Cm/Am)} = 2.7$ for the Me-TODGA – TS-BTPhen combination. The region in which a mutual separation of Am and Cm is possible is shifted to even higher nitric acid concentrations compared to TODGA, making a selective separation possible even at nitric acid concentrations > 1.5 mol/L.

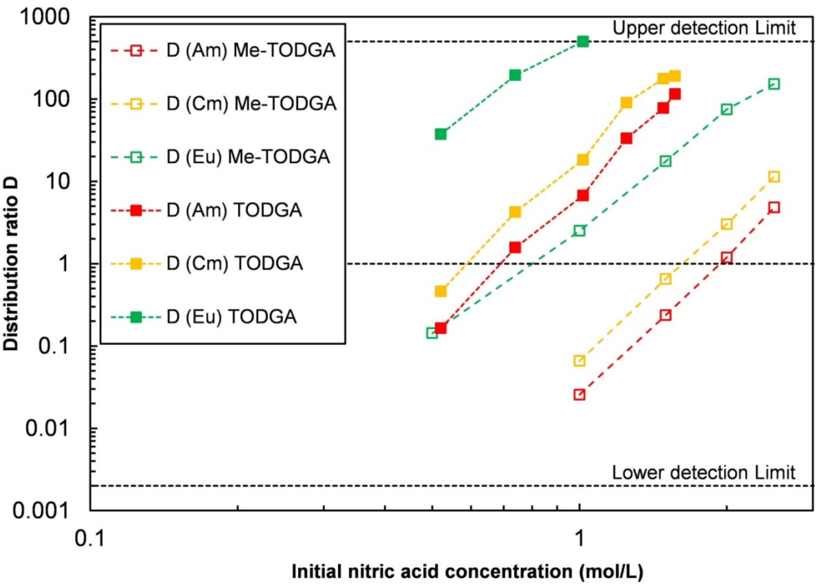

Figure 31: Comparison of TODGA and Me-TODGA as organic extractants for the selective stripping of Am(III). Organic phase: 0.2 mol/L TODGA (filled symbols) or Me-TODGA (open symbols) in TPH + 5 vol.-% 1-octanol; aqueous phase: 10 mmol/L TS-BTPhen in different nitric acid concentrations; 30 min of extraction at 22°C; 5 min of centrifugation.

5.2.3. Pytri-Diol

Pytri-diol (Figure 29) is a hydrophilic complexant based on a pyridine system connected to two triazole systems as backbone.[119] Its hydrophilicity is increased by substitution of two hydroxy-alkanes of the triazole systems. The complexant was developed at the University of Parma in cooperation with the University of Milan. Its focused application is a CHON compliant stripping of An(III) from Ln(III) in selective partitioning processes. Pytri-diol shows high separation factors for An(III) over Ln(III). Its "soft" complexation with nitrogen atoms and a lack of data regarding its Am/Cm selectivity makes it an interesting complexant for the screening. Figure 32 shows the distribution ratios of Am(III), Cm(III), and Eu(III) with TODGA in the organic and Pytri-diol in the aqueous phase as a function of the initial nitric acid concentration.

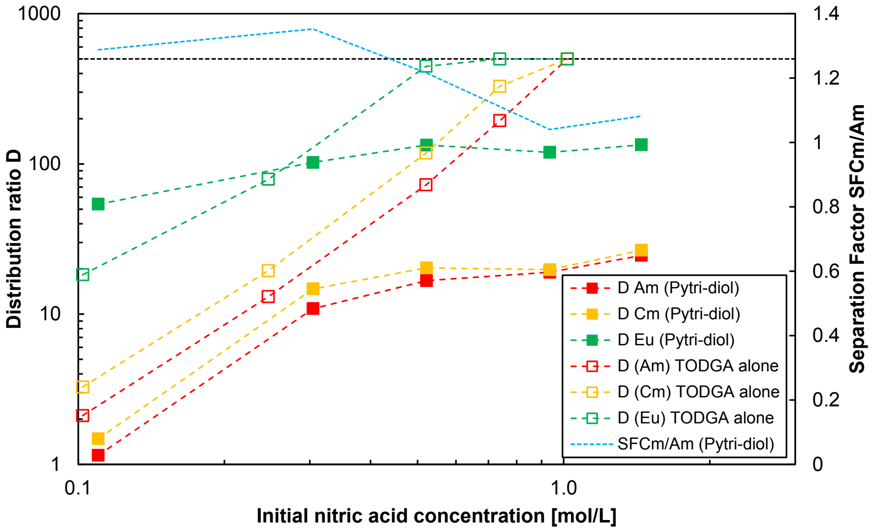

Figure 32: Distribution ratios of Am(III), Cm(III), and Eu(III) as a function of the initial nitric acid concentration. Org: 0.2 mol/L TODGA in TPH +5 vol.-% 1-octanol; aq: 10 mmol/L Pytri-diol in different nitric acid concentrations. 30 min of contact time at 22 °C, 5 min of centrifugation.

The distribution ratios of Am(III), Cm(III) and Eu(III) are similar to TODGA alone in the region of low acidity up to 0.3 mol/L nitric acid. However, at higher acidity the trivalent actinides are held back in the aqueous phase by the Pytri-diol and distribution ratios of the An(III) of ~20 are observed. The separation factor $SF_{Cm/Am}$ decreases with increasing nitric acid concentration and does not reach the separation factor achieved with TODGA alone. However, the selectivity of the separation of Ln(III) over An(III) is high providing a separation factor of $SF_{(Eu/Am)} > 50$ at 0.1 mol/L nitric acid which would be the region for a separation of An(III) from Ln(III). The reduced separation factor $SF_{Cm/Am}$ compared to TODGA alone may indicate an inversed selectivity of the Pytri-diol, forming complexes more likely with Cm(III) compared to Am(III). Therefore, additional experiments were carried out using Pytri-diol in combination with DMDOHEMA. Figure 33 shows the distribution ratios of Am(III), Cm(III) and Eu(III) using Pytri-diol in combination with DMDOHEMA as a function of the initial nitric acid concentration.

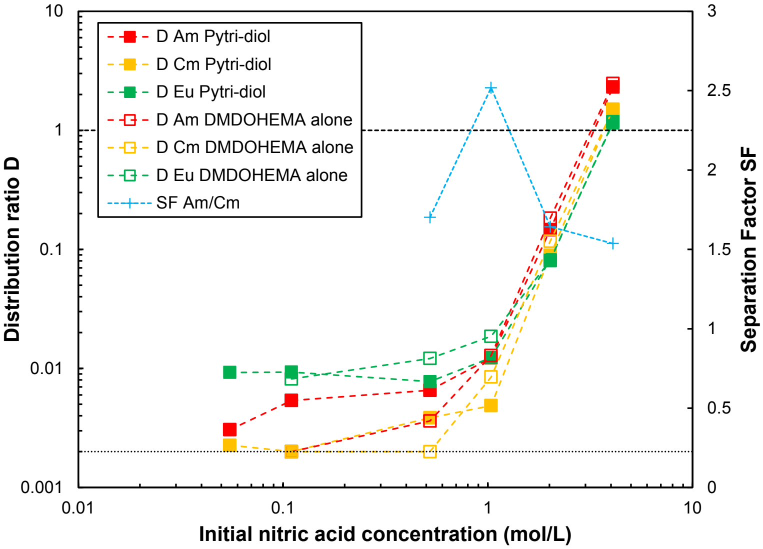

Figure 33: Distribution ratios of Am(III), Cm(III), and Eu(III) as a function of the initial nitric acid concentration. Org: 0.2 mol/L DMDOHEMA in TPH; aq: 10 mmol/L Pytri-diol in different nitric acid concentrations. 30 min of contact time at 22 °C, 5 min of centrifugation.

From Figure 33 it is visible that the distribution ratios of An(III) and Eu(III) are low compared to the application with TODGA. There is a steep increase of the distribution ratios for acidities > 1 mol/L nitric acid. The separation factor $SF_{Am/Cm}$ is in the range of the separation factor expected for DMDOHEMA alone ($SF_{Am/Cm} = 1.7$) except for the data at 1 mol/L nitric acid. The selectivity of Pytri-diol for An(III) over Eu(III) cannot be obtained with DMDOHEMA in the organic phase.

5.2.4. H_4TPAEN

The hydrophilic ligand H_4TPAEN was developed for a medical application with Ln(III) ions in NMR spectrometry.[123] H_4TPAEN (cf. Figure 29) as an EDTA analogue consists of an ethylenediamine-bridge were each amino-function is connected to two pyridinyl-carboxylic acid groups by a methylene-linker. Its selectivity for actinides was first discovered at CEA Marcoule, France.[124] To analyze the suitability of H_4TPAEN for a selective Am(III) separation a screening in combination with a TODGA based organic phase was carried out.

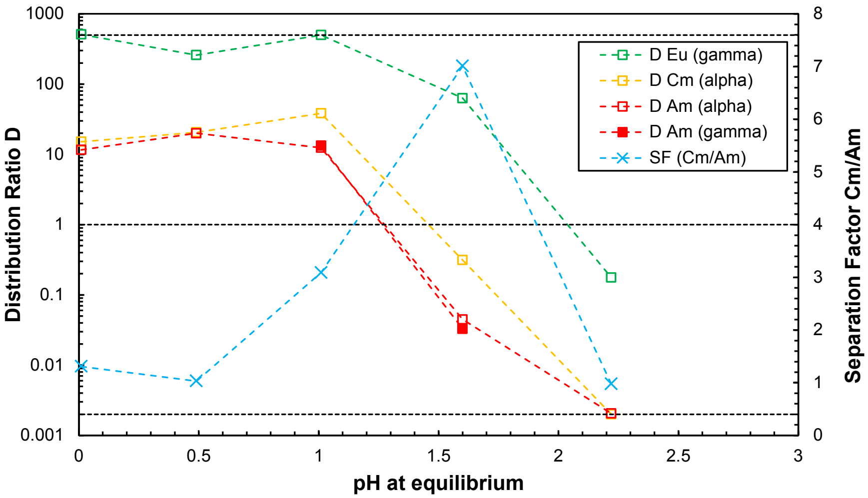

Figure 34: Distribution ratios of Am(III), Cm(III), and Eu(III) as a function of the equilibrium pH. Org: 0.2 mol/L TODGA in TPH +5 vol.-% 1-octanol; aq: 10 mmol/L H_4TPAEN and 3.0 mol/L $NaNO_3$ in different nitric acid concentrations. 30 min of contact time at 22 °C, 5 min of centrifugation.

Figure 34 shows the distribution ratios of Am(III), Cm(III), and Eu(III) using TODGA in the organic and H_4TPAEN in the aqueous phase as a function of the equilibrium pH. It has to be kept in mind that there are 3 mol/L $NaNO_3$ present representing a similar ionic strength compared to 3 mol/L nitric acid. TPAEN shows a very high selectivity for Am(III) over Cm(III) of up to $SF_{Cm/Am} = 7$. However, it has to be mentioned that the alpha spectrometric measurements performed for Am(III) and Cm(III) are very prone to self-absorption in the sample which is highly probable with the high concentration of sodium nitrate. A comparison of the Am(III) distribution ratios measured by gamma and alpha spectrometry showed that only the points at pH 1 and pH 1.5 are fully reliable for Am(III). A comparison for Cm is not possible due to the missing gamma emission of ^{244}Cm. H_4TPAEN is an efficient hydrophilic Am(III) complexing agent. It has to be further analyzed related to the determination of a reliable separation factor and the necessity to apply $NaNO_3$ in the aqueous phase.

5.2.5. Promising ligand-complexant combinations for a selective separation of Am(III)

Three hydrophilic complexing agents were tested for their selectivity regarding either Cm(III) or Am(III) in combination with different lipophilic ligands. Two of the analyzed combinations show a significant selectivity for Am(III) over Cm(III). Figure 35 shows an overview of the most promising combinations of lipophilic ligand and hydrophilic complexant tested during the screening. The selectivity for Am(III) in the aqueous phase enforces a previous co-extraction of at least Am(III) and Cm(III) together into the organic phase. The organic ligands with a selectivity for Cm(III) over Am(III) are the DGA based ligands TODGA and Me-TODGA. TS-BTPhen reaches separation factors of $SF_{(Cm/Am)} = 3.6$ using TODGA in the organic phase. A selective back-extraction would be possible between 0.4 and 0.7 mol/L nitric acid which is sufficient for a TODGA based separation process (e.g. i-SANEX process, chapter 5.1). H_4TPAEN shows a very high selectivity for Am(III) in the aqueous phase and a possible application in combination with TODGA. The major drawbacks of H_4TPAEN are the high sodium nitrate concentrations in the aqueous phase and the low acidity for a selective stripping. The $SF_{Cm/Am} = 7$ at pH 1.5 was rated as not reliable due to alpha self-absorption.

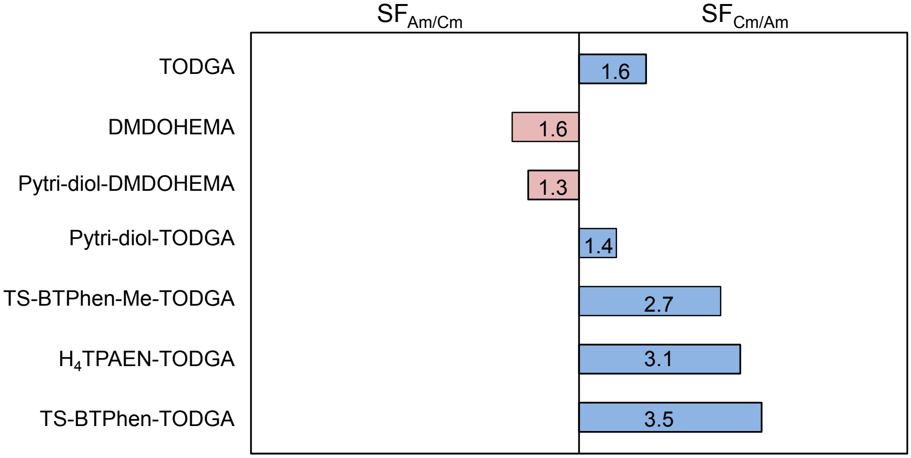

Figure 35: Overview of the separation factors achieved with the ligand/complexant combinations analyzed.

The combination of TS-BTPhen as well as H_4TPAEN with TODGA shows promising results for the development of an Am(III) selective single cycle process. Both combinations will be analyzed in detail with respect to process relevant properties and complexation mechanism.

5.3. TS-BTPhen as Am(III) selective complexant

The novel hydrophilic back-extraction agent TS-BTPhen was tested for its selectivity towards Am(III) over Cm(III) and the fission and corrosion products with a TODGA-based solvent.[110] Different batches of TS-BTPhen have been synthesized at the University of Reading, UK. Table 9 shows a comparison of the properties of the received batches of TS-BTPhen. The solubility of was tested using 0.1 mol/L nitric acid.

Table 9: Comparison of the visual properties of the different TS-BTPhen batches.

Batch no.	Date of synthesis	color	form	Additional information
Batch 1	2013	Yellow	Powder	Fully soluble
Batch 2	June 2014	Green	Powder	Fully soluble
Batch 3	July 2014	Green	Powder	Insoluble particles included

Table 10 shows the distribution ratios of Am(III), Cm(III) and Eu(III) for the different batches received for solvent extraction tests. Figure 36 shows a comparison of the different TS-BTPhen batches in nitric acid solution. It is visible that batch one has a clear yellow color while the batches 2 and three have a green color.

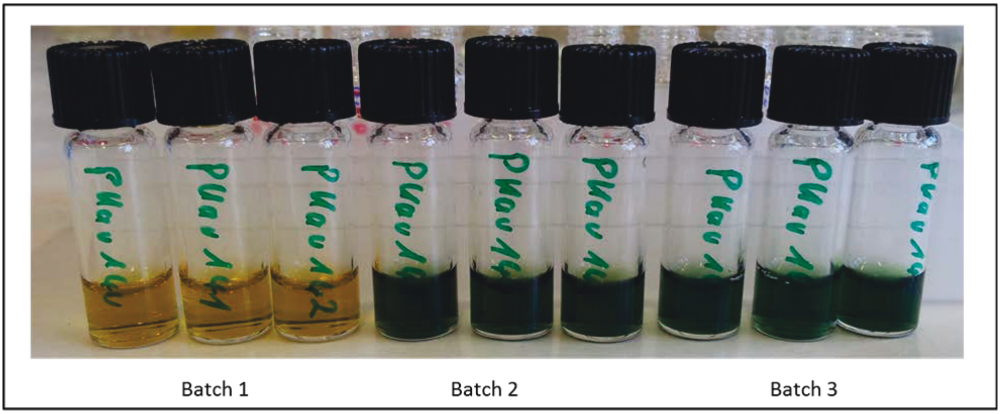

Figure 36: 10 mmol/L of the different TS-BTPhen batches diluted in nitric acid solution.

Table 10: Distribution ratios of Am(III), Cm(III) and Eu(III) at 0.5 mol/L initial nitric acid concentration. Org: 0.2 mol/L TODGA in TPH + 5 vol.-% 1-octanol; aq: 10 mmol/L TS-BTPhen in 0.5 mol/L nitric acid.

Batch no.	$\mathbf{D_{Am}}$	$\mathbf{D_{Cm}}$	$\mathbf{D_{Eu}}$	$\mathbf{SF_{Cm/Am}}$
Batch 1	0.12	0.28	56.1	2.45
Batch 2	0.06	0.25	34.7	4.0
Batch 3	0.15	0.46	37.5	3.0

Batch 1 was used for studies regarding nitric acid concentration, complexation mechanisms and stoichiometry. Batch 2 was used to study the influence of the TODGA concentration. Batch 3 was not used for further studies.

5.3.1. Influence of the nitric acid concentration

Batch extraction experiments were carried out to analyze the influence of the nitric acid concentration on the extraction of Am(III), Cm(III) and Eu(III), using a 10 mmol/L solution of TS-BTPhen in different nitric acid concentrations spiked with ^{152}Eu(III), ^{241}Am(III), and ^{244}Cm(III). TS-BTPhen of Batch 1 was used for these experiments. The results are shown in Figure 37. Open symbols represent the distribution ratios of americium, curium and europium using TODGA + 5 vol.-% 1-octanol without the addition of TS-BTPhen to the aqueous phase. The distribution ratios of Am(III), Cm(III) and Eu(III) increase with increasing nitric acid concentrations which is known to be the classical behavior of neutral extractants such as TODGA.[35] The influence of TS-BTPhen addition to the aqueous phase is shown by the filled symbols. The addition of the hydrophilic ligand decreased the distribution ratios of An(III) by approx. three orders of magnitude, while the Eu(III) distribution ratios were only decreased by one order of magnitude, resulting in a high Eu over Am separation factor of $SF_{Eu/Am}$ = 300 at 0.65 mol/L nitric acid. However, lanthanides lighter than Eu may have a significantly lower separation factor $SF_{Ln/Am}$.[33] The distribution ratios of Am(III) were affected slightly more than those of Cm(III). The separation factor for Cm(III) over Am(III) therefore increased from $SF_{Cm/Am}$ = 1.6 for a TODGA-nitric acid system to $SF_{Cm/Am}$ = 2.4 to 4.5 using TS-BTPhen in the nitric acid concentration range covered by Figure 37 (0.01 – 1 mol/L). The separation factors for Eu(III) over Am(III) using TS-BTPhen ($SF_{Eu/Am}$ = 70-1000) in the aqueous phase are similar to the $SF_{Eu/Am}$ values reached using SO_3-Ph-BTP (250-1000)[62], and are in agreement with the separation factors previously reported for TS-BTPhen.[110] A high nitric acid concentration in the stripping step is favorable, as it simplifies scrubbing and gives robustness to the system. The region of interest for Am(III) selective separation using 10 mmol/L TS-BTPhen is around 0.65 mol/L initial nitric acid concentration, providing separation factors of $SF_{Eu/Am} \approx 300$ and $SF_{Cm/Am} = 3.6$. The distribution ratios of Am(III), Cm(III), and Eu(III) all show a linear increase with increasing TODGA concentration in the log(D) vs. log([TODGA]) plot.

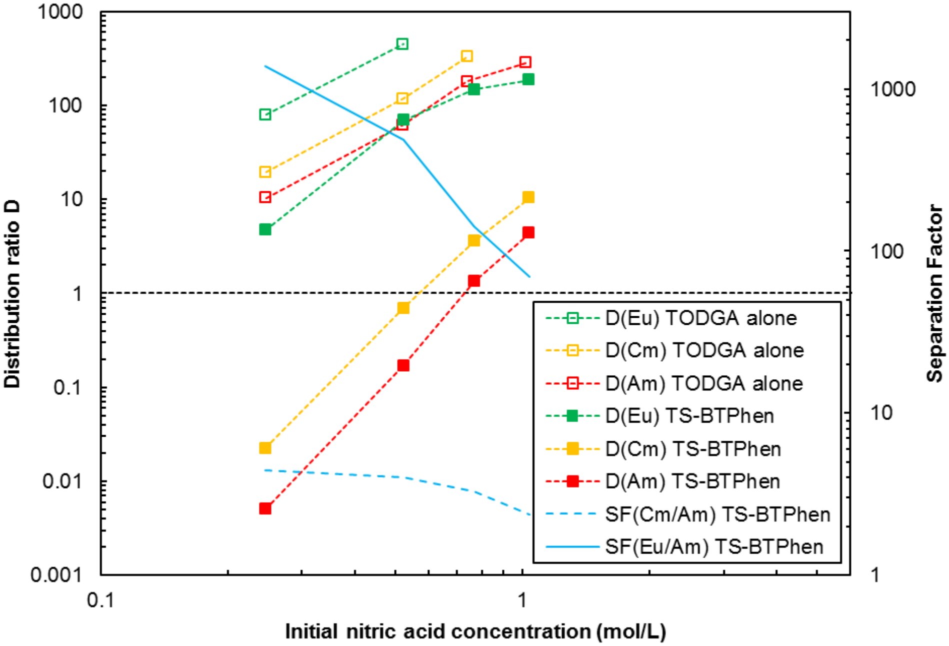

Figure 37: Distribution ratios of Eu(III), Am(III) and Cm(III) and separation factors of Eu(III) and Cm(III) over Am(III) as a function of the initial nitric acid concentration in the radiotracer experiments. Organic phase: 0.2 mol/L TODGA in TPH + 5 vol.-% 1-octanol; aqueous phase: filled symbols: 10 mmol/L TS-BTPhen in nitric acid, open symbols: no addition of TS-BTPhen.

5.3.2. Behavior of the lanthanides

Not only the mutual separation between the trivalent actinides Am(III) and Cm(III) play an important role for a selective back extraction of Am(III) from a loaded organic phase, but also the separation from co-extracted lanthanides. Distribution ratios of Ln(III) are known to be high for TODGA-based organic phases at relevant nitric acid concentrations.[94] Within the lanthanide group, the distribution ratios increase with decreasing ionic radius of the lanthanide.[39] Figure 38 shows the comparison of the distribution ratios of Ln(III) and An(III) using TODGA in combination with nitric acid (Figure 37 A) and TODGA in combination with nitric acid containing 10 mmol/L TS-BTPhen (Figure 37 B). Without using the hydrophilic complexing agent, the distribution ratios of Am(III) and Cm(III) are located between neodymium and samarium within the lanthanide group. The actinides are selectively removed from all of the lanthanides by using TS-BTPhen in nitric acid solution. The separation factor between the least extracted lanthanide La(III) and Am(III) is $SF_{La/Am} \approx 20$ at 0.25 mol/L nitric acid. The selectivity for stripping of An(III) from Ln(III) is lower compared to SO_3-Ph-BTP used for the An(III) stripping in the innovative-SANEX test ($SF_{La/An} \approx 50$), but the $SF_{Cm/Am}$ is significantly higher.[62] The initial concentration of the Ln(III) in the aqueous phase was 10^{-5} mol/L each lanthanide. TS-BTPhen of Batch 1 was used for this experiment.

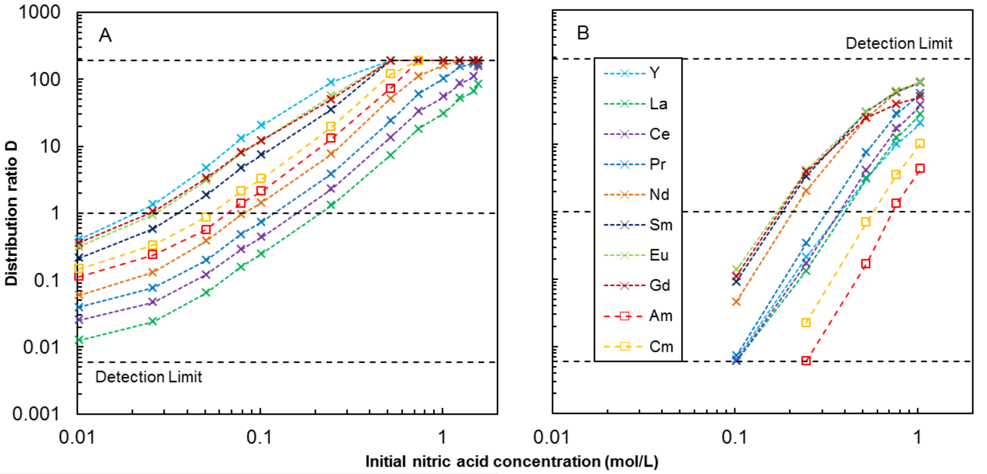

Figure 38: Distribution ratios of Ln(III), Am(III) and Cm(III) with and without TS-BTPhen in the aqueous phase. Left side (A) without addition of TS-BTPhen, right side (B) with 10 mmol/L TS-BTPhen. Organic phase: 0.2 mol/L TODGA in TPH + 5 vol.-% 1-octanol. Aqueous phase: A: 10^{-5} mol/L Ln(III) in nitric acid without addition of TS-BTPhen; B: 10^{-5} mol/L Ln(III) and 10 mmol/L TS-BTPhen in nitric acid; 30 minutes phase contact at 22 °C.

5.3.3. Effect of the TS-BTPhen-concentration

The influence of the TS-BTPhen concentration on the Am(III), Cm(III) and Eu(III) distribution ratios was tested in the range from 1 to 50 mmol/L. Figure 39 shows the distribution ratios as a function of the TS-BTPhen concentration on a logarithmic scale at constant nitric acid and TODGA concentrations. A slope of -0.8 was observed in the solvent extraction experiment for the linear regression of the Am(III) and Cm(III) data with increasing TS-BTPhen concentration. The Eu(III) data did not follow a linear trend in the double-logarithmic plot. In solvent extraction studies, the structurally similar lipophilic ligand CyMe$_4$BTPhen preferentially forms 1:2 (Am(III)- CyMe$_4$BTPhen) complexes, as demonstrated by TRLFS and NMR studies.[110, 113] Therefore, a slope of -2 would also have been expected if the hydrophilic TS-BTPhen forms 1:2 complexes with An(III) in the aqueous phase. Equation 4 shows the simplified possible complexation reactions with An(III) in the TODGA/TS-BTPhen system. Similar deviations were also observed in the TODGA/SO$_3$-Ph-BTP and TODGA/SO$_3$-Ph-BTBP systems.[62-63, 98]

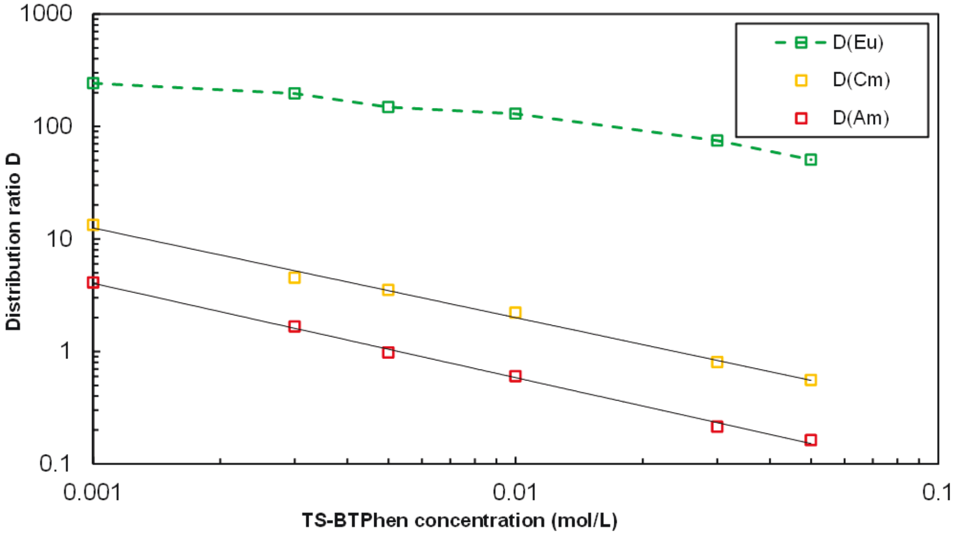

Figure 39: Distribution ratios of Am(III), Cm(III) and Eu(III) as a function of the TS-BTPhen concentration. Organic phase: 0.2 mol/L TODGA in TPH + 5 vol.-% 1-octanol. Aqueous phase: different TS-BTPhen concentrations in 0.66 mol/L nitric acid; 30 minutes of phase contact at 22 °C.

The slopes of the sulphonated hydrophilic N-donor complexant suggest a complex stoichiometry which is reduced by 1 complexant molecule compared to the complexes of their organic derivative. This is even the case for SO_3-BTP complexant, showing a slope of -2 while its lipophilic derivative is known to form 1:3 complexes. The differences between a slope of -0.8 in the slope analysis and the expected slope of -2 may be related to the formation of mixed complexes. To analyze the deviation between the slopes (n=1 or 2) of the hydrophilic BTPhen and the literature stoichiometry of the lipophilic BTPhen and to obtain comprehensive data on the complex properties, time resolved laser fluorescence (TRLFS) studies were carried out (described below).

Equation 4: Possible complexation reactions of An(III) in the biphasic TS-BTPhen-TODGA system.

$$\mathbf{An(III)_{aq} + n\ TS\text{-}BTPhen_{aq} \rightarrow [An(III)(TS\text{-}BTPhen)_n]_{aq}}$$

$$\mathbf{An(III)_{aq} + 3\ TODGA \rightarrow [An(III)(TODGA)_3]}$$

5.3.4. Influence of TODGA concentration

The ligand concentration in the organic phase and the complexant concentration in the aqueous phase play an important role for an effective stripping. Therefore, the influence of the TODGA concentration was tested, keeping the nitric acid and TS-BTPhen complexant concentrations constant. Figure 40 shows the log(D) values of Eu(III), Am(III) and Cm(III) as a function of log([TODGA]) in the organic phase. From Figure 40 it can be seen that the data for the actinides follow a nonlinear trend with decreasing slope for increasing TODGA concentrations. The formation of mixed [M(III)-TODGA-TS-BTPhen] complexes may be an explanation for the deviation from linear behavior. However, to compare the data with the literature, linear regressions were applied. The slopes of the function added to the data are similar to the slope of TODGA without TS-BTPhen in the aqueous phase (slope of An(III)= 2.7).[39] TS-BTPhen of Batch 2 was used for this experiment.

For TODGA, the metal-to-ligand stoichiometry is known to be 1:3 predicting a slope of 3. Furthermore, with a constant concentration of the complexant TS-BTPhen in the aqueous phase, the slope of $\log(D_{An(III)})$ as a function of log([TODGA]) is close to the slopes of $\log(D_{An(III)})$ as a function of the log[TODGA] of the TODGA-nitric acid system.

Plotting log(D) vs. log(free ligand concentration) is commonly used in the literature to study complex stoichiometries by slope analysis.[125] The extraction equilibria can be expressed mathematically with the extraction constant and the obtained slope gives the number of complexing ligands. As a complex mixture of lipophilic and hydrophilic complexes may form here and is yet unknown, extraction equilibria were not formulated here. First, the complexation shall be studied in more detail using spectroscopic techniques.

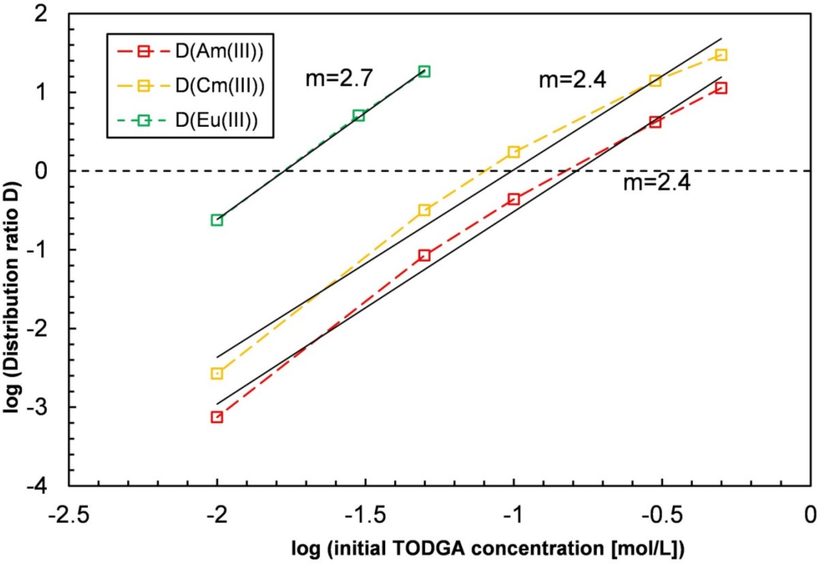

Figure 40: Logarithm of the distribution ratios of Am(III) and Cm(III) as a function of the logarithm of the initial TODGA concentration. Organic phase: 0.01 to 0.5 mol/L TODGA in TPH + 5 vol.-% 1-octanol; aqueous phase: 10 mmol/L TS-BTPhen in 0.7 mol/L nitric acid; Forward extraction experiment.

5.3.5. Batch kinetics

Batch test tube shaking experiments were carried out as back-extraction experiments from a loaded organic phase with varying mixing times. The loaded organic phase was prepared in advance by extraction of Am, Cm and Eu tracer from 0.6 mol/L nitric acid. Figure 41 shows that the back extraction kinetics is fast. The equilibrium D values and separation factors of Am(III), Cm(III) and Eu(III) were achieved within only one minute using a fast shaking device (described in the methods chapter). The equilibrium distribution ratios and separation factor in the batch kinetics experiment were $D_{Am,eq}$=0.26, $D_{Cm,eq}$=0.87, $SF_{Cm/Am,eq}$= 3.3 which is in good agreement with the data from the equilibrium batch extraction experiments.

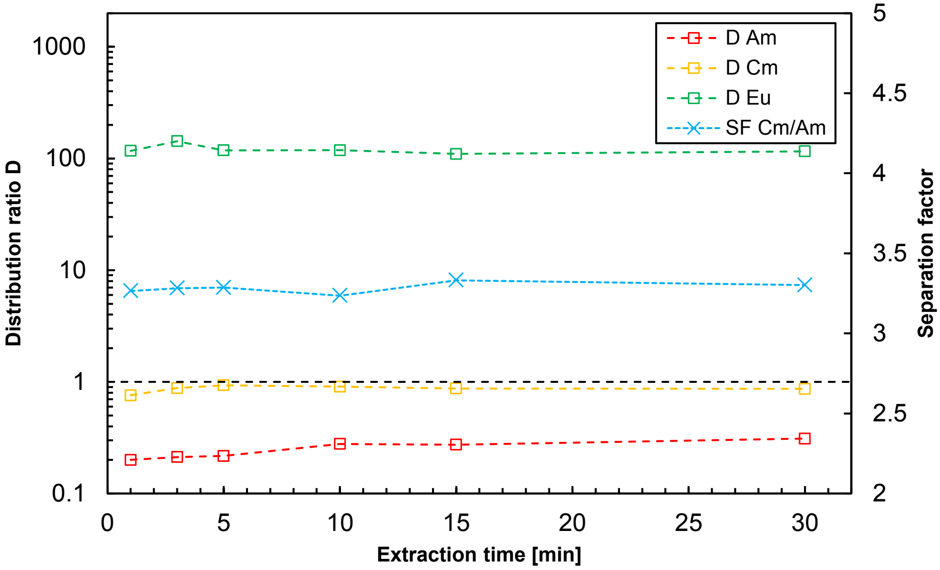

Figure 41: Batch stripping kinetic experiment. Org: 0.2 mol/L TODGA in TPH + 5 vol.-% 1-octanol loaded with tracers of Am(III), Cm(III) and Eu(III) at 0.6 mol/L nitric acid.; Stripping aq: 10 mmol/L TS-BTPhen in 0.6 mol/L nitric acid; diff. time of phase contact at 22°C; 3 min of centrifugation.

5.3.6. Time resolves laser spectrometry with TS-BTPhen

Time resolved laser fluorescence spectrometric studies of TS-BTPhen with curium and europium were conducted to analyze the complexation of TS-BTPhen with trivalent actinides and lanthanides and to gain comprehensive data on the complex stoichiometry of the TS-BTPhen complexes. The experiments were carried out in aqueous perchloric acid at pH3 and and in aqueous nitric acid at 0.5 mol/L.

5.3.6.1. Cm(III) TRLFS -studies of TS-BTPhen complexes

Complexometric titrations were carried out by adding TS-BTPhen to a 10^{-7} mol/L Cm(III) solution in 10^{-3} mol/L $HClO_4$ as well as in 0.5 mol/L HNO_3. As ClO_4^- is a very weakly coordinating anion, 10^{-3} mol/L $HClO_4$ was used as an idealized system with little influence of ionic strength, concurring anions or protonation of TS-BTPhen. For more realistic conditions in contrast, biphasic extraction experiments were performed with the aqueous phase consisting of nitric acid (0.01 - 1.5 mol/L). Therefore, 0.5 mol/L nitric acid was also used as medium in monophasic investigations to study the complexation of Cm(III) with TS-BTPhen under extraction conditions. Figure 42 shows the Cm(III) fluorescence emission spectra of the $^6D'_{7/2} \rightarrow {}^8S'_{7/2}$ transition as a function of the TS-BTPhen concentration in 10^{-3} mol/L $HClO_4$.

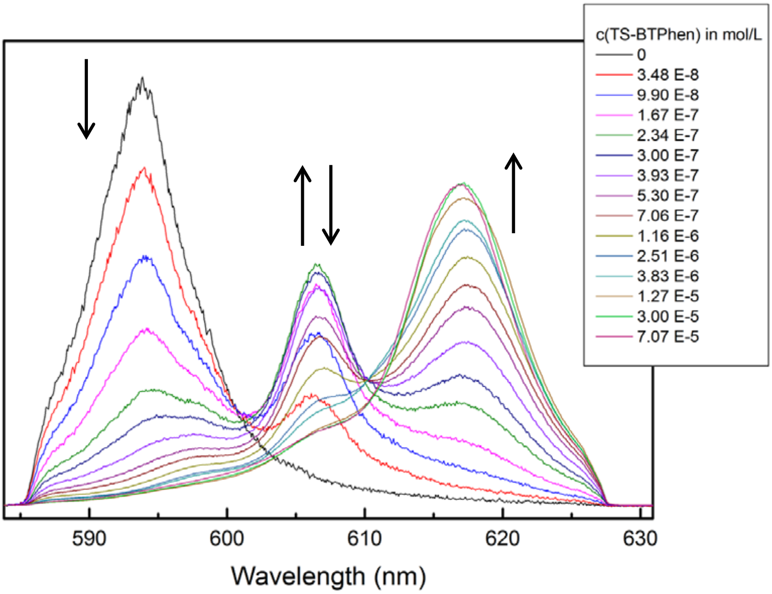

Figure 42: Normalized fluorescence spectra of Cm(III) at increasing TS-BTPhen concentration (0 – 7.07 x 10^{-5} mol/L) in 10^{-3} mol/L $HClO_4$ ([Cm(III)] = 1 x 10^{-7} mol/L)

The fluorescence spectra in Figure 42 show three emission bands, the Cm(III) aquo ion (Cm(III) solvent species) at 593.9 nm and the emission bands of two complex species at 606.5 nm and 617.0 nm. The observed bathochromic shifts of the emission bands of the complex species are characteristic of the formation of a 1:1 and a 1:2 complex with a strong tetradentate N-donor ligand like TS-BTPhen.[113, 126-127] Peak de-convolution was carried out, providing the spectra of the pure components shown in Figure 43. The spectra of both complex species exhibit a hot band caused by population of a higher energy level by thermal effects. The hot bands are visible as shoulders at higher energy at 597 nm and 607 nm, respectively.[128]

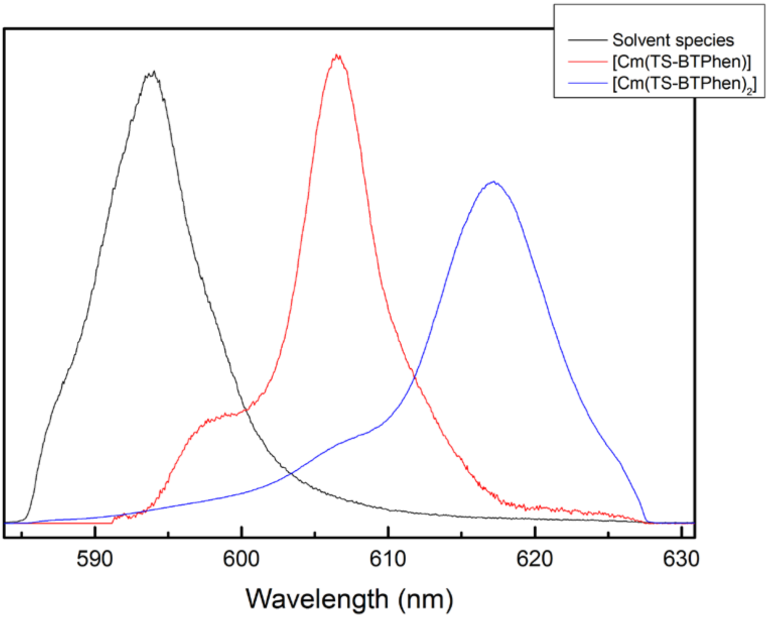

Figure 43: Normalized fluorescence spectra of the [Cm(TS-BTPhen)n] complexes in 10^{-3} mol/L $HClO_4$ (n= 0, 1, 2).

The relative distribution of the different Cm(III) species after each titration step was obtained by peak de-convolution of the fluorescence spectra using the emission bands of the individual species (cf. Figure 43). As the fluorescence intensity increases strongly upon complexation as a result of intramolecular energy transfer processes,[129] fluorescence intensity factors (FI) of the Cm-TS-BTPhen complexes have to be considered when calculating the concentrations of the formed Cm(III) species from the peak areas obtained by peak de-convolution. The FI factors were determined by fitting the increase of the Cm(III) fluorescence intensity as a function of TS-BTPhen concentration (FI[Cm(TS-BTPhen)] = 5, FI[Cm(TS-BTPhen)$_2$] = 560). The species distribution as a function of the TS-BTPhen concentration is shown in Figure 44.

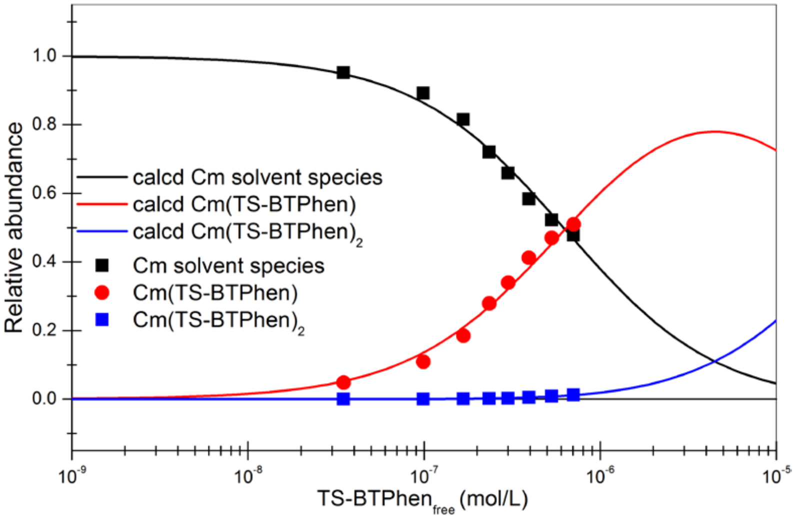

Figure 44: Species distribution of Cm(III) as a function of the TS-BTPhen concentration in 10^{-3} mol/L $HClO_4$. Symbols represent experimental data, lines are calculated with $\log\beta_{01} = 6.2$ and $\log\beta_{02} = 10.7$.

The complexation of Cm(III) started at a TS-BTPhen concentration of 3.48×10^{-8} mol/L with a maximum fraction of species 1 ([Cm(TS-BTPhen)]) of 78 % at 4.48×10^{-6} mol/L TS-BTPhen. At concentrations above 3.45×10^{-5} mol/L complex species 2 ([Cm(TS-BTPhen)$_2$]) was the major species in solution.

A plot of the concentration ratios of the different species vs. the free ligand concentration in double logarithmic scale and subsequent linear regression yields slopes of 1.1 for the stepwise formation of the 1:1 and 1:2 complexes. The slopes depict the stoichiometric factor of TS-BTPhen added to the Cm(III) during transition from one species to another species. The overall transition from Cm(III) solvent species to the final complex yields a slope of 2.2, depicting a final 1:2 Cm(III) to TS-BTPhen complex ([Cm(TS-BTPhen)$_2$]). Therefore, the species with emission bands at 606.5 nm and 617.0 nm were identified as 1:1 and 1:2 complexes, respectively (Figure 45). Furthermore, conditional stability constants were derived from the speciation yielding $\log\beta_{01} = 6.2$ for the 1:1 complex and $\log\beta_{02} = 10.7$ for the 1:2 complex.

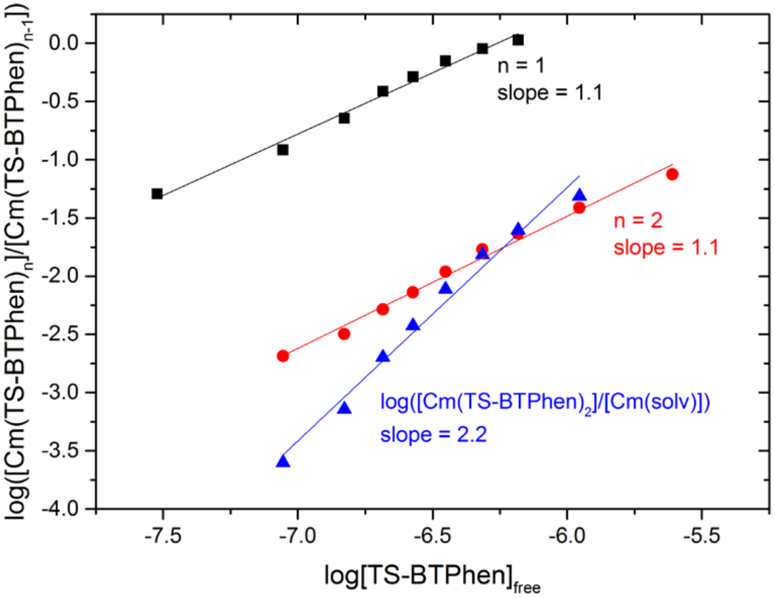

Figure 45: Linear regression of the logarithm of the species ratios of the solvent species and the two complex species observed in titration experiments in 10^{-3} mol/L $HClO_4$ vs. the logarithm of the free TS-BTPhen concentration.

The determination of the number of water molecules in the inner coordination shell by measurement of the fluorescence lifetime of the two complex species was not possible, due to the fluorescence quenching properties of TS-BTPhen. Further experiments were performed in 0.5 mol/L HNO_3 to study the complexation of Cm(III) under extraction conditions. Figure 46 shows the normalized fluorescence emission spectra of Cm(III) with increasing TS-BTPhen concentration in 0.5 mol/L nitric acid. The Cm(III) solvent species displays two emission maxima at 595 nm and 597 nm. These emission bands correspond to the formation of a mixture of Cm(III) aquo ion and Cm(III) mononitrato complex and are in excellent agreement with the literature.[130] An additional species at 618.8 nm was observed at higher TS-BTPhen concentrations with a similar bathochromic shift as the [Cm(TS-BTPhen)$_2$] complex observed in 10^{-3} mol/L $HClO_4$. The peak intensity of an additional 1:1 species at 606 nm was very low in nitric acid.

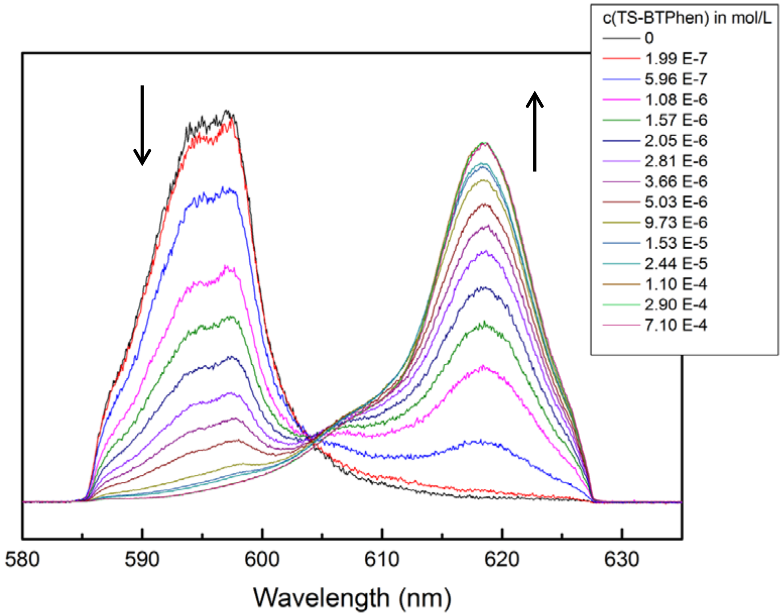

Figure 46: Normalized fluorescence spectra of Cm(III) at increasing TS-BTPhen concentration (0 – 7.10 × 10^{-4} mol/L) in 0.5 mol/L HNO_3 ([Cm(III)] = 1 x 10^{-7} mol/L)

The pure component spectra of the Cm(III) solvent species and the [Cm(TS-BTPhen)$_2$] complex were obtained from the titration experiment. In addition, the spectrum of the [Cm(TS-BTPhen)] complex derived in 10^{-3} mol/L $HClO_4$ was used for peak deconvolution. Considering the fluorescence intensity factors (FI[Cm(TS-BTPhen)] = 5, FI[Cm(TS-BTPhen)$_2$] = 620), the species distribution as a function of the free TS-BTPhen concentration was derived (Figure 47).

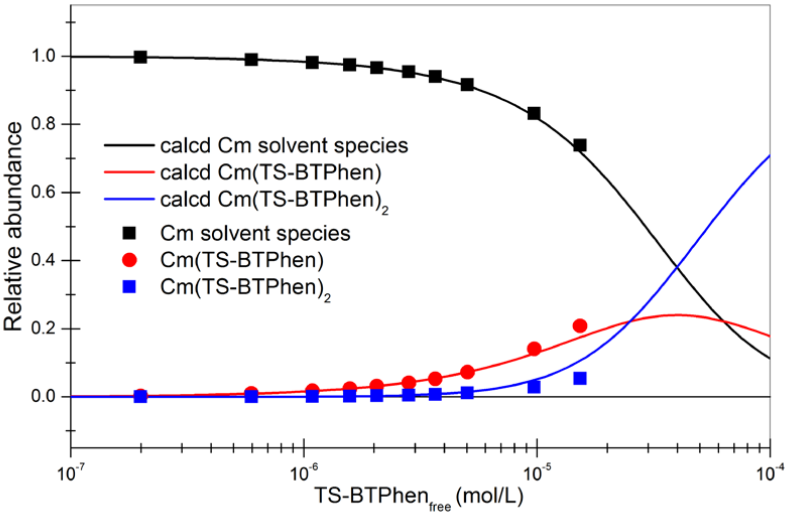

Figure 47: Species distribution of Cm(III) as a function of the TS-BTPhen concentration in 0.5 mol/L nitric acid. Symbols represent experimental data, lines are calculated with logβ_{01} = 4.2 and logβ_{02} = 8.8.

The complexation of Cm(III) with TS-BTPhen starts at 2×10^{-7} mol/L TS-BTPhen and exhibits a maximum of species 1 ([Cm(TS-BTPhen)]) of 24% at 4.05×10^{-5} mol/L. At concentrations above 4.1×10^{-5} mol/L species 2 ([Cm(TS-BTPhen)]) is the major species present in the system. The relatively low amount of species 3 in the speciation diagram in comparison to the normalized fluorescence spectra in Figure 46 can be explained by the high fluorescence intensity factor of species 3 resulting in low amounts of substance even for very high fluorescence signals.

The slope analyses calculated from the species distribution are given in Figure 48. A slope of 1.0 for species 1/solvent, 0.8 for species 2/species 1 depict the addition of 1 TS-BTPhen molecule for each complexation step. A slope of 1.8 for species 2/solvent depicts an overall complexation stoichiometry from the solvated curium ion to the 1:2 complex. The results confirm the assignment of the observed emission bands. The results show that a 1:1 complex is formed under extraction conditions as an intermediate minor species whereas the 1:2 complex predominates at high ligand concentrations. The conditional stability constants were calculated to be logβ_{01} = 4.2 for the 1:1 complex and logβ_{02} = 8.8 for the 1:2 complex. A summary of the obtained conditional stability constants in different media is given in Table 11.

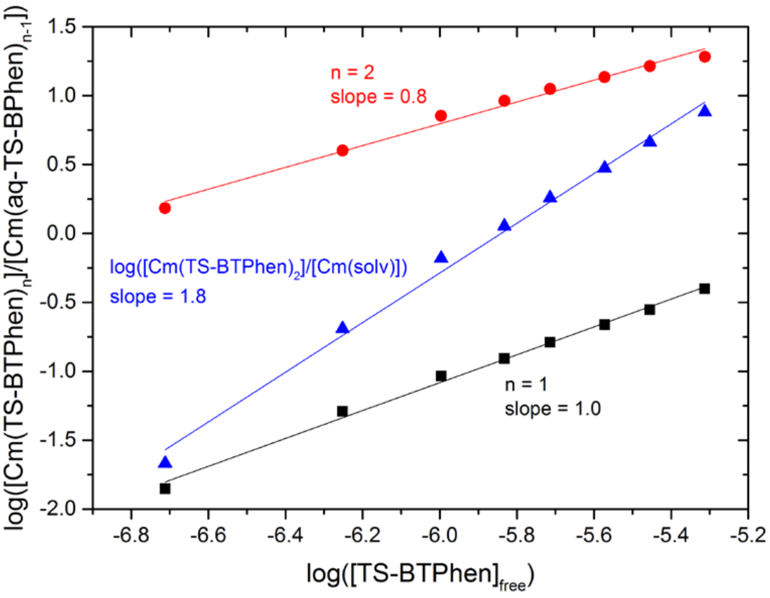

Figure 48: Linear regression of the logarithm of the peak ratios of the solvent species and the two complex species observed in the titration experiments in 0.5 mol/L HNO_3 vs. the logarithm of the free ligand concentration.

The minor amounts of the 1:1 complex obtained in HNO_3 compared to the titration experiment performed in 10^{-3} mol/L $HClO_4$ is explained by the effects of the applied medium. As already observed by Wagner *et al.*[127], the increase of ionic strength destabilizes the mono anionic $[Cm(TS\text{-}BTPhen)]^-$ complex relative to the penta anionic $[Cm(TS\text{-}BTPhen)_2]^{5-}$ complex due to the increased charge density. Furthermore, the decrease of $\log\beta_{02}$ resulting from the change of the medium from 10^{-3} mol/L $HClO_4$ to 0.5 mol/L HNO_3 (10.7 → 8.8) is explained by two different factors: a change of the activity of TS-BTPhen and Cm(III) due to the increased ionic strength, and the competing reaction between protonated TS-BTPhen ligands and nitrate ions caused by the protonation of the N-atoms of TS-BTPhen. These effects result in a decreased activity of the free TS-BTPhen. Previous studies have shown the protonation of the free ligand to be the major contribution to the decrease of the conditional stability constants.[127]

Table 11 shows the conditional stability constants of TS-BTPhen in comparison to the stability constants of the SO_3-Ph-BTBP complexant used in the AmSel process.[63] Both complexants form an intermediate 1:1 Cm(III) to complexant and a final 1:2 Cm(III) to complexant complex.

TS-BTPhen shows a slightly stronger complexation with Cm(III) compared to SO_3-Ph-BTBP of the final 1:2 Cm(III) to complexant complex in both diluents. This effect was also observed for lipophilic BTBP and BTPhen ligands[113] and is attributed to the greater degree of preorganization of the BTPhen ligand. The formation of the 1:1 Cm(III) to TS- BTPhen complex is stronger in the $HClO_4$ system which can be explained by a concurrency of the $[Cm(III)(NO_3)_x]$ complexes in nitric acid. Furthermore, the change of the solvent from 10^{-3} mol/L $HClO_4$ to 0.5 mol/L HNO_3 has a smaller effect on the final stability constant of the TS-BTPhen complex compared to that of SO_3-Ph-BTBP.

Table 11: Conditional stability constants of $[Cm(TS\text{-}BTPhen)_n]$ (n = 1,2) and $[Cm(SO_3\text{-}Ph\text{-}BTBP)_n]$ (n = 1,2) complexes in 10^{-3} mol/L $HClO_4$ and 0.5 mol/L HNO_3.[20]

Solvent	$\log\beta_{01}$	$\log K_{12}$	$\log\beta_{02}$
TS-BTPhen 10^{-3} mol/L $HClO_4$	6.2	4.5	10.7
TS-BTPhen 0.5 mol/L HNO_3	4.2	4.6	8.8
SO_3-Ph-BTBP 10^{-3} mol/L $HClO_4$	5.3	5.1	10.4
SO_3-Ph-BTBP 0.5 mol/L HNO_3	-	-	7.3

5.3.6.2. Biphasic Cm(III) TRLFS -Experiments

To analyze the complexes formed during the solvent extraction experiments, a two phase TRLFS experiment was performed. An aqueous phase containing Cm(III) and TS-BTPhen dissolved in 0.13 mol/L nitric acid was contacted with an organic phase containing TODGA in Exxsol D80 (a diluent very similar to TPH) + 5 vol.-% 1-octanol. After extraction, the phases were analyzed using TRLFS.

Figure 49 shows the spectra of the organic (left) and aqueous phases (right). The spectra of $[Cm(TS\text{-}BTPhen)_2]$ and $[Cm(TODGA)_3](NO_3)_3$ [39] were added for comparison.

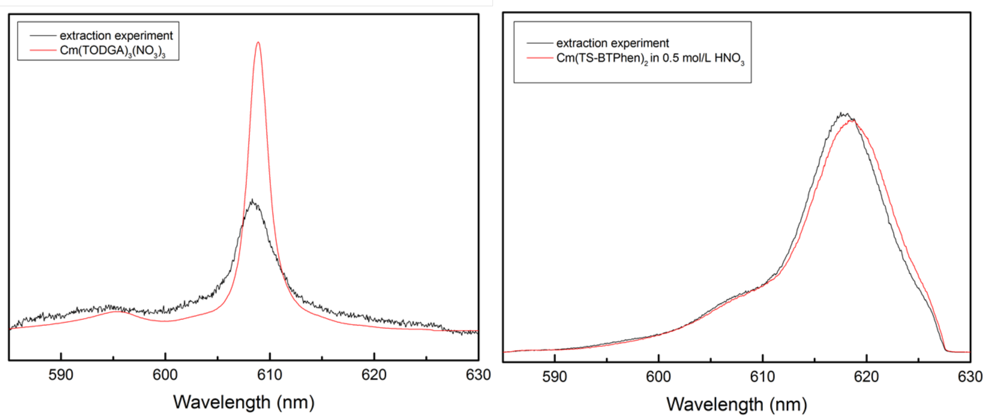

Figure 49: TRLFS-Spectra of the organic phase (left) and the aqueous phase (right) of a solvent extraction experiment. Organic phase: 0.2 mol/L TODGA in Exxsol D80 + 5 vol.-% 1-octanol; aqueous phase: 10^{-7} mol/L Cm(III), 1 mmol/L TS-BTPhen in 0.13 mol/L nitric acid. 30 minutes of extraction at RT, 5 minutes of centrifugation. For comparison, spectra of the [Cm(TODGA)$_3$](NO$_3$)$_3$ and [Cm(TS-BTPhen)$_2$] complexes from single phase experiments are added in red.

Figure 49 confirms the formation of a 1:2 Cm(III) TS-BTPhen complex in the aqueous phase of the extraction experiment. Furthermore, a comparison with the [Cm(TODGA)$_3$(NO$_3$)$_3$] spectrum shows the exclusive formation of [Cm(TODGA)$_3$(NO$_3$)$_3$] in the organic phase. The formation of mixed [Cm(TS-BTPhen)$_n$] complexes in the organic phase could not be observed within the sensitivity of the TRLFS measurement. However, due to the low Cm(III) distribution ratios under these experimental conditions, the concentration of Cm(III) in the organic phase was low leading to a broadened peak with a low signal to noise ratio.

5.3.6.3. Eu(III) TRLFS-studies with TS-BTPhen

As the fluorescence of an atom or ion is generated by the de-excitation of electrons, the fluorescence intensity and wavelength is strongly depending on the state of the electronic shell. A deviation in the electronic properties of the atom or ion results in a change of the fluorescence emission wavelength and intensity. The electronic properties of Eu(III) allow for several de-excitation transfers which are different in wavelength and probability resulting in different emission bands. Due to their different properties, the individual fluorescence emission bands of Eu(III) show an increased sensitivity towards different properties of the complex, e.g. symmetry ($^5D_0$ to $^7F_0$) or changes of the ligand field ($^5D_0$ to $^7F_4$). Additional complexometric titrations were carried out adding defined amounts TS-BTPhen to a 5x10^{-6} mol/L Eu(III) solution in HNO_3 and $HClO_4$, respectively. In the following studies, the $^5D_0$ to $^7F_4$ or a combination of $^5D_0$ to $^7F_1$ and $^7F_2$ transitions were used to analyse the Eu(III) spectra. Figure 50 shows the $^5D_0$ to $^7F_4$ emission spectra of the titration of an Eu(III)- solution with increasing TS-BTPhen concentration in a perchloric acid solution at pH 3. The consecutive formation of two new species was observed during the titration.

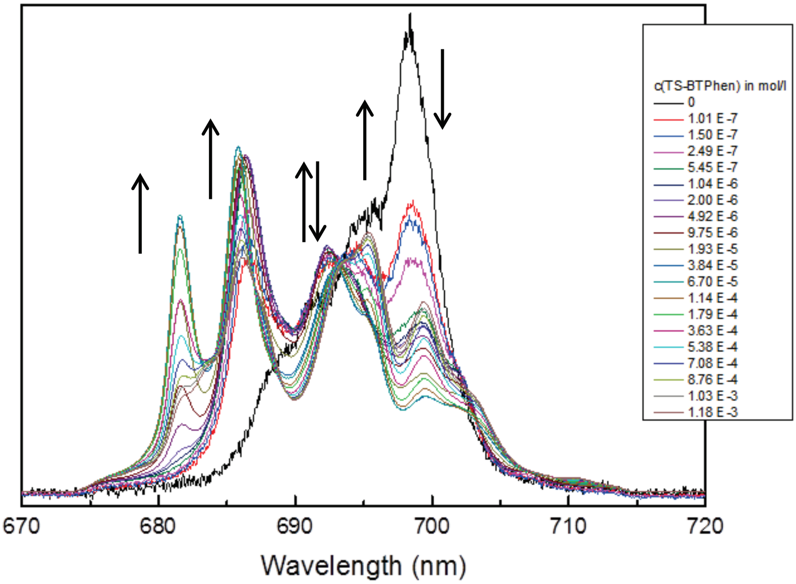

Figure 50: Normalized Eu $^5D_0$ to $^7F_4$ fluorescence emission spectra for the titration of a 10^{-5} mol/L Eu(III) solution with TS-BTPhen in pH 3 $HClO_4$.

Starting from the solvent species, five additional maxima were observed during the titration being related to the formation of new species in combination with symmetry and hot band effects. The spectra of the individual species used for peak de-convolution are given in Figure 51.

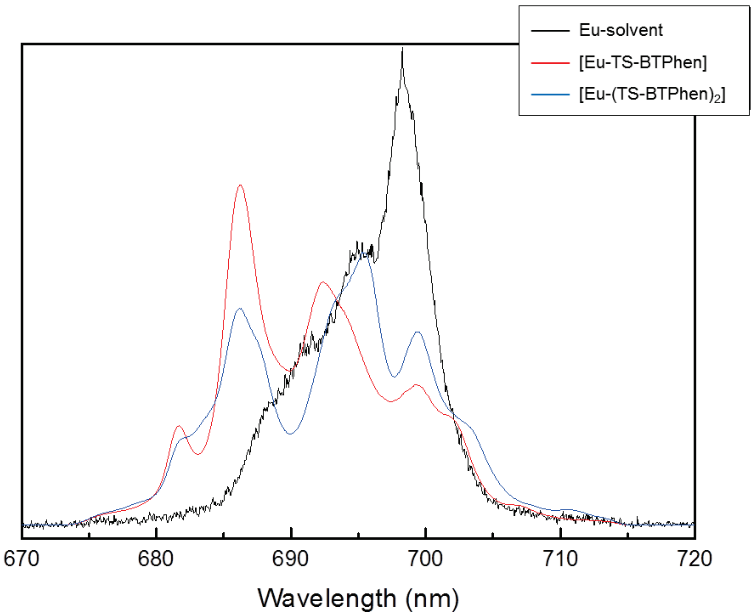

Figure 51: Normalized fluorescence spectra of the [Eu(TS-BTPhen)n] complexes in 10^{-3} mol/L $HClO_4$ (n= 0, 1, 2).

A peak de-convolution of the individual spectra of the titration experiment was carried out also considering the FI factors of the individual species ($FI_{[EuTS\text{-}BTPhen]}=80$; $FI_{[Eu(TS\text{-}BTPhen)2]}=2000$). The resulting speciation diagram of Eu(III) with TS-BTPhen is given in Figure 52.

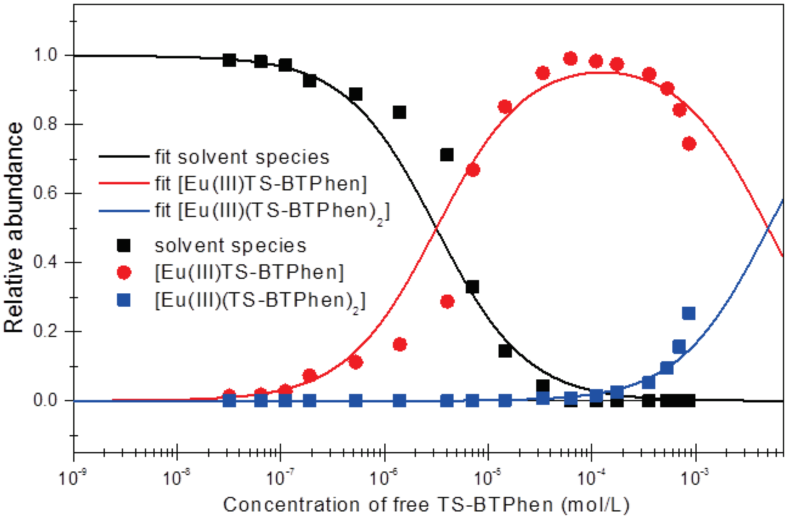

Figure 52: Species distribution of Eu(III) as a function of the TS-BTPhen concentration in 10^{-3} mol/L $HClO_4$. Symbols represent experimental data. Lines are calculated using $\log\beta_{01} = 5.5$ and $\log\beta_{02} = 7.8$.

Figure 52 shows the formation of a new species (red) with increasing TS-BTPhen concentration and a simultaneous decrease of the solvent species (black). The novel species shown in red gets dominant over the solvent species at a ligand concentration of 5×10^{-6} mol/L TS-BTPhen. The maximum abundance of the species in red occurs at 5×10^{-5} mol/L TS-BTPhen. A third species (blue) is formed consecutively at higher TS-BTPhen concentration starting from a TS-BTPhen concentration of 1×10^{-4} mol/L.

A slope analysis was carried out identifying the new species as the [Eu(III)(TS-BTPhen)] and [Eu(III)(TS-BTPhen)$_2$] complexes, respectively. The individual slopes calculated from the species distribution are given in Figure 53. A slope of 0.9 for species 1/solvent and 1.0 for species 2/species 1 depict the consecutive addition of 1 TS-BTPhen molecule. A slope of 1.9 for species 2/solvent was calculated by the sum of the individual slopes and depicts an overall complexation stoichiometry from the solvated europium ion to the 1:2 complex. However, due to insufficient data density for the species 2 / solvent species, the slope was not analyzed by simultaneous observation of the two species and was therefore not added to the figure.

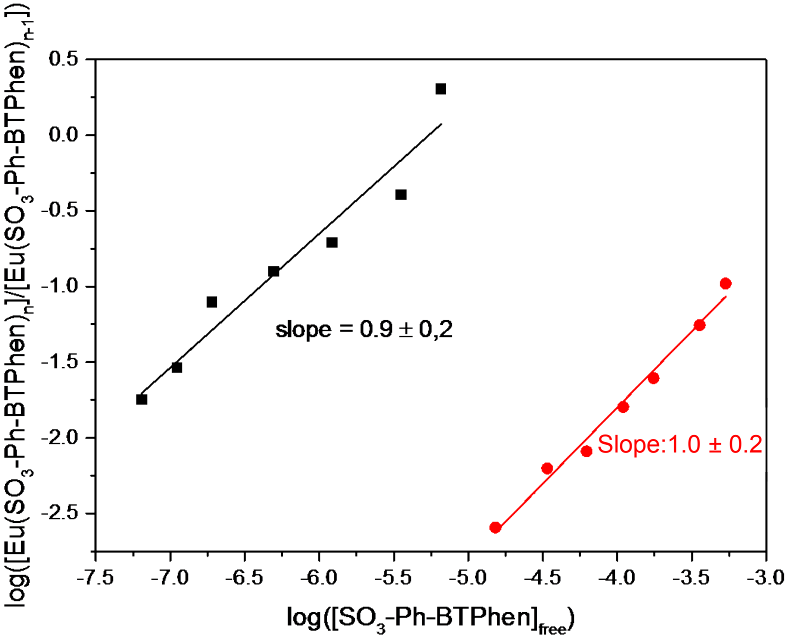

Figure 53: Linear regression of the logarithm of the peak ratios of the solvent species and the two complex species observed in the titration experiments in pH 3 $HClO_4$ vs. the logarithm of the free ligand concentration.

The results show the formation of the [Eu(TS-BTPhen)] complex as an intermediate and the formation of the $[Eu(TS\text{-}BTPhen)_2]$ complex as the final species predominating at high ligand concentrations. The conditional stability constants were calculated to be $\log\beta_{01} = 5.5$ for the 1:1 complex and $\log\beta_{02} = 7.8$ for the 1:2 complex.

Additional experiments were carried out to analyze the complexation behavior of Eu(III) with TS-BTPhen in nitric acid. Figure 54 shows the Eu(III) $^5D_0$ to $^7F_4$ fluorescence emission spectra for the consecutive addition of TS-BTPhen to a $5x10^{-6}$ mol/L Eu(III) solution in 0.5 mol/L nitric acid.

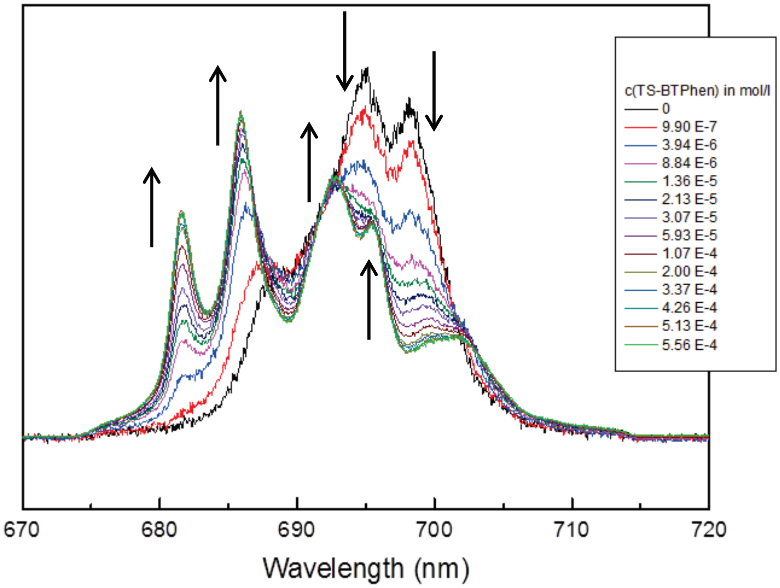

Figure 54. Normalized Eu $^5D_0$ to $^7F_4$ fluorescence emission spectra for the titration of a 10^{-5} mol/L Eu(III) solution with TS-BTPhen in 0.5 mol/L HNO_3.

In addition to the solvent species, four additional maxima were observed during the titration of Eu(III) with TS-BTPhen in 0.5 mol/L nitric acid. The formation of the different maxima can be explained by the formation of new species in combination with symmetry and hot band effects. A peak de-convolution was carried out resulting in the formation of two additional species during the titration. The species distribution resulting from the peak de-convolution is given in Figure 55. It shows the relative abundance of the individual species as a function of the free TS-BTPhen concentration. Starting from the solvent species in black a new species is formed starting at $4 \cdot 10^{-6}$ mol/L TS-BTPhen.

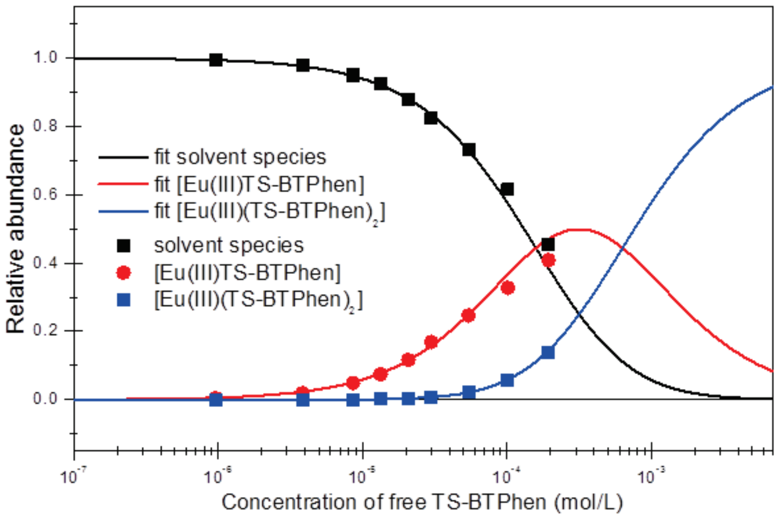

Figure 55: Speciation diagram for the titration of a 10^{-5} mol/L Eu(III) solution with TS-BPThen in 0.5 mol/L HNO_3. Symbols, experiment; lines, calculated with $\log\beta_{01} = 3.8$ and $\log\beta_{02} = 7.0$.

The amount of solvent species decreases with increasing TS-BTPhen concentration. During the titration, a third species is formed consecutively, starting at $5\cdot10^{-5}$ mol/L TS-BTPhen concentration. A slope analysis carried out from the species distribution identifies the new species as [Eu(III)(TS-BTPhen)] and [Eu(III)(TS-BTPhen)$_2$] complexes, respectively. The slope analysis is given in Figure 56. The conditional stability constants were calculated to be $\log\beta_{01} = 3.8$ for the 1:1 complex and $\log\beta_{02} = 7.0$ for the 1:2 complex. From Figure 55 it is visible that the formation of [Eu(III)(TS-BTPhen)] in nitric acid is hindered compared to the species distribution in pH 3 $HClO_4$ (Figure 53). The formation of the [Eu(III)(TS-BTPhen)] complex starts at significant higher TS-BTPhen concentrations and reaches lower maximum abundance in the progress of the titration. This effect was already observed in the Cm(III) TRLFS experiments and can be explained by a de-stabilization of the [Eu(III)(TS-BTPhen)] complex due to the increased ionic strength in the medium. Furthermore, the decrease of the logβ resulting from the change of the medium from 10^{-3} mol/L $HClO_4$ to 0.5 mol/L HNO_3 is explained by two different impacts: a change of the activity of TS-BTPhen and Eu(III) due to the increased ionic strength, and the competing reaction between protonated TS-BTPhen ligands and nitrate ions caused by the protonation of the coordinating N-atoms of TS-BTPhen.

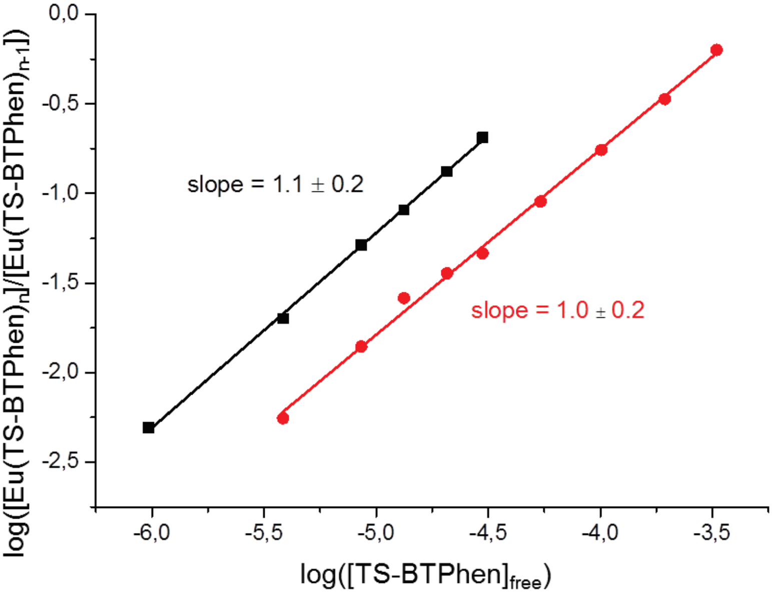

Figure 56: Slope analysis for the titration of a 10^{-5} mol/L Eu(III) solution with TS-BTPhen in 0.5 mol/L HNO_3.

Figure 56 shows the species ratio as a function of the free TS-BTPhen concentration. The slopes of 1.1 and 1.0 for the two new species, respectively, depict the addition of one TS-BTPhen molecule for the formation of the consecutive species. A slope of 2.1 for species 2/solvent was calculated by the sum of the individual slopes and depicts an overall complexation stoichiometry from the solvated europium ion to the 1:2 complex. However, due to insufficient data density for the species 2 / solvent species, the slope was not analyzed by simultaneous observation of the two species and was therefore not added to the figure. Due to the hindered formation of the [Eu(III)(TS-BTPhen)] complex in nitric acid, the functions are closer to each other compared to the slope analysis in pH 3 $HClO_4$ (Figure 53).

Table 12 shows the conditional stability constants of TS-BTPhen for Cm(III) and Eu(III). Both metals form an intermediate 1:1 metal(III) to TS-BTPhen and a final 1:2 metal(III) to TS-BTPhen complex. TS-BTPhen shows a stronger complexation with Cm(III) compared to Eu(III) for both, the 1:1 and the final 1:2 metal(III) to TS-BTPhen complex in both diluents. The formation of the

1:1 metal(III) to TS- BTPhen complex is stronger in the $HClO_4$ system for both, Eu and Cm. This can be explained by a concurrency of the $[Me(III)(NO_3)_1]$ complexes in nitric acid. The observed stability constants for Eu(III) and Cm(III) with TS-BTPhen in both media confirm the selectivity of TS-BTPhen for An(III) over Ln(III) which was already observed in the solvent extraction experiments.

Table 12: Conditional stability constants for the Cm(III)-BTPhen and Eu(III)-BTPhen complexes.

Aqueous solution	$\log\beta_{01}$ Cm(III)	$\log\beta_{02}$ Cm(III)	$\log\beta_{01}$ Eu(III)	$\log\beta_{02}$ Eu(III)
0.5 mol/L HNO_3	4.2	8.8	3.8	7.0
1 mmol/L $HClO_4$	6.2	10.7	5.5	7.8

5.3.7. Synthesis of TS-BTPhen

The synthesis of TS-BTPhen was developed at the University of Reading, UK. The sulfonated tetraphenyl-BTPhen used in this work was synthesized according to the literature.[110] However, the synthesis of TS-BTPhen only shows little reproducibility in distribution ratios and separation factors making an analysis of the complexation properties of TS-BTPhen difficult.

5.3.8. Conclusions for TS-BTPhen

The hydro-soluble TS-BTPhen showed increased selectivity for the selective back extraction of americium from a TODGA based loaded solvent. Detailed solvent extraction studies on the influence of the TS-BTPhen concentration, the TODGA-concentration and the behavior of the lanthanides were carried out. A stripping of americium, leaving curium and the lanthanides in the organic phase was found to be possible at moderate nitric acid concentrations. The behavior of the lanthanides showed to play a minor role, providing better separation between americium and the lanthanides compared to curium. Batch extraction kinetic studies showed fast kinetics for both, actinide and lanthanide elements. The solvent extraction based slope analysis with trivalent actinides proposed a 1:1 actinide to TS-BTPhen complex which is unusual for BTPhen type-ligands. Time resolved laser fluorescence studies showed the formation of a 1:1 and a 1:2 curium to TS-BTPhen complex with the 1:2 complex being the final species. The conditional stability constants obtained by TRLFS experiments confirmed the stronger complexation of curium compared to europium. Biphasic TRLFS experiments under extraction conditions with curium showed the formation of a 1:3 curium to TODGA complex in the organic phase and a 1:2 curium to TS-BTPhen complex in the aqueous phase. The synthesis of TS-BTPhen was carried out by project partners. Due to the complex synthesis strategy in the sulfonation step, it is challenging task to provide batches with stable distribution ratios and separation factors. A supply of TS-BTPhen quality would be necessary to carry out further invesgigations on the system.

5.4. H_4TPAEN as selective stripping agent for Am(III)

The experiments concerning H_4TPAEN were carried out in cooperation with KIT-INE (TRLFS) and CEA Marcoule. Experiments at KIT-INE were carried out in cooperation with Christoph Wagner who is member of the team of Prof. Panak. A three month student exchange to CEA Marcoule was funded by the SACSESS project of the European Commission. Solvent extraction experiments using high An(III) concentrations were carried out at the ATALANTE facility at the laboratoire concéption de procéss éxtraction (L28, LCPE) within the CEA Marcoule.

The polyaminocarboxylic acid H_4TPAEN was investigated in detail regarding its ability to separate Am(III) from Cm(III) as well as the fission and corrosion products. An organic phase consisting of 0.2 mol/L TODGA dissolved in TPH + 5 vol.-% 1-octanol was used for the H_4TPAEN extraction experiments. Preliminary studies were described in chapter 5.2 using nitric acid in an acidity range from pH 0 to pH 2.2 with the addition of 3 mol/L sodium nitrate. H_4TPAEN showed an enhanced selectivity for americium over curium providing a separation factor of $SF_{Cm/Am} = 7$ in combination with a TODGA-based organic phase. However, $NaNO_3$ was used to ensure sufficiently high distribution ratios. With respect to the extraction properties of TODGA regarding An(III) and Ln(III), it may be required/beneficial to use diluted nitric acid instead of high concentrations of $NaNO_3$.

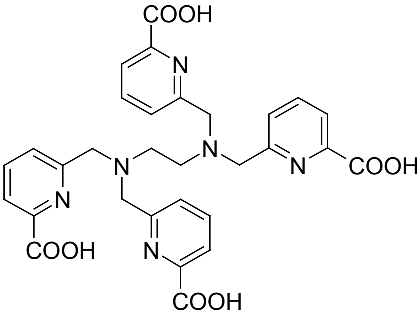

Figure 57: Structure of the hydrophilic complexing agent H_4TPAEN.

5.4.1. Solvent Extraction studies on TPAEN

Detailed solvent extraction studies on the TODGA-H_4TPAEN system were carried out to analyze its suitability for an application in an americium selective process. Different process relevant properties like the influence of the nitric acid concentration, lanthanide behavior, and extraction kinetics play an important role to find the optimal conditions for the separation of americium and will be discussed in detail in this chapter.

5.4.1.1. Influence of the nitric acid concentration

Figure 58 shows the distribution ratios of Am(III), Cm(III) and Eu(III) and separation factors of Cm(III) over Am(III) using TODGA in combination with H_4TPAEN at different nitric acid concentrations. Data of the system without H_4TPAEN are added for comparison. The distribution ratios of Am(III), Cm(III) and Eu(III) follow the general trend of increasing distribution ratios with increasing nitric acid concentrations as known for DGA-based organic phases. However, distribution ratios of Cm(III) and especially Am(III) using H_4TPAEN in the aqueous phase are significantly lower compared to the distribution ratios using TODGA alone.

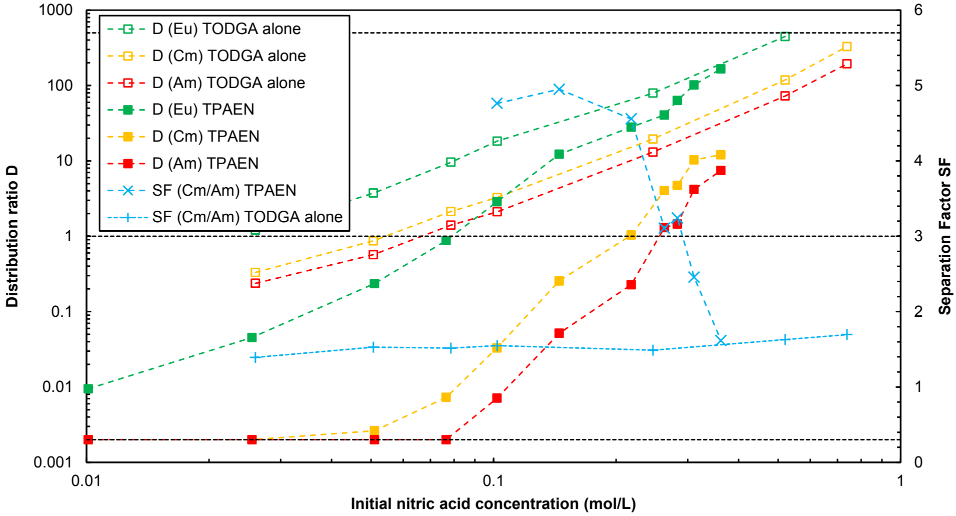

Figure 58: Distribution ratios of europium, americium and curium as a function of the nitric acid concentration with H_4TPAEN and TODGA. Org: 0.2 mol/L TODGA in TPH + 5 vol.-% 1-octanol, aq: 10 mmol/L H_4TPAEN in different initial nitric acid concentrations; 30 min of extraction at 22 °C.

The separation factor between Cm(III) and Am(III) increases from $SF_{Cm(III)/Am(III)}$ = 1.6 for TODGA up to $SF_{Cm(III)/Am(III)}$ = 5 for TODGA in combination with H_4TPAEN in the aqueous phase. The region providing the possibility of a selective separation of Am(III) from Cm(III) is between 0.2 mol/L and 0.25 mol/L initial nitric acid concentration. The separation factor in this region is $SF_{Cm(III)/Am(III)}$= 3-4 which is still high enough for process application.

5.4.1.2. Solubility of H_4TPAEN

The solubility of a hydrophilic complexing agent and its resulting complexes is of major concern for its performance in liquid-liquid extraction. Different solubilities were obtained for different batches of H_4TPAEN. Concentrations of 10 mmol/L as used for the previously described experiments caused precipitation of either H_4TPAEN or H_4TPAEN-metal complexes in experiments performed at CEA Marcoule. Therefore, solubility tests were carried out at CEA Marcoule and at the University of Parma. The solubility of H_4TPAEN was found to be related to its purity. It was found that the origin of the impurities is the last step of the synthesis during which a hydrolysis of the ester-precursor results in the H_4TPAEN product. A non-quantitative hydrolysis, leaving impurities of single or multi ester groups in H_4TPAEN molecules results in a more lipophilic impurity. However, even with an optimized synthesis the solubility of some Ln(III)-TPAEN complexes (e.g. Ce(III)) and the stability of the complexant H_4TPAEN itself in nitric acid solutions remains an important issue which has to be considered to find the optimal conditions for the experiments and a consecutive process development.

To address the solubility issues of H_4TPAEN in nitric acid solutions, the complexant was dissolved in de-ionized water to give a stable stock solution. Aqueous phases were prepared from this solution by diluting with nitric acid solution and adjust the pH using concentrated nitric acid solution. Furthermore, detailed experiments at different H_4TPAEN concentrations were carried out to analyze the optimal concentration for process development.

The solubility of the H_4TPAEN batch used in Jülich was tested. A solution of up to 20 mmol/L H_4TPAEN in 0.1 mol/L nitric acid was found to be stable for several hours.

5.4.1.3. Influence of the H_4TPAEN concentration

Experiments were carried out varying the concentration of H_4TPAEN keeping all other parameters constant. Figure 59 shows the distribution ratios of Am(III), Cm(III) and Eu(III) as a function of the H_4TPAEN concentration in the aqueous phase. The pH value of the equilibrium aqueous phase was measured to be pH 1.03± 0.05. Figure 59 shows that Am(III) and Cm(III) behave similarly in the log(D) vs. log[c(H_4TPAEN)] plot. The distribution ratios of the An(III) and Eu(III) decrease with increasing H_4TPAEN concentration. However, the change of the distribution ratio per log unit of the H_4TPAEN concentration (the slope of the curve) decreases with increasing H_4TPAEN concentration. The separation factor for Cm over Am shows a maximum of $SF_{Cm/Am}$ = 5.2 at a H_4TPAEN concentration of 0.05 mmol/L (log[TPAEN] = -3.3). The separation factor of Cm/Am varies between 4.1 and 5.2 for the range of H_4TPAEN concentration shown in Figure 59. Distribution ratios of Eu(III) are less affected by the variation of the H_4TPAEN concentration and show an inverse change of the slope compared to the An(III).

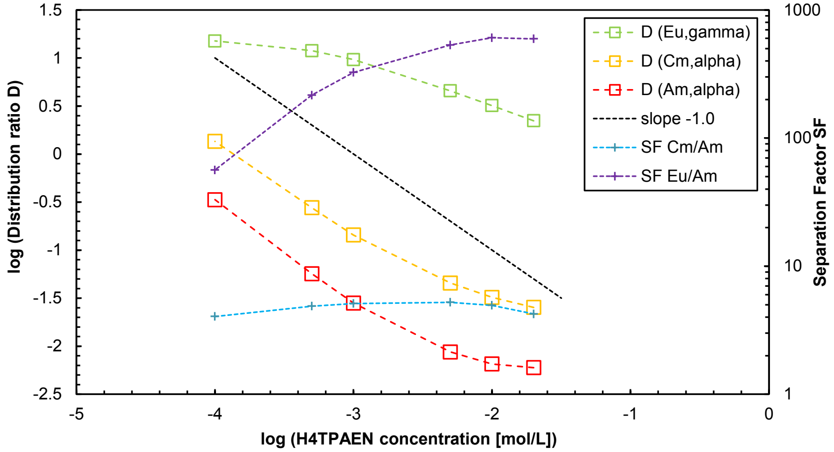

Figure 59: Distribution ratios of Am(III), Cm(III), and Eu(III) as a function of the H_4TPAEN concentration. Org: 0.2 mol/L TODGA in TPH + 5 vol.-% 1-octanol, Aq: different H_4TPAEN concentrations in 0.10 mol/L HNO_3; 30 min of extraction at 22 °C.

The separation factor of Eu(III) over Am(III) first increases with increasing H_4TPAEN concentration to show a maximum of $SF_{Eu/Am}$ = 607 at a H_4TPAEN concentration of 10 mmol/L. For simple metal-ligand complexes, information of the complex stoichiometry can be gained by plotting the logarithm of the distribution ratios against the logarithm of the free H_4TPAEN concentration. The slope of the linear functions in the log(D) vs. log(c_{TPAEN}) plot depicts the number of ligands attached to the metal to form the complex. Figure 59 does not show a linear trend for any of the analyzed elements. The pattern of the log(D) vs. log(c_{TPAEN}) shows curved lines with opposite trends for An(III) and Eu(III). This behavior indicates an additional effect which may be explained by protonation or de-protonation effects of H_4TPAEN. As a polyaminocarboxylic acid, H_4TPAEN has a number of functional groups prone to protonation and de-protonation which are shown in Figure 60.

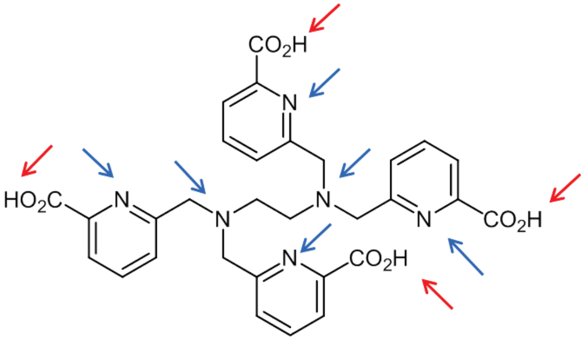

Figure 60: Theoretically possible protonation (blue) and de-protonation (red) spots in the H_4TPAEN molecule.

From Figure 60 eleven different H_4TPAEN species can be derived. The change of the electronic properties of the molecule due to protonation or de-protonation influences the complexation of metals by H_4TPAEN. From the rapid change in distribution ratios and separation factors with varying acidity, it can be assumed that only a small number or even a single one of the H_xTPAEN protonation species is responsible for the selectivity of the complexation. This effect may also be the reason for the non-linear behavior observed in the slope analysis. Due to the high number of H_xTPAEN species, an analytic determination of the H_xTPAEN species is very difficult. Chatterton et al. published protonation constants of H_xTPAEN obtained by potentiometric titration.[120] Five protonation constants were published based on potentiometric titrations of H_6TPAEN^{2+}. Figure 61 shows the relative abundance of the individual H_xTPAEN species as a function of the equilibrium pH calculated from the values published by Chatterton.

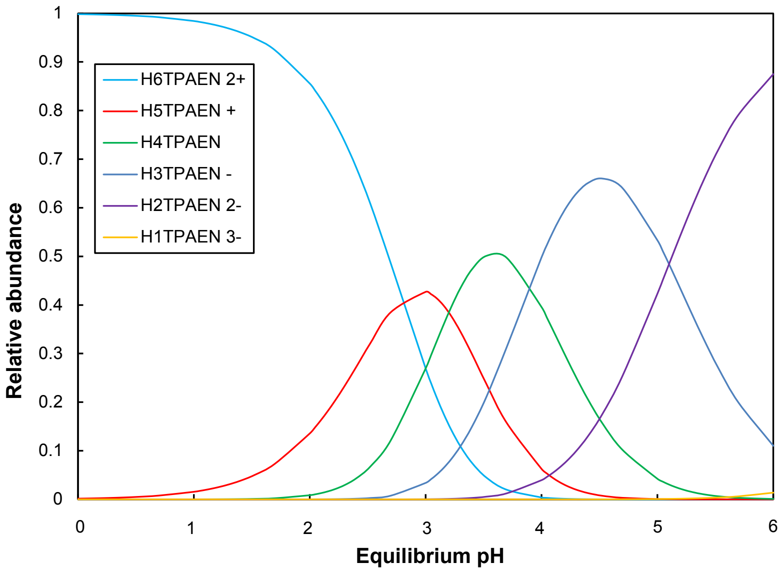

Figure 61: Relative abundance of the H_4TPAEN protonation species as a function of the pH calculated from published pK_a values.[120]

Due to the origin of the data by potentiometric titration, there is a lack of information on the two possible species H_7TPAEN^{3+} and H_8TPAEN^{4+} with increasing acidity which may be formed at high H^+ concentrations. This is due to the relation of the high proton concentration in the solution in combination with the limited amount of H^+ absorbed by a further protonation of the complexant, which is within the uncertainty of the measurement technique. The species H_6TPAEN^{2+} appears very dominant which may be reduced by the additional species to lower pH values which were not determined. From Figure 61 it can be seen that the major species in the region of the maximum separation factor $SF_{Cm/Am}$ at pH 1 is the H_6TPAEN^{2+} species which would however be strongly influenced by the missing information of the H_7TPAEN^{3+} and H_8TPAEN^{4+} species preventing detailed information on the accountable species for selectivity. Due to the unclear speciation of the H_xTPAEN in the solutions used for the experiments, it is denoted as H_4TPAEN without further statement of its protonation number in the following text.

5.4.1.4. Behavior of the Lanthanides

A good separation between Cm(III) and Am(III) is the basis for the Am selective stripping step in a novel Am(III) selective separation process. However, the trivalent 4f lanthanide elements co-extracted by TODGA together with the An(III) have to be separated together with Cm(III). Figure 62 shows the distribution ratios of the Ln(III) contained in spent fuel (La – Gd + Y) as well as the distribution ratios of An(III) for TODGA alone (left side) and for TODGA in combination with H_4TPAEN in the aqueous phase (right side). To provide data without significant influences of loading the lanthanides were contained in 10^{-5} mol/L concentration each. Figure 62 shows that An(III) as well as Ln(III) are affected by the addition of H_4TPAEN. The trend of the distribution ratios of An(III) and the separation factor $SF_{Cm/Am}$ is similar to the trend of the distribution ratios in the tracer experiments (c.f. Figure 58). Generally, the distribution ratios in the H_4TPAEN system are lower compared to the distribution ratios achieved in the experiments without hydrophilic complexant. Starting from low nitric acid concentrations in the TODGA-H_4TPAEN experiment (right side), the distribution ratios of Am(III) are below all distribution ratios of the Ln(III). At an initial nitric acid concentration of approximately 0.3 mol/L the distribution ratios of Am(III) exceed the distribution ratios of La(III). The distribution ratios of Cm(III) do not fall below the distribution ratios of the light Ln(III) La and Ce within the entire range of the analyzed initial nitric acid concentration.

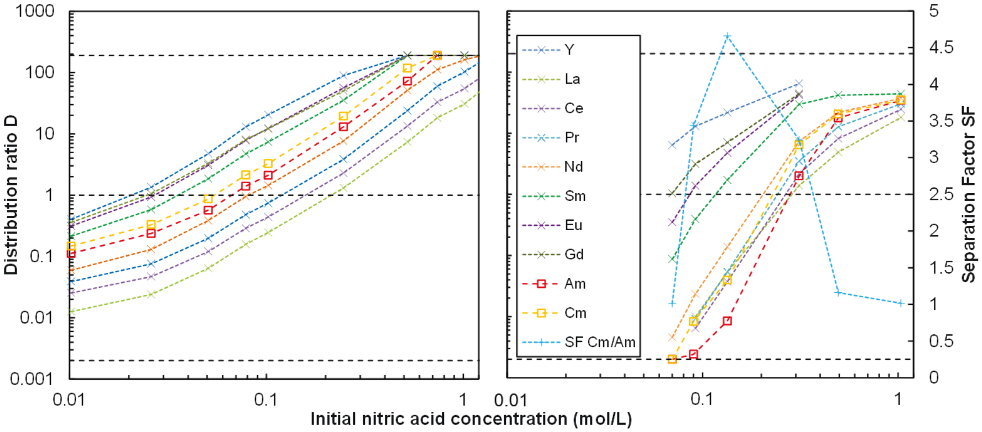

Figure 62: Distribution ratios of Am(III), Cm(III) and selected Ln(III) as a function of the initial nitric acid concentration. Org: 0.2 mol/L TODGA in TPH + 5 vol.-% 1-octanol; Aq, left: different initial nitric acid concentrations, $c_{Ln(III)}=10^{-5}$ mol/L. Aq, right: 10 mmol/L H_4TPAEN dissolved in different initial nitric acid concentrations, $c_{Ln(III)}=10^{-5}$ mol/L. 30 min of phase contact at 22 °C; 5 min of centrifugation.

Therefore, a selective separation of Am(III) using H_4TPAEN is limited by the separation from Cm(III) and the light lanthanides La(III) and Ce(III) as well. The conditions of the experiment with trace lanthanide concentrations do not depict the Ln(III) concentrations in a TODGA based process starting from PUREX raffinate. Therefore further experiments were carried out to analyze the effect of loading of a simulated PUREX raffinate on the distribution ratios of An(III) and Ln(III).

5.4.1.5. Stripping from a spiked, simulated loaded solvent

The batch tests using H_4TPAEN as Am(III)-selective stripping agent showed good results for the separation of Am(III) from Cm(III). The separation of Am(III) from the light Ln(III), however, is still an issue. Batch stripping tests from a loaded organic solvent using more realistic concentrations of metal ions were carried out to study the behavior of H_4TPAEN in combination with a simulated raffinate in comparison to the 10^{-5} mol/L Ln(III) experiments. For this test, a simulated HAW solution comparable to the solution used for the innovative-SANEX spiked process test was used.[43] Extraction was carried out using 0.2 mol/L TODGA in TPH + 5 vol.-% 1-octanol, extracting from a simulated HAW solution at 4.46 mol/L nitric acid containing 0.05 mol/L CDTA and spiked with Am(III), Eu(III), and Cm(III) tracer. Then, the organic phase was scrubbed with 0.5 mol/L nitric acid solution. The loaded organic phase was then divided and contacted with H_4TPAEN solutions in different nitric acid concentrations. Figure 63 shows the distribution ratios of An(III) and Ln(III) as a function of the nitric acid concentration.

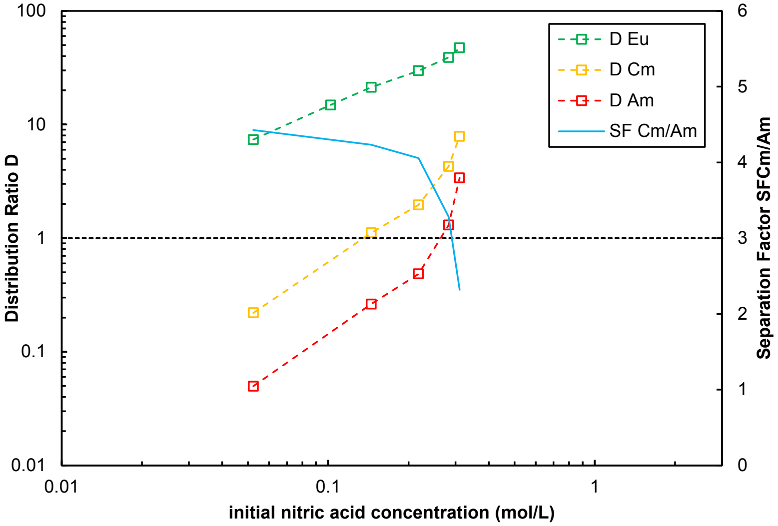

Figure 63: Distribution ratios of Am(III) Cm(III) and Eu(III) as a function of the initial nitric acid concentration. Org: 0.2 mol/L TODGA in TPH + 5 vol.-% 1-octanol loaded with spiked simulated HAW at 4.46 mol/L nitric acid solution containing 0.05 mol/L CDTA, scrubbed subsequently with 0.5 mol/L nitric acid solution. Aq: 10 mmol/L H_4TPAEN dissolved in different initial nitric acid concentrations. 30 min of stripping; 22 °C; 5 min of centrifugation.

Figure 63 shows an interesting effect of the distribution ratios of Am(III) and Cm(III). In tracer experiments the An(III) distribution ratios showed a more or less linear trend (c.f. Figure 58). However, the trend in the distribution ratios of An(III) in Figure 63 changes to a progressive increase of the distribution ratios with increasing initial nitric acid concentrations > 0.2 mol/L. The separation factor of Cm over Am is $SF_{Cm/Am}$ = 4.4 for low nitric acid concentrations but decreases rapidly to $SF_{Cm/Am}$ = 2.3 in the region where the progressive increase of the An(III) distribution ratios occurs (> 0.2 mol/L HNO_3). The distribution ratios of Eu(III) are high compared to the distribution ratios of the An(III) and follow a rather linear trend.

Using H_4TPAEN as stripping agent for an Am(III) selective process also affects the lanthanides. Figure 64 shows the distribution ratios of Am(III), Cm(III) and Ln(III) in the same experiment as shown in Figure 63. Distribution ratios of Cm(III) are greater than distribution ratios of La, Ce, and Pr in the D versus c(HNO_3) plot. Am(III) was separated from the group of Ln(III) + Cm(III) only at initial nitric acid concentrations < 0.2 mol/L. However, the distribution ratios of the Ln(III) + Cm(III) in this region are below 1 as well, hindering a separation of Am(III) from Ln(III) and Cm(III) under these conditions.

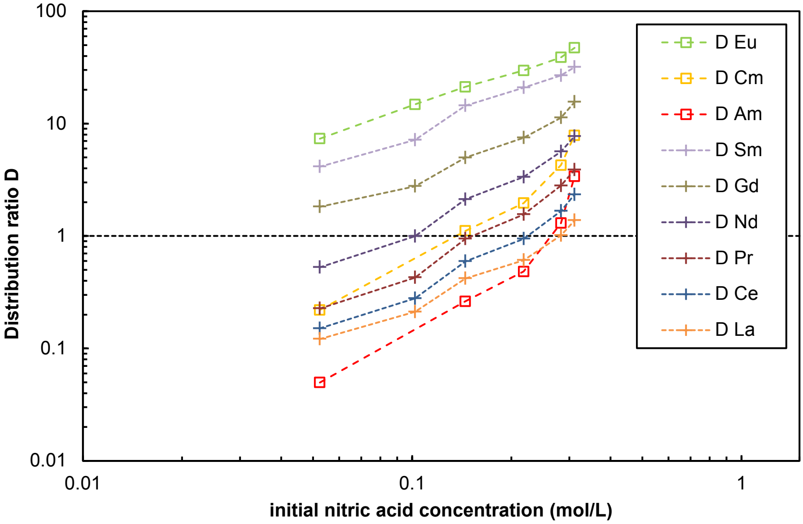

Figure 64: Distribution ratios of Am(III), Cm(III) and Eu(III) and selected Ln(III) as a function of the initial nitric acid concentration. Org: 0.2 mol/L TODGA in TPH + 5 vol.-% 1-octanol loaded with spiked simulated HAW at 4.46 mol/L nitric acid solution containing 0.05 mol/L CDTA, scrubbed subsequently with 0.5 mol/L nitric acid solution. Aq: 10 mmol/L H_4TPAEN dissolved in different initial nitric acid concentrations. 30 min of stripping; 22 °C; 5 min of centrifugation.

The stripping experiments of Am(III) and Cm(III) from a spiked, loaded organic phase indicated the behavior of the lanthanides to be one of the major problems for the separation of Am(III) from Cm(III) and the fission products using H_4TPAEN. Comparing the experiment using 10^{-5} mol/L Ln(III) in Figure 62 with the experiments in Figure 64 results in a reduced separation between Ln(III) and An(III). The concentration of Ln(III) has an important effect on the distribution ratios of the An(III) and the separation factors $SF_{Cm(III)/Am(III)}$ and $SF_{Ln(III)/Am(III)}$.

5.4.1.6. Effect of the Am(III) concentration on the TODGA-TPAEN-system.

In spent fuel recycling processes, the amount of actinides is much higher compared to the tracer experiments in the laboratory. Even if tracer-based experiments are a good tool to predict the behavior of a system, high actinide and lanthanide concentrations may cause loading effects significantly influencing the performance of the system. However, to handle high amounts of actinides, special requirements regarding radiation protection and criticality safety have to be met. The An(III) loading experiments containing significant concentrations of Am(III) were carried out at the Laboratoire de la Conception de Procéss Éxtraction (LCPE) of the ATALANTE facility at CEA Marcoule. Due to the relatively low concentration of TPAEN in the aqueous phase, even low amounts of coordinating elements can cause loading effects in the system. Especially Am(III) which forms very stable complexes with TPAEN may decrease the free TPAEN concentration rapidly. Even the relatively low amount of Am(III) in the PUREX raffinate of about 100 mg/L (0.5 mmol/L) may be sufficient to change the stripping properties of the TODGA-TPAEN system. The TPAEN/Am(III) ratio for the considered TPAEN concentration of 2.5 mmol/L would be 5 [109] Experiments were carried out using macro-concentrations of Am(III) to analyze its loading effect on TPAEN. Figure 65 shows the distribution ratios of Am(III) and Cm(III) as a function of the Am(III) concentration in a stripping experiment. The experimental conditions were chosen to contain Ln(III) and An(III) in concentrations which are present in PUREX raffinate. Different concentrations of Am(III) were provided in a Ln(III)-containing 1 mol/L nitric acid solution. The An(III) and Ln(III) were co-extracted out of these solutions using 0.2 mol/L TODGA in TPH + 5 vol.-% 1–octanol. Subsequently, the loaded organic phases were used for stripping experiments using 2.5 mmol/L TPAEN. From Figure 65 it is obvious that an increase in Am(III) concentration increases the distribution ratios of both Am(III) and Cm(III). However, even at an americium concentration of 1.74 mmol/L, depicting a ligand to metal ratio of 1.4, the distribution ratios of Am(III) are still below 1. The separation factor between Cm(III) and Am(III) starts at around 4 for trace amounts of Am(III) but decreases with increasing Am(III) concentration. This may be related to the increasing influence of TODGA on the distribution ratios of An(III) at high Am(III) concentrations as the free TPAEN concentration decreases and complexation with TODGA gains more relevance.

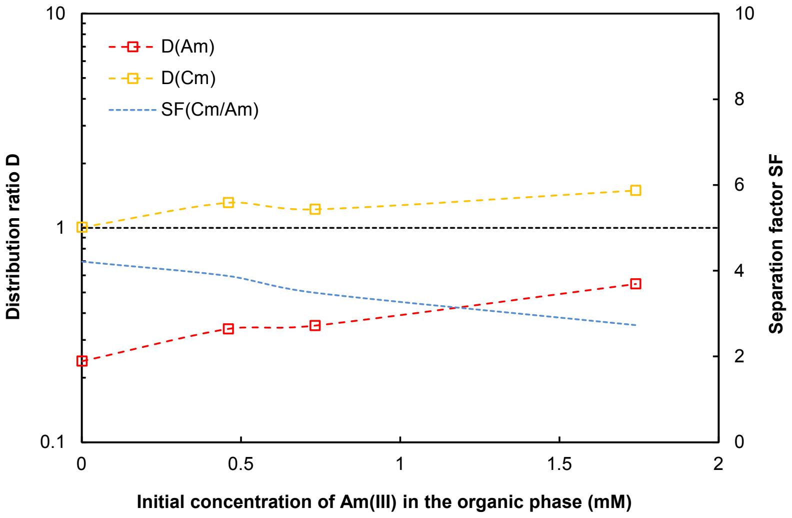

Figure 65: Distribution ratios of Am(III) and Cm(III) as a function of the initial Am(III) concentration in the organic phase. Org: 0.2 mol/L TODGA in TPH + 5 vol.–% 1-octanol loaded by 1 mol/L nitric acid containing different concentrations of Am(III) and Ln(III) in 0.75 equivalent amount to UOx fuel raffinate. Aq: 2.5 mmol/L H_4TPAEN in diluted nitric acid at initially pH 1.1; 15 min of extraction at 25 °C; 5 min of centrifugation; equilibrium pH 0.94 – 0.96.

Besides the variation of the Am(III) concentration, a variation of the TPAEN concentration in presence of high Am(III) concentrations will give additional data to understand the complexation of Am(III) with TPAEN and enable flow sheet calculations. Figure 66 shows the distribution ratios of Am(III) and Cm(III) as a function of the TPAEN concentration. The Am(III) concentration in the experiment shown in Figure 66 correlates to the Am(III) concentration of the third data point in Figure 65 (0.74 mmol/L Am(III)). Loading of the organic phase was carried out using a 1 mol/L nitric acid solution containing Am(III) and the Ln(III). The loaded organic phase was consecutively divided and contacted to the individual stripping solutions.

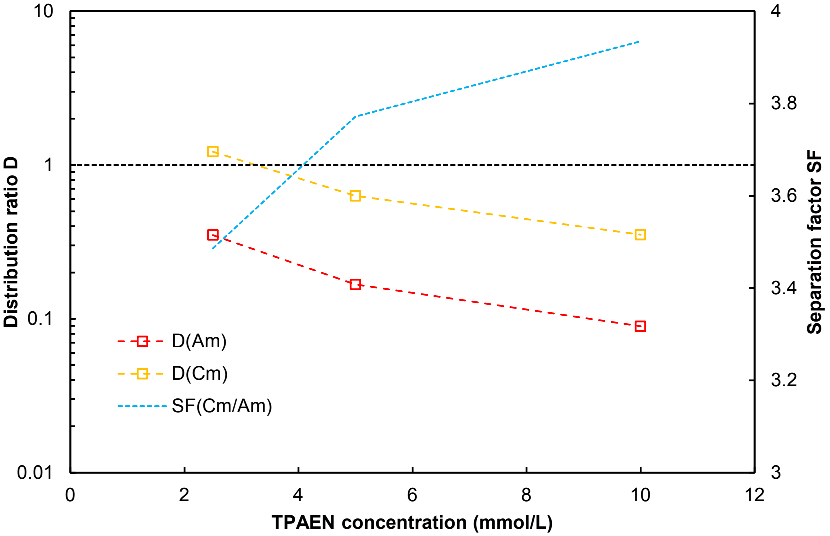

Figure 66: Distribution ratios of Am(III) and Cm(III) as a function of the H_4TPAEN concentration. Org: 0.2 mol/L TODGA in TPH + 5vol. % 1-octanol loaded by 1 mol/L nitric acid containing 0.73 mmol/L Am(III), Cm(III) and Ln(III) in 0.75 equivalent amount to UOx fuel raffinate. Aq: 2.5 mmol/L H_4TPAEN in diluted nitric acid at initially pH 1.1; 15 min of extraction at 25 °C; 5 min of centrifugation; equilibrium pH 0.94-0.96.

With increasing H_4TPAEN concentration, the distribution ratios of Am(III) and Cm(III) decrease. The separation factor $SF_{Cm/Am}$ increases with increasing H_4TPAEN concentration which is in contrast to the tracer data were the separation factor $SF_{Cm/Am}$ shows a maximum of 5, at 5 mmol/L H_4TPAEN. However, the separation factor in the tracer experiments is higher compared to the separation factor in the experiments with high Am(III) concentrations. This effect can be explained by the reduced free H_4TPAEN concentration at low H_4TPAEN concentrations where the Am(III) to H_4TPAEN ratio is relatively high. With increasing H_4TPAEN concentration the share of H_4TPAEN bound by Am(III) decreases relative to the total H_4TPAEN concentration. An increased H_4TPAEN concentration may therefore be an option to compensate An(III) loading effects on H_4TPAEN under process conditions. However, the low solubility of H_4TPAEN causes a limitation to the increase of the H_4TPAEN concentration.

Experiments were carried out using a constant Am(III) concentration of 1 mmol/L. To vary the concentration of the lanthanides the organic phase was loaded using different Ln(III) concentrations in the aqueous phase. The composition of the Ln(III) in the solution for organic phase loading is based on the concentration of the Lanthanides in UOx spent fuel raffinate, the concentration of the individual Ln(III) is given in Table 13. The resulting loaded organic phases were subsequently contacted with the TPAEN containing stripping solution. Figure 67 shows the distribution ratios of Am(III), Cm(III), and the Ln(III) La, Ce, Pr, Nd, and Sm as a function of the initial Ln(III) concentration in the aqueous phase which was used for loading the organic phase. The elements Eu, Gd, and Y are not shown in the diagram as the concentrations where inappropriate to be analyzed in the hot cell ICP-MS. The number of ICP-MS samples unfortunately had to be reduced for technical reasons missing the dataset at 2.4 mmol/L Ln(III) which is given for Am(III) and Cm(III) in Figure 67.

Table 13: Ln(III) concentrations of the initial loading aqueous phase.

Ln(III) UOx factor	**0.1**	**0.5**	**0.75**	**1**
Ce	0.57	2.87	4.30	5.74
Eu	0.04	0.21	0.32	0.43
Gd	0.03	0.16	0.24	0.32
La	0.30	1.49	2.24	2.98
Nd	0.80	4.00	6.00	8.00
Pr	0.26	1.31	1.97	2.63
Sm	0.20	0.98	1.47	1.96
Y	0.15	0.75	1.12	1.50
Sum [mmol/L]	**2.36**	**11.78**	**17.66**	**23.55**

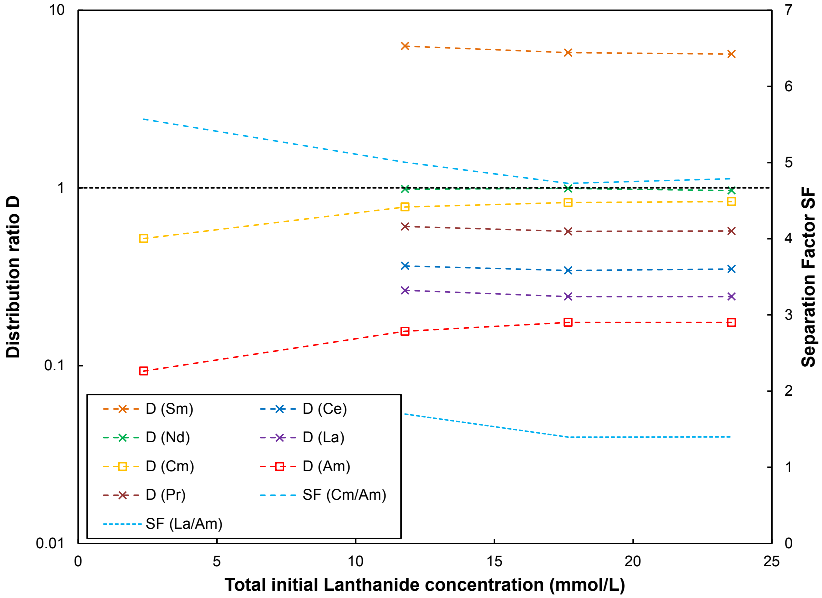

Figure 67: Distribution ratios of Am(III) and Cm(III) and the Ln(III) Ce, Pr, Sm, La, and Nd as a function of the initial Ln(III) concentration. Org: 0.2 mol/L TODGA in TPH + 5 vol.-% 1-octanol loaded by 1 mol/L nitric acid containing different Ln(III) concentrations; 1 mmol/L Am(III) and Cm(III) in equivalent amount to UOx fuel raffinate; Aq: 2.5 mmol/L H_4TPAEN in diluted nitric acid at initially pH 1.1; 15 min of extraction at 25 °C; 5 min of centrifugation; equilibrium pH 0.92 - 0.95.

Figure 67 shows increasing distribution ratios for both Am(III) and Cm(III) with increasing initial lanthanide concentration. This is a result of two effects being on the one hand the loading of the TPAEN by lanthanides. On the other hand, an increasing concentration of lanthanides in the aqueous phase is known to increase extraction by TODGA as the extraction is guided by the ionic strength of the aqueous phase. An increase of the lanthanide concentration in the aqueous phase will therefore cause increasing distribution ratios. With respect to the concentration of Am(III) and the higher stability of Am(III) complexes compared to Ln(III), the loading effect of TPAEN by lanthanides can be assumed to be the dominant effect. The distribution ratios of all measured Ln(III) stay constant over the whole lanthanide concentration range. The separation factor $SF_{Cm/Am}$ as well as the separation factor $SF_{La/Am}$ slightly decreases with increasing lanthanide concentration. The separation factor of La(III) from Am(III) is the lowest for the studied lanthanides, providing a maximum separation factor of $SF_{La/Am}$ = 1.7. The separation factor of La(III) over Am(III) is significantly lower compared to the $SF_{Cm/Am}$ making a selective separation of Am(III) without contamination by light lanthanides difficult. The distribution ratios and separation factors as a function of the Ln(III) concentration for high Am(III) concentration show the same trend with respect to the comparable experiment with trace amounts of americium.

The extraction temperature may also influence the separation between Am(III) and Cm(III) as well as the Ln(III). Experiments with high Am(III) concentrations were carried out to analyze the effect of temperature on the distribution ratios. Figure 68 shows the distribution ratios of Am(III), Cm(III), and the Ln(III) Sm, Nd, Pr, Ce, and La as a function of the stripping temperature. From Figure 68 it is visible that the distribution ratios of Am(III) and Cm(III) as well as the distribution ratios of the Ln(III) decrease with increasing temperature. The separation factor $SF_{Cm/Am}$ increases with increasing temperature to values close to 7 at 45 °C. The increase of the separation factor indicates a slightly more endothermic complexation of Am(III) compared to Cm(III) with TPAEN.

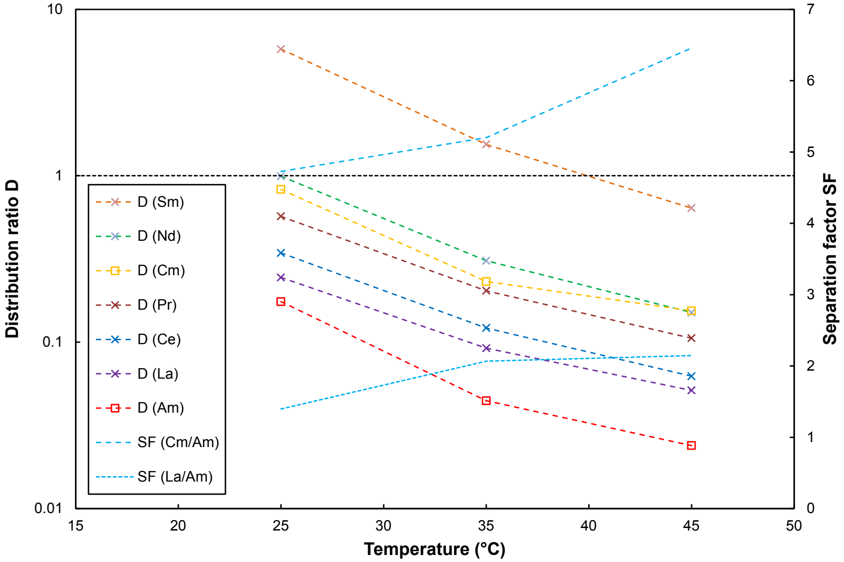

Figure 68: Distribution ratios of Am(III) and Cm(III) as a function of the stripping temperature. Org: 0.2 mol/L TODGA in TPH + 5 vol.-% 1-octanol loaded by 1 mol/L nitric acid containing 1 mmol/L Am(III), Cm(III) and 17.7 mmol/L total Ln(III). Aq: 2.5 mmol/L H_4TPAEN in diluted nitric acid at initially pH 1.1; 15 min of phase contact at different temperatures; 5 min of centrifugation; equilibrium pH 0.92 - 0.93.

The separation factor $SF_{La/Am}$ increases as well with increasing temperature from $SF_{La/Am} = 1.4$ at 25 °C to $SF_{La/Am} = 2.2$ at 45 °C. It can be explained by the decreased affinity of the Ln(III) to TPAEN. A process at elevated temperatures may be useful to achieve a better separation of Am(III) from Cm(III). Unfortunately, the separation factors at elevated temperature are still quite low for an effective separation of Am(III) from Ln(III) in a counter-current process.

5.4.1.7. Radiolysis of H_4TPAEN

For the development of a process dealing with spent nuclear fuel the performance is also related to the radiolytic behavior of the system. TODGA is already known to be quite stable towards radiolysis and provides a stable extraction system also with respect to genuine highly radioactive spent fuel solutions.[131-132] To get an impression of the radiolytic stability of H_4TPAEN, irradiation experiments were carried out on H_4TPAEN dissolved in 0.1 mol/L nitric acid. The irradiation was carried out at the University of Chalmers in Gothenbourg, Sweden. Table 14 shows the details of the irradiation. The dose rate applied to the samples was constant at 160 Gy/min for all the samples.

Table 14: Irradiation time and resulting absorbed dose for the irradiation of H_4TPAEN at Chalmers University.
Conditions: 160 Gy/min ^{60}Co-gamma source; 10.0 mmol/L H_4TPAEN in 0.1 mol/L nitric acid.

Time (min)	Absorbed dose (kGy)
153	24.0
303	47.6
610	95.8
900	141.3
1205	189.1

A color change of the initially clear and colorless solution was observed during the irradiation. Figure 69 shows the evolution of the color change with increasing absorbed dose from clear-colorless over yellow to a brown solution. Furthermore, a precipitate was observed in the last three samples. The photograph in Figure 69 was taken after the arrival of the samples back in Jülich. Figure 70 shows a close-up of the precipitate.

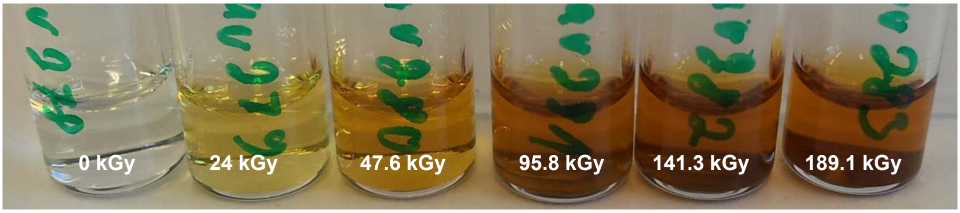

Figure 69: Color change during the irradiation of H_4TPAEN. For comparison a fresh H_4TPAEN solution was added at the left side.

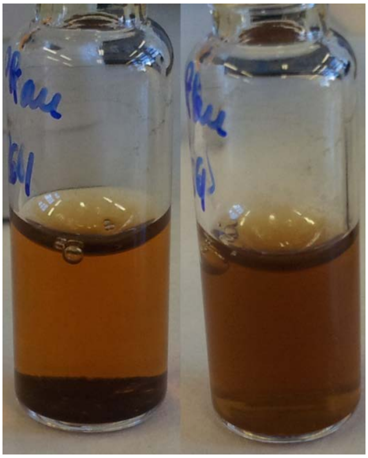

Figure 70: Settled precipitate (left side) and re-suspended precipitate (right side) of the 189 kGy absorbed dose sample.

Extraction experiments were carried out using the irradiated H_4TPAEN containing aqueous phases. The samples containing the precipitate were homogenized, giving a suspension, and used as aqueous phase. The extraction was carried out using 0.2 mol/L TODGA in TPH + 5 vol.-% 1-octanol as organic phase. Trace amounts of Eu(III), Am(III) and Cm(III) were added to the aqueous phases before phase contact. Figure 71 shows the distribution ratios and the Cm/Am separation factor as a function of the absorbed dose. For comparison, distribution ratios of Am(III), Cm(III) and Eu(III) using TODGA in combination with the same nitric acid concentration were added as horizontal lines.

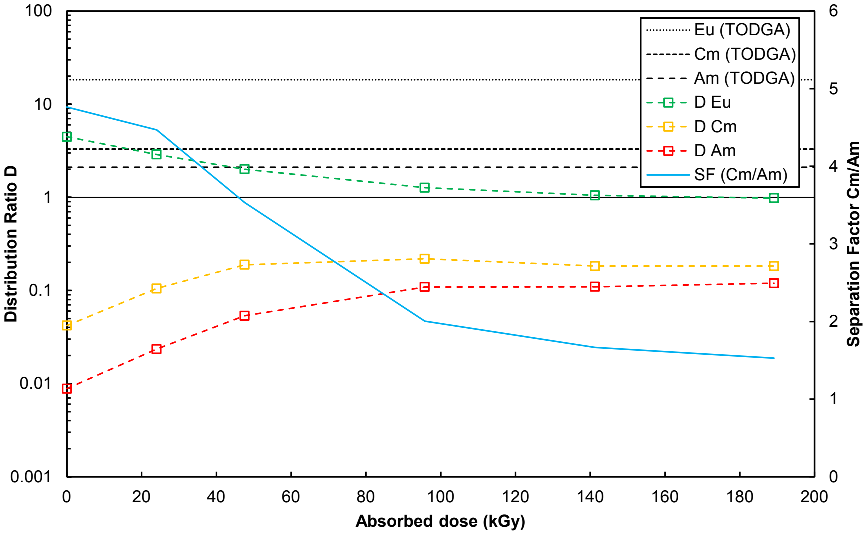

Figure 71: Distribution ratios of Am, Eu and Cm and Cm/Am separation factor (SF) as a function of the absorbed dose. Conditions: Aq: 10 mmol irradiated H_4TPAEN in 0.118 mol/L nitric acid; Org: 0.2 mol/L TODGA in TPH + 5 vol.-% 1-octanol; 30 min of extraction at 22 °C, 5 min of centrifugation. The distribution ratios of Am, Cm and Eu of TODGA with nitric acid (0.102 mol/L) without H_4TPAEN are given by the black dashed lines in the diagram.

From Figure 71 it is visible that the first effects already occur between 0 and 24 kGy. The distribution ratios of europium decrease with increasing absorbed dose which is probably caused by Ln complexation withradiolysis products of TPAEN. The distribution ratios of americium and curium increase with increasing absorbed dose which may be caused by the radiolytic decomposition of H_4TPAEN. The distribution ratios of Am(III) Cm(III) and Eu(III) using the same organic phase in contact with nitric acid of comparable concentration are not reached during the whole range of absorbed dose analyzed. The Cm/Am separation factor of the system decreases over the whole analyzed region and reaches values close to the separation factor of TODGA ($SF_{(Cm/Am)}$:1.6) at about 100 kGy. The organic and aqueous phases were visually inspected after phase separation. No change in the color of organic and aqueous phase was observed during the extraction. For the precipitate-containing samples, the precipitate remains in the aqueous phase. The radiolysis experiments of H_4TPAEN show a relatively high sensitivity towards radiolysis compared to elaborated organic ligands like TBP.[133] However, applying a process for selective Am(III) separation consecutively to a PUREX process would reduce the radiolysis in a H_4TPAEN based process to the radioisotopes present in the Am(III) selective process step. For an Am(III) selective stripping consecutive to a TODGA based co-extraction of An(III) and Ln(III) the dose is reduced to the radiation resulting from the An(III) as most of the Ln(III) are already decayed to a stable isotope at this time.

5.4.1.8. Batch extraction kinetics

Kinetics tests carried out by batch forward extraction experiments with different contact times. Figure 72 shows the distribution ratios of Am(III), Cm(III) and Eu(III) as a function of the contact time.

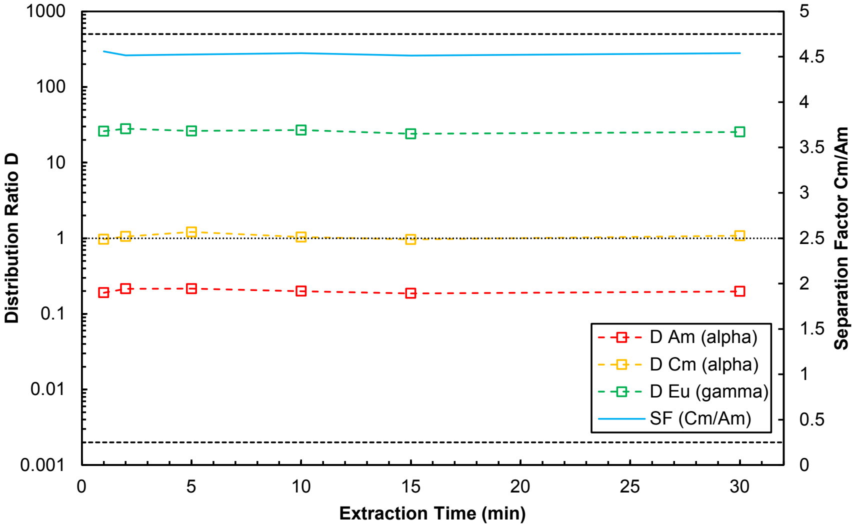

Figure 72: Distribution ratios of Am(III), Cm(III) and Eu(III) and separation factor $SF_{Cm/Am}$ as a function of the contact time in batch test tube experiments. Org: 0.2 mol/L TODGA in TPH + 5 vol.-% 1-octanol; aq: 10 mmol/L H_4TPAEN in 0.21 mol/L nitric acid; T=22 °C.

Equilibrium was reached very fast, after only two minutes no significant variation of the distribution ratios was detectable. Fast kinetics of the extraction system simplifies the design of a separation process and is therefore an important factor. However, batch experiments in test tubes only provide an idea of the kinetics as the hydrodynamics of a counter current system is much more complicated compared to the test tube hydrodynamics.

5.4.1.9. Kinetics experiments in mixer cell system

To provide sufficient data for the calculation of an americium selective flow-sheet and to ensure that this system will be compatible with a test in centrifugal contactors (with a short residence time), kinetics experiments in a mixer cell were carried out at CEA Marcoule. To provide an organic phase close to process conditions, a 0.2 mol/L TODGA in TPH + 5 vol.-% *n*-octanol solution was preloaded with lanthanides. The concentrations of Ln in the organic phase are given in Table 15. Measurements were provided by ICP-AES analysis after quantitative back-extraction of Ln from the loaded organic phase.

Table 15: Concentration of different lanthanides in the loaded organic phase used for the stripping kinetic experiment.

Element	Y	La	Ce	Pr	Nd	Sm	Eu	Gd
c (mg/L)	134	284	617	335	277	272	49	40

An aqueous phase containing 2.5 mmol/L H_4TPAEN with different pH was used for the stripping experiments. To determine the distribution ratios as a function of time, aliquots of the mixing emulsion were sampled and both phases were analyzed by ICP-AES. Figure 73 shows the variation of the distribution ratios of different lanthanides over time at pH 1.2. The results of the experiments at pH 0.8 and pH 1.0 show very similar metal distribution ratios. The experiment at pH 1.2 is therefore discussed in detail to be representative for the stripping at different pH.

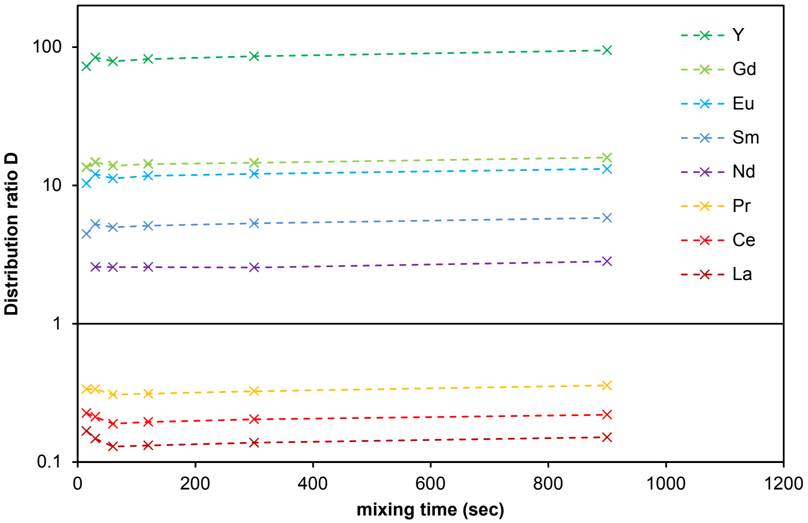

Figure 73: Distribution ratios of selected lanthanides as a function of the mixing time. Org: 0.2 mol/L TODGA in TPH + 5 vol.-% n-octanol loaded by lanthanides using 0.5 mol/L HNO_3. Aq: 2.5 mmol/L H_4TPAEN in aqueous HNO_3 at pH 1.2; T=20 °C; initial volume: 3 ml org + 3 ml aq phase.

Figure 73 shows that all lanthanides quickly reach distibution ratios close to their equilibrium values, already after 15 seconds of stirring. The distribution ratios of cerium and lanthanum are quite low and reach values similar to the americium distribution ratios under these conditions. Kinetics experiments on americium in trace amounts have been carried out following the same procedure used for the lanthanide stripping experiment in Figure 73. Figure 74 shows the distribution ratios of Am(III), Cm(III), Eu(III) and Ce(III) as a function of the mixing time in a radiotracer experiment.

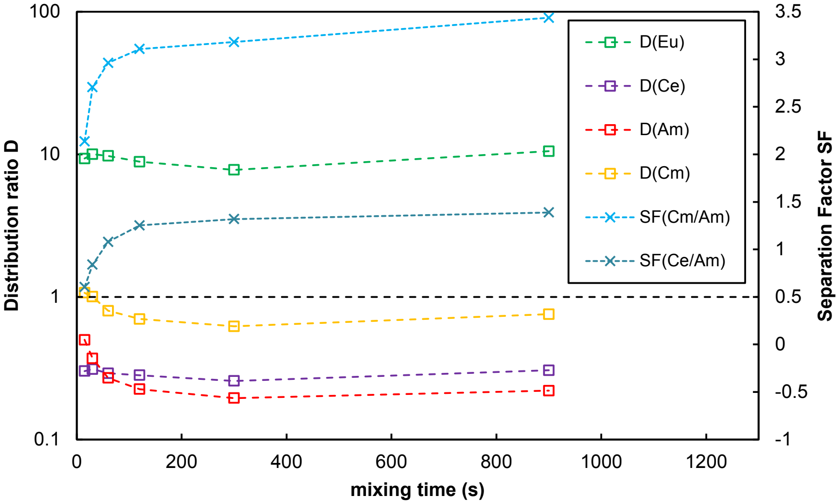

Figure 74: Distribution ratios of Am(III), Cm(III) and Ln(III) radiotracers as a function of the mixing time. Org: 0.2 mol/L TODGA in TPH + 5 vol.-% n-octanol loaded by lanthanides using 0.5 mol/L HNO_3. Aq: 1.86 mmol/L H_4TPAEN in aqueous HNO_3 at pH 1.1; T=20 °C; initial volume: 3 ml org+3 ml aq phase.

From Figure 74 it can be taken that there are significantly slower kinetics for the An(III) compared to the Ln(III). Distribution ratios similar to the equilibrium distribution ratios of the An(III) are reached after 120 seconds of phase mixing which is quite a long time for the application in a counter-current liquid-liquid extraction process. Eu(III) and Ce(III) show similar results in the radiotracer experiment compared to the stable element experiment in Figure 73 even if the concentration of H_4TPAEN in the radiotracer experiment is lower. Within the distribution ratios of the trivalent actinides, americium shows faster kinetics resulting in an increased change in the distribution ratios for the first three time-steps compared to Cm(III). Separation factors between Cm(III) and Am(III) as well as Ce(III) and Am(III) develop relatively slow due to the slow kinetics of the An(III).

5.4.1.10. Effect of Temperature on the TODGA – TPAEN system

To provide comprehensive data for the process modelling under An(III) and Ln(III) trace conditions, extraction experiments were carried out at different temperatures. A solution of 0.2 mol/L TODGA in TPH + 5 vol.-% *n*-octanol was loaded with trace amounts of ^{241}Am, ^{244}Cm, ^{152}Eu and ^{139}Ce from a 0.5 mol/L nitric acid solution. The stripping was carried out using a 2.5 mmol/L H_4TPAEN solution in diluted HNO_3 at pH 0.7 at different temperatures between 278 K and 318 K. Figure 75 shows the distribution ratios of Am(III), Cm(III), Ce(III) and Eu(III) as a function of the temperature. From Figure 75 it can be taken that the stripping of Am(III), Cm(III), Ce(III) and Eu(III) by H_4TPAEN from TODGA-1-octanol/TPH is exothermic in its gross energy balance. However, the complexation of An(III) and Ln(III) using TODGA alone is known to be strongly exothermic at least for Am(III) and Eu(III).[134] As the complexation using H_4TPAEN in the aqueous phase is competing with the TODGA complexation in the organic phase, this may indicate an endothermic complex formation of H_4TPAEN with An(III) and Ln(III).

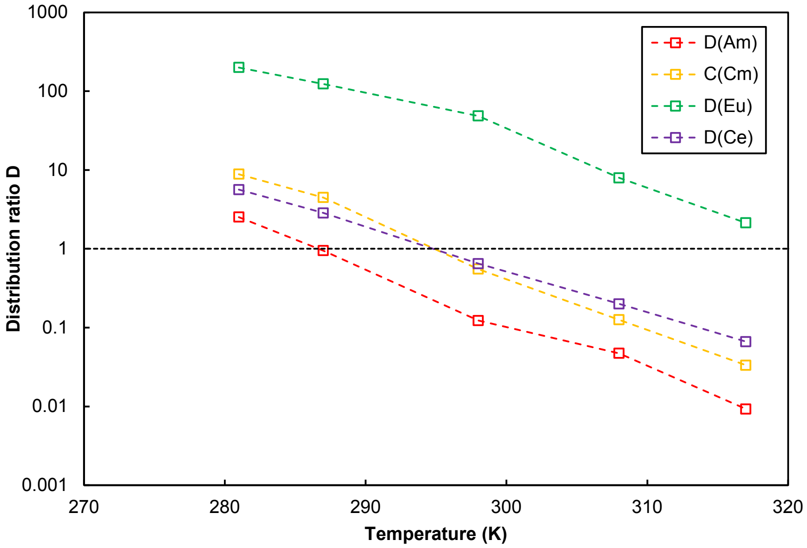

Figure 75: Distribution ratios of An(III) and selected Ln(III) as a function of the temperature. Org: 0.2 mol/L TODGA in TPH + 5 vol.-% *n*-octanol loaded with tracers of Am, Cm, Eu and Ce. Aq: 2.5 mmol/L H_4TPAEN in aqueous HNO_3 at pH 0.7; different temperatures between 278 K and 318°K; mixing time = 30 min, 3 min of centrifugation.

Nevertheless, a very strong impact of the temperature on the distribution ratios is clearly visible for all elements tested. Compared to Ce(III), the influence of temperature on the An(III) is higher, resulting in a better Ce(III)/Am(III) separation at higher temperatures ($SF_{Ce/Am}$(317 K) ≈ 7). This effect is also obtained for Eu(III) with the separation factor increasing from $SF_{Eu/Am} = 80$ at 281 K to $SF_{Eu/Am} = 230$ at 317 K. The separation factor of Cm(III) over Am(III) stays constant at $SF_{Cm/Am} = 3.8$ within the measurement uncertainties. Basic information about the temperature behavior of the distribution ratios can be expressed as slopes in a log(D) vs. 1/T plot. The slopes for Am(III), Cm(III), Ce(III), and Eu(III) in a log(D) vs. 1/K plot can be taken from Table 16.

Table 16: Slopes of log(D) vs. 1/T of Am(III), Cm(III), Ce(III) and Eu(III) in the TODGA-TPAEN-system.

	Am(III)	Cm(III)	Ce(III)	Eu(III)
slope (log(D) K)	13465	14145	10953	11179

The slopes of the log(D) vs. 1/T function of the individual elements depict the sensitivity of its distribution ratio to the temperature. According to the van ‘t Hoff plot (log(K) vs. 1/T) the slopes of the elements indicate the thermodynamic sensitivity of the system. Different slopes may indicate a difference in the thermodynamic regime which can be related to differences in the complexation mechanism or in the final complexes. The slopes of the different elements given in Table 16 show differences for the analyzed An(III) (slope ~ 14000) and the Ln(III) (slope ~11000). The different temperature sensitivity can be used in process development to improve the separation of Ln(III) over An(III).

5.4.2. TRLFS Studies on TPAEN

Time resolved laser fluorescence spectroscopic studies on the complexation of H_4TPAEN with solutions of Eu(III) and Cm(III) in 0.1 mol/L HNO_3, $HClO_4$ at pH 3 and 0.1 mol/L $HClO_4$ were titrated with a solution of H_4TPAEN in the appropriate aqueous medium. An initial kinetics test pointed out that 90 min were required for equilibration before recording an emission spectrum and adding further H_4TPAEN. The ClO_4^- ion can be considered as a very weakly coordinating anion which reduces the emission spectra of the solvent species of Eu(III) and Cm(III) to the appropiate aquo-ion without a change of the spectrum by batochromic shifts caused by coordinating anions e.g. NO_3^-.[128]

5.4.2.1. Cm(III) TRLFS with H_4TPAEN

The titration of Cm(III) with H_4TPAEN in perchloric acid can be seen as an idealized system without coordination effects from the solvent.[128] Figure 76 shows the normalized Cm(III) fluorescence emission spectra of the $^6D'_{7/2} \rightarrow {}^8S'_{7/2}$ transition as a function of the H_4TPAEN concentration in $HClO_4$ at pH 3.

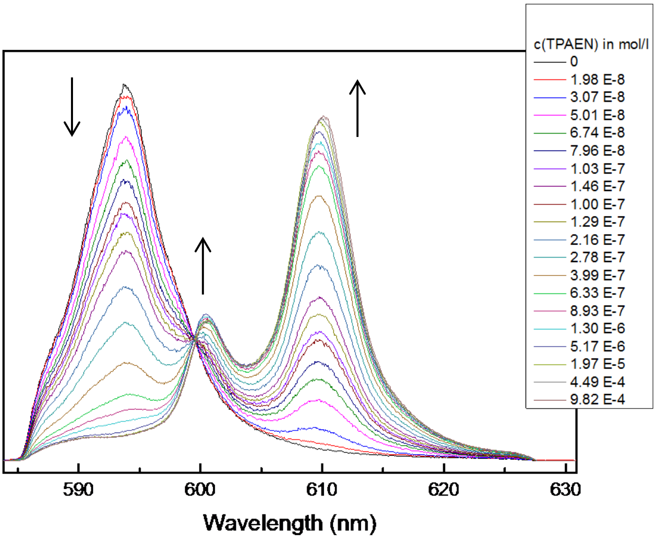

Figure 76: Normalized fluorescence emission spectra for the titration of Cm(III) with TPAEN in pH 3 $HClO_4$. $[Cm(III)]_{ini} = 10^{-7}$ mol/L; [TPAEN] = 0–0.982 mmol/L.

The titration of Cm(III) with H_4TPAEN in $HClO_4$ at pH 3 shows three maxima at 594 nm; 601 nm and 610 nm. The first maximum depicts the solvent species in $HClO_4$.[128] With increasing H_4TPAEN concentration two additional maxima are formed simultaneously depicting a new Cm(III) species at 610 nm and a hot band at 601 nm. The bathochromic shift of the final H_4TPAEN species of 610 nm is significantly higher compared to the bathochromic shift of cognate complexants at pH 3, e.g. EDTA (603.8 nm).[128] A peak de-convolution was carried out showing the formation of a single new species. The FI factors were determined by fitting the increase of the Cm(III) fluorescence intensity as a function of TPAEN concentration (FI[Cm(III)TPAEN] = 3.3). Figure 77 shows the normalized emission spectra of the pure Cm(III) aquo-ion and pure Cm(III)-TPAEN species taken from the titration spectra.

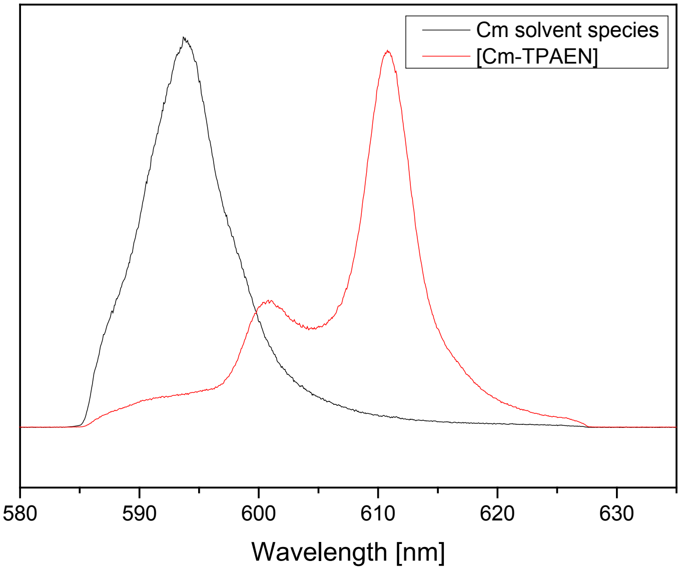

Figure 77: Normalized fluorescence spectra of the pure Cm solvent species (black) and [Cm-TPAEN] complex (red).

Figure 78 shows the species distribution calculated from the peak de-convolution of the titration spectra.

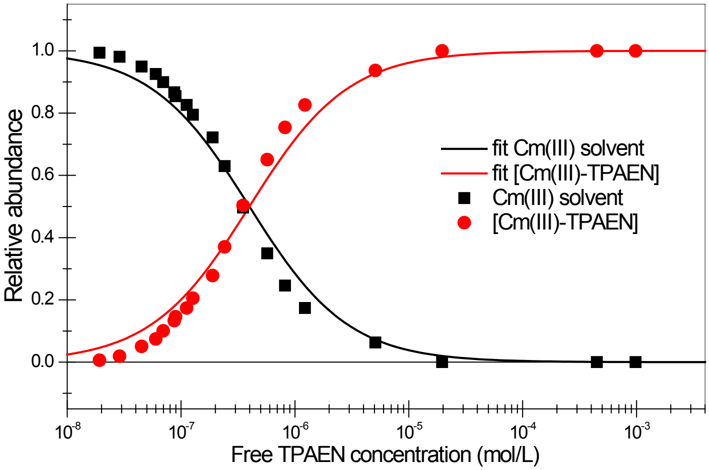

Figure 78: Experimental and calculated species distribution for the titration of Cm(III) with H_4TPAEN in pH 3 $HClO_4$.

In Figure 78, the data of the peak de-convolution is given as dots. The formation of a new species with increasing H_4TPAEN concentration is visible with a 50:50 species ratio at $\approx 4 \cdot 10^{-7}$ mol/L free TPAEN. At $2 \cdot 10^{-5}$ mol/L, the solvent species is quantitatively transferred into the new Cm(III) species depicting the final species of the titration. The free TPAEN concentration was calculated by subtracting the amount of TPAEN bound in Cm(III) complexes from the total TPAEN concentration assuming a 1:1 Cm(III) to TPAEN complex. The continuous lines depict mathematical fits for the individual species based on $\log\beta = 6.4$. A slope analysis was carried out, identifying the new species as [Cm(III)-TPAEN] complex. The slope analysis is given in Figure **79**.

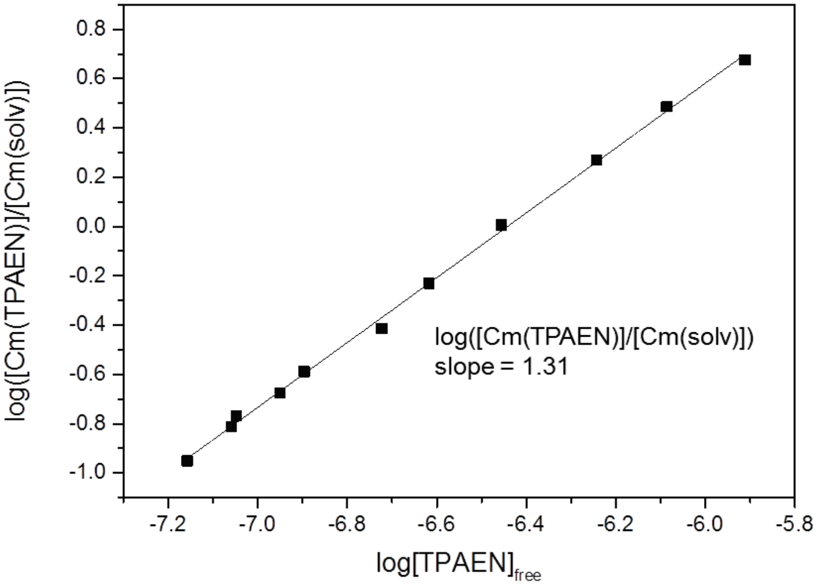

Figure 79: Slope analysis for the titration of Cm (III) with H_4TPAEN in $HClO_4$ at pH3.

The slope analysis in Figure 79 results a slope of 1.31 for the logarithm of the species ratio as a function of the free TPAEN concentration in logarithmic scale. The slope close to one depicts the addition of one TPAEN molecule per Cm(III) ion for the formation of the new species and confirms the new species to be the Cm(III)-TPAEN 1:1 complex.

Additional experiments were carried out using a higher ionic strength and proton concentration of 0.1 mol/L $HClO_4$ as titration medium. Figure 80 shows the Cm(III) fluorescence emission spectra of the ${}^6D'_{7/2} \rightarrow {}^8S'_{7/2}$ transition as a function of the H_4TPAEN concentration in 0.1 mol/L $HClO_4$.

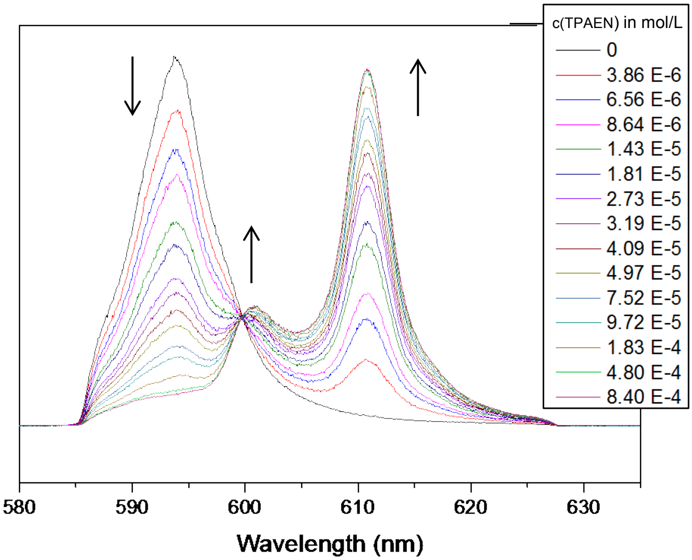

Figure 80: Normalized fluorescence emission spectra for the titration of Cm(III) with TPAEN in 0.1 mol/L $HClO_4$. $[Cm(III)]_{ini} = 10^{-7}$ mol/L; [TPAEN] = 0 – 0.840 mmol/L.

The emission spectra in Figure 80 exhibit two maxima at 594 nm and 611 nm and a hot band at 601 nm. With increasing TPAEN concentration, the species at 594 nm decreases and the second species at 611 nm grows in. The titration was stopped when further addition of the complexant did not change the emission spectrum. A peak de-convolution was carried out using the normalized spectra in Figure 77 The resulting species distribution was corrected for the fluorescence intensity factor and is shown in Figure 81 as data points. The continuous lines depict the species distribution calculated using the logβ as determined from the emission spectra. The FI factors were determined by fitting the increase of the Cm(III) fluorescence intensity as a function of TPAEN concentration (FI[Cm(III)TPAEN] = 3.5).

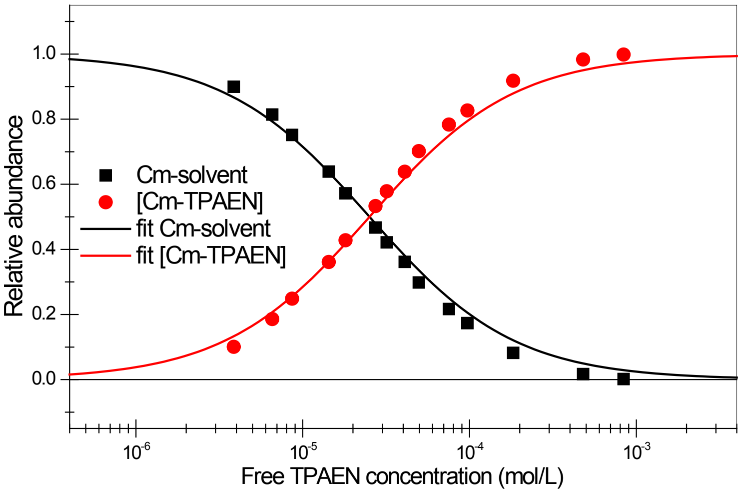

Figure 81: Experimental and calculated species distribution for the titration of Cm(III) with H_4TPAEN in 0.1 mol/L $HClO_4$.

The formation of a new species with increasing free H_4TPAEN concentration is visible with a 50:50 species ratio at ≈$3\cdot10^{-5}$ mol/L free H_4TPAEN. The free H_4TPAEN concentration was calculated by subtracting the amount of H_4TPAEN bound in Cm(III) complexes from the total H_4TPAEN concentration assuming a 1:1 Cm(III) to TPAEN complex. At $9\cdot10^{-4}$ mol/L free H_4TPAEN the solvent species is quantitatively transferred into the new Cm(III) species depicting the final species of the titration. The significant points of the speciation diagram develop at much higher H_4TPAEN concentrations in comparison to the pH 3 experiments (50:50 at $4\cdot10^{-7}$ mol/L and Cm(III)H_4TPAEN quantitatively at $2\cdot10^{-5}$ mol/L free H_4TPAEN) which can be explained by the increased proton concentration in 0.1 mol/L $HClO_4$ compared to $HClO_4$ at pH 3.[127] A conditional stability constant of $\log K = 4.6$ was calculated for the formation of a [Cm(III)-H_4TPAEN] complex in 0.1 mol/L perchloric acid being nearly two orders of magnitude lower compared to the pH 3 experiment ($\log K_{pH3} = 6.4$). The continuous lines depict mathematical fits for the individual species based on $\log K$.

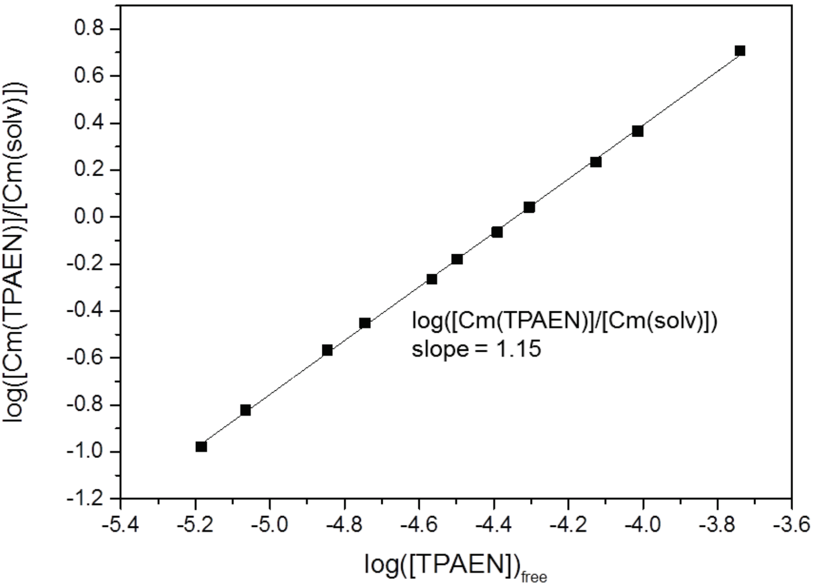

Figure 82: Slope analysis for the titration of Cm(III) with H_4TPAEN in 0.1 mol/L $HClO_4$.

A slope analysis was carried out using the relative abundance of the species, giving a slope of 1.15 and confirming the formation of a [Cm(III)-TPAEN] complex. Figure 82 shows the plot of the relative species distribution vs. the free TPAEN concentration both in logarithmic scale.

Additional experiments were carried out titrating Cm(III) in 0.1 mol/L nitric acid with H_4TPAEN depicting comparable conditions to the aqueous phase in solvent extraction experiments using H_4TPAEN. The nitrate anion is known to form distinct complexes with Cm(III) which results in a different behavior of the system in comparison to the $HClO_4$ based system. Figure 83 shows the normalized Cm(III) fluorescence emission spectra of the ${}^6D'_{7/2} \rightarrow {}^8S'_{7/2}$ transition as a function of the H_4TPAEN concentration in 0.1 mol/L HNO_3.

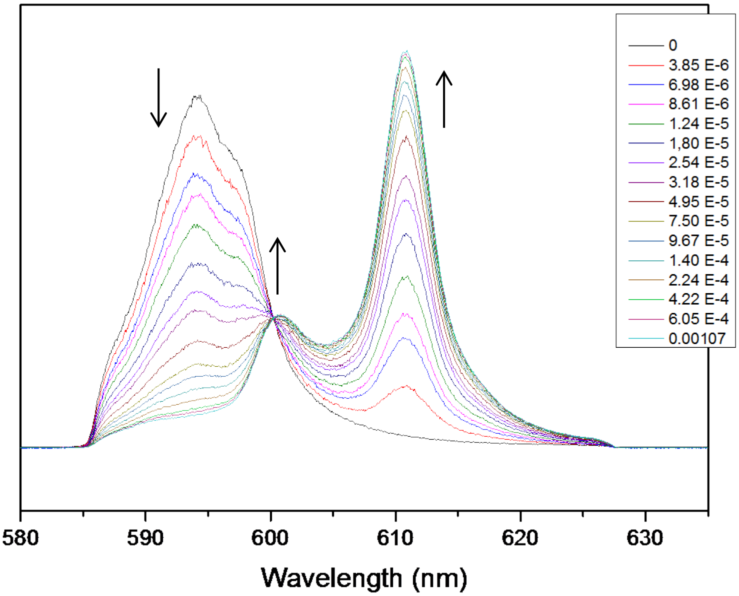

Figure 83: Normalized fluorescence emission spectra for the titration of Cm(III) with H_4TPAEN in 0.1 mol/L HNO_3. $[Cm(III)]_{ini} = 10^{-7}$ mol/L; $[H_4TPAEN]$ = 0 – 1.07 mmol/L.

The initial emission spectrum in Figure 83 corresponds to a mixture of hydrated Cm(III) at 593.9 nm and the mono-nitrato complex as a shoulder at 597.1 nm which is in good agreement with the literature.[130] Upon the consecutive addition of small portions of H_4TPAEN only one new complex is formed having an emission maximum at 610.7 nm with a hot band at 600.7 nm. In comparison to the $HClO_4$ experiments the solvent species in nitric acid is broadened by the shoulder of the Cm(III) mono-nitrato complex at 597 nm. The broadening leads to an overlap with the hot band of the final species. A peak de-convolution was carried out from the titration spectra using the normalized spectra shown in Figure 77. The resulting species distribution was corrected for the fluorescence intensity factor and is shown in Figure 84 as data points. The FI factor was determined to be FI[Cm(III)TPAEN] = 3.3.

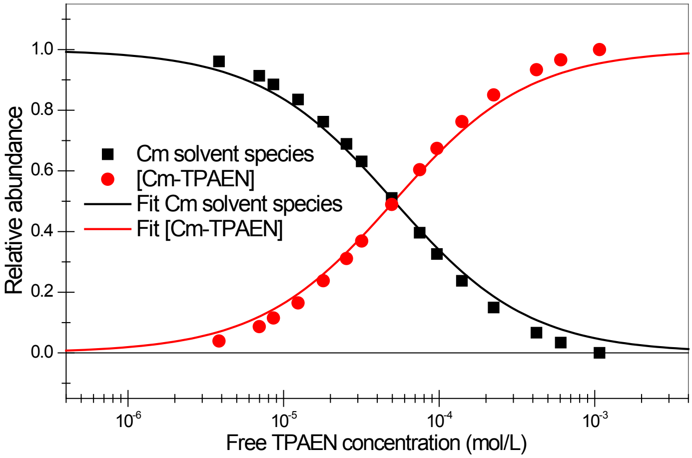

Figure 84: Experimental and calculated species distribution for the titration of Cm(III) with H_4TPAEN in 0.1 mol/L HNO_3.

From Figure 84 the formation of a single new species with increasing H_4TPAEN concentration is visible. The solvent species decreases equivalent to the increase of the new species, having a 50:50 ratio at about $4 \cdot 10^{-5}$ mol/L $\text{TPAEN}_{\text{free}}$ and showing the quantitative formation of the new species at ≈ $1 \cdot 10^{-3}$ mol/L $\text{TPAEN}_{\text{free}}$. A conditional stability constant of $\log K = 4.3$ was calculated for the formation of a [Cm(III)-TPAEN] complex in 0.1 mol/L nitric acid. Figure 84 shows the comparison of the species distribution calculated using the log$K$ value as continuous lines and the species distribution determined from the emission spectra as data points. A comparison to the experiments using $HClO_4$ at pH 3 shows a significantly lower log$K$ value for the complexation of Cm(III) with TPAEN ($\log K_{\text{pH3}} = 6.4$). However, in comparison with the results from the 0.1 mol/L $HClO_4$ experiments, just minor differences can be found. The log$K$ calculated for 0.1 mol/L $HClO_4$ experiment is 4.6 which is similar to the log$K$ value at 0.1 mol/L nitric acid. This finding can be explained by the similar ionic strength of the media and is in line with the literature.[127] The difference can be explained by the concurring reaction between TPAEN and nitrate for the complexation of Cm(III).

A slope analysis was carried out using the relative abundance of the species, giving a slope of 1.18 and confirming the formation of a 1:1 Cm(III) to TPAEN complex. Figure 85 shows the plot of the relative species distribution vs. the free TPAEN concentration both in logarithmic scale.

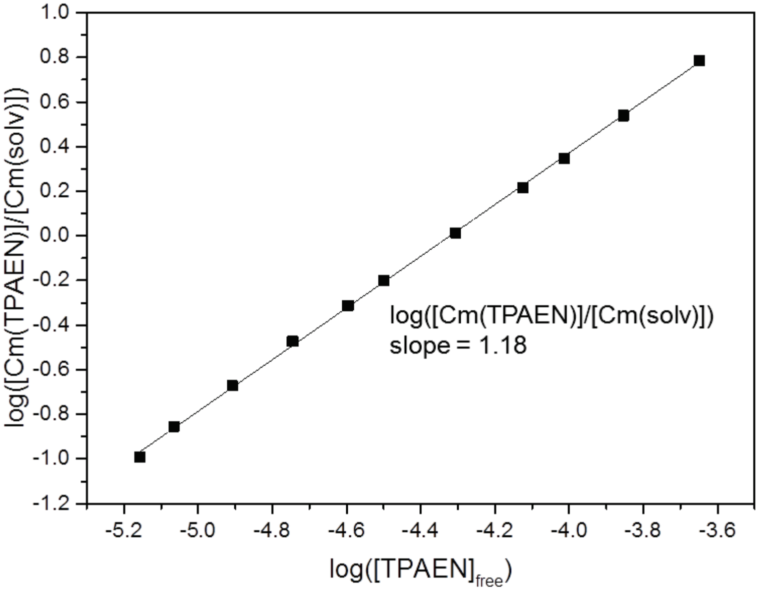

Figure 85: Slope analysis for the titration of Cm(III) with H_4TPAEN in 0.1 mol/L HNO_3.

5.4.2.2. Eu(III)-TRLFS with H_4TPAEN

In analogy to the studies with Cm(III), the complexation of Eu(III) with H_4TPAEN was analyzed in perchloric acid as well as in nitric acid. Figure 86 shows the emission spectra of the Eu(III) $^5D_0$ to $^7F_1$ and $^7F_2$ transition during the titration with H_4TPAEN in 10^{-3} mol/L perchloric acid.

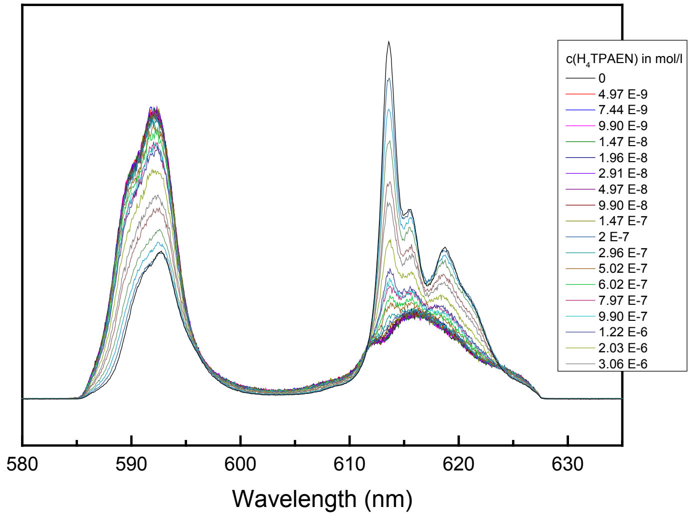

Figure 86: Normalized fluorescence spectra of the Eu(III) $^5D_0$ to $^7F_1$ and $^7F_2$ emission for the titration of Eu(III) with H_4TPAEN in $HClO_4$ at pH 3. *[Eu(III)]*$_{\mathrm{ini}}$ = 10^{-5} mol/L; *[TPAEN]* = $0 - 3.06 \cdot 10^{-6}$ mol/L.

The different relaxation pathways to the $^7F_1$ and $^7F_2$ state yield emission maxima at ca. 592 nm and ca. 613 nm. The intensity of the $^7F_1$ fluorescence at 592 nm decreases with increasing H_4TPAEN concentration while the intensity of the $^7F_2$ fluorescence at 613 nm increases. Both peaks contain the solvent species as well as the complex species. The changes in the intensity and splitting of the $^7F_1$ and $^7F_2$ emission bands are caused by changes in the symmetry of the Eu(III) complex ion resulting from a complexation with TPAEN. A peak de-convolution was carried out, the resulting speciation diagram is shown in Figure 88. The pure spectra for the $^7F_1$ and $^7F_2$ fluorescence of the Eu(III) solvent and [Eu(III)(TPAEN)] complex for the peak de-convolution are shown in Figure 87. It has to be mentioned that the spectrum of the 1:1 species changes slightly for high TPAEN concentrations which is assumed to be caused by symmetric effects. The FI factors were determined by fitting the increase of the Eu(III) fluorescence intensity as a function of TPAEN concentration (FI[Eu(III)TPAEN] = 11.5).

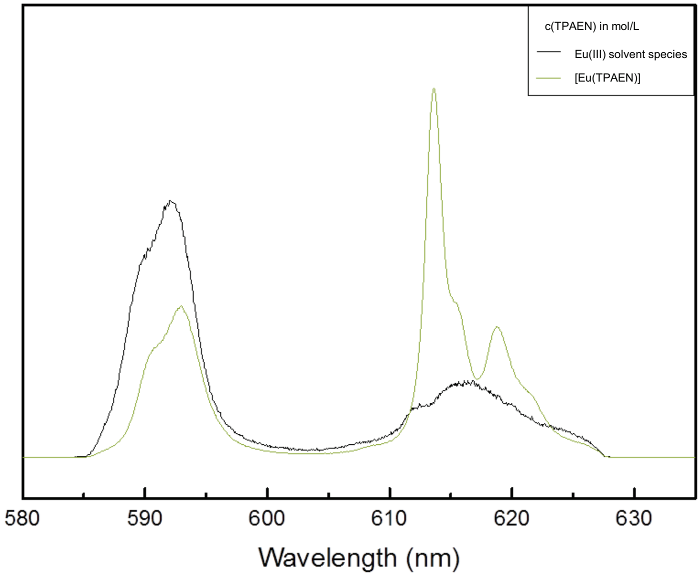

Figure 87: Normalized fluorescence spectra of the $^7F_1$ and $^7F_2$ transition of the pure Eu(III) solvent species (black) and [Eu-TPAEN] complex (green).

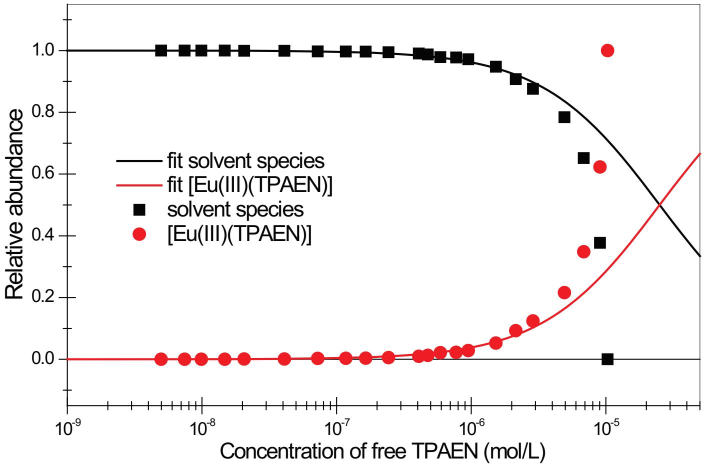

Figure 88: Experimental and calculated species distribution for the titration of Eu(III) with H_4TPAEN in pH 3 $HClO_4$.

From the peak de-convolution a single new species was found during the titration of Eu(III) with TPAEN. In Figure 88 the experimental species ratios of the Eu(III) solvent species and the new Eu(III) species is given as black and red dots for each titration step. The calculation of the fit is based on a log*K* = 4.6 for the formation of the new species out of the Eu(III) solvent species. The calculated fit describes well the region of low H_4TPAEN concentration. However, the last two points of the titration are not described very well by the fit based on the log*K*. This can be explained by the low area of the Eu(III) solvent species in the peak de-convolution which leads to an overestimation of the Eu(TPAEN) complex at high H_4TPAEN concentrations. A slope analysis allowed to identify the new species as [Eu(III)-TPAEN] complex. Figure 89 shows the slope analysis of the formation of [Eu(III)-TPAEN] complex out of the Eu(III) solvent species. A slope of 1.29 can be calculated from the data confirming the new species to be the 1:1 Eu(III) to TPAEN complex.

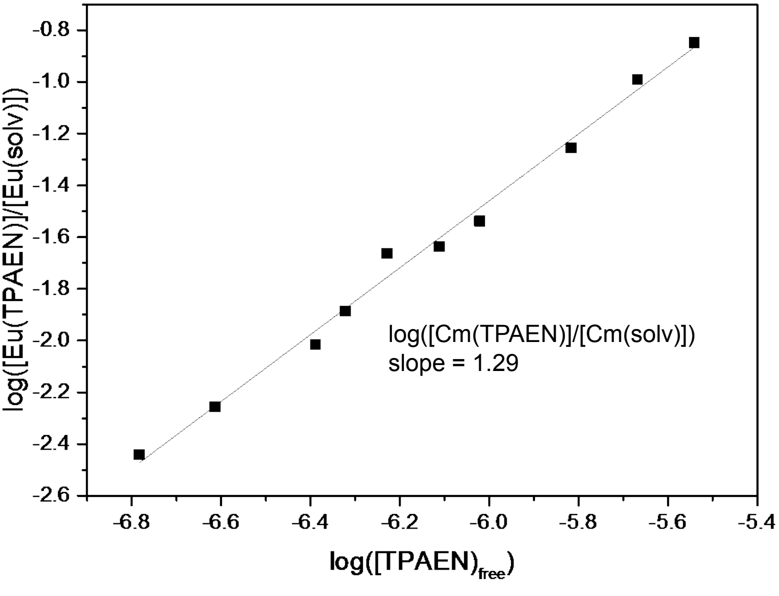

Figure 89: Slope analysis for the titration of Eu(III) with H_4TPAEN in pH 3 $HClO_4$.

The high deviation from slope = 1 in the slope analysis can be explained by the changes of the spectra at high TPAEN concentrations mentioned before. The titration of Eu(III) with TPAEN in $HClO_4$ at pH 3 can be seen as an idealized system with low ionic strength and negligibly weak coordination of the Eu(III) species by the perchlorate anion.

To analyze the species distribution in the extraction relevant nitric acid system used for solvent extraction, additional experiments were carried out using aqueous nitric acid solutions as solvent for the titration. A concentration of 0.1 mol/L HNO_3 was chosen for the experiments being close to the expected ideal stripping conditions in batch experiments. Figure 90 shows the Eu(III) fluorescence emission spectra of the titration of Eu(III) with H_4TPAEN in 0.1 mol/L nitric acid.

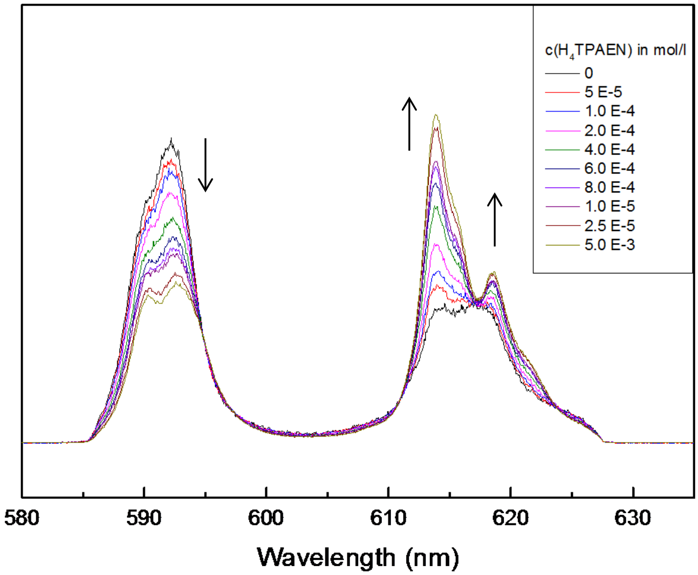

Figure 90: Normalized fluorescence spectra of the Eu(III) $^5D_0$ to $^7F_1$ and $^7F_2$ emission for the titration of Eu(III) with H_4TPAEN in 0.1 mol/L nitric acid. *[Eu(III)]*$_{\text{ini}}$ = 10^{-5} mol/L; *[TPAEN]* = 0 – $3.06 \cdot 10^{-6}$ mol/L.

Figure 90 shows the development $^5D_0$ to $^7F_1$ and $^7F_2$ transition emission spectra of Eu(III) during the titration with H_4TPAEN. Like in the experiment using $HClO_4$ at pH 3, the $^7F_1$ emission intensity decreases during the titration while the $^7F_2$ emission intensity increases.

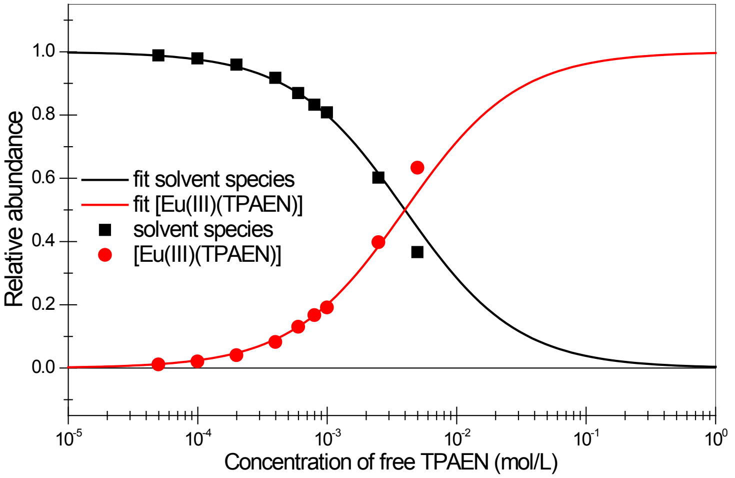

Figure 91: Experimental and calculated species distribution for the titration of Eu(III) with H_4TPAEN in 0.1 mol/L nitric acid.

A peak de-convolution was carried out giving a single new species for the titration of Eu(III) with TPAEN in nitric acid. The data of the peak de-convolution for every titration step are given as dots in Figure 91. Continuous lines represent the calculated species distribution using Log$K$ = 2.4 for the formation of the new Eu(III) species out of the solvent species. In comparison with the experiments in $HClO_4$ at pH 3 the log$K$ decreases from log$K$ = 4.6 by approximately two orders of magnitude which is consistent with the TRLFS results of Cm(III) with TPAEN. The lower stability of the formed Eu(III)-TPAEN complexes in the 0.1 mol/L nitric acid solution can be explained by a combination of the increased ionic strength, the increased acidity, and the concurrency of nitrato complexes.

A slope analysis was calculated based on the data of the peak de-convolution resulting in a slope of 1.04. Figure 92 shows the slope analysis for the formation of the [Eu(III)-TPAEN] complex out of the Eu(III) solvent species.

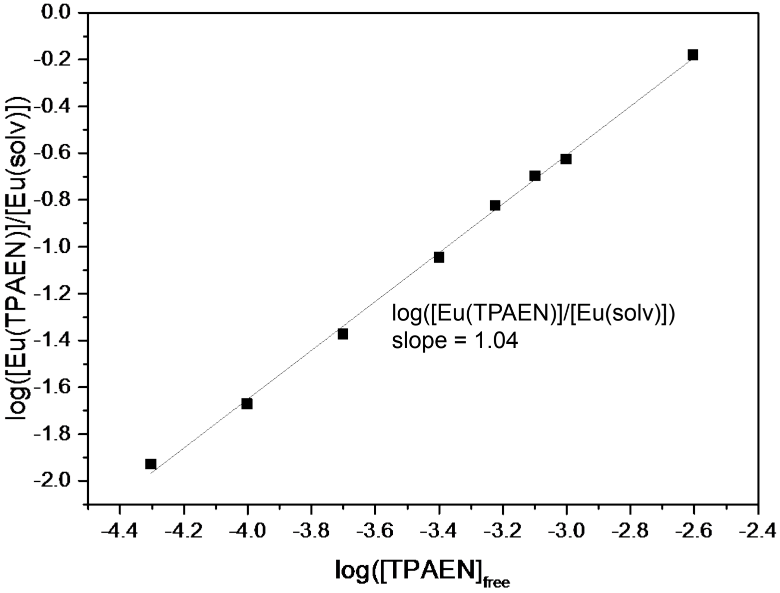

Figure 92: Slope analysis for the titration of Eu(III) with H_4TPAEN in 0.1 mol/L nitric acid.

The slope analysis in Figure 92 results in a slope of 1.04, depicting the addition of one TPAEN molecule per Cm(III) molecule for the formation of the new species. In Table 17, the conditional stability constants obtained by TRLFS titration experiments are compared for Cm(III) and Eu(III) in the individual media. The preferential complexation of Cm(III) over Eu(III) can be explained by comparing the stability constants in Figure 92. The complex stability constant of Cm(III) complexes is higher by approx. two orders of magnitude compared to the Eu(III) complex stability constants in the individual medium, respectively. Additionally, the complex stability constants of the individual metals vary with the medium. Stability constants in perchloric acid at pH 3 are significantly higher compared to the stability constants in highly acidic media. For Cm(III), the type of the medium seems to be less important compared to the acidity as the stability constants for [Cm(III)-TPAEN] in 0.1 mol/L nitric acid and 0.1 mol/L perchloric acid are similar.

Table 17: Comparison of the conditional stability constants of Cm(III) and Eu(III) in different media.

Medium	logK Cm(III)	logK Eu(III)	ΔlogK
$HClO_4$ pH 3	6.4	4.6	1.8
$HClO_4$ 0.1 mol/L	4.6	-	-
HNO_3 0.1 mol/L	4.3	2.4	1.9

The change of the complex stability can be explained by two different reasons. On the one hand, the ionic strength and proton concentration of the media are important factors for the stability of the complexes. On the other hand, a concurrency of the complexation of Cm(III) between the complexant and complexing anionic species in the solvent influences the stability of the complexes. The experiments concerning the complexation of Cm(III) in different media showed that the ionic strength of the media provides the guiding effect for the change in the stability of the final [Cm(III)-TPAEN] complex. The change from perchlorate anion to nitrate anion at similar ionic strength points out to have only minor effects on the stability of the final [Cm(III)-TPAEN] complex. For Eu(III) the effects of the two variables can be assumed to be similar. However, due to the time – consuming TRLFS experiments related to the equilibrium complex formation for Cm(III) and Eu(III) in the TPAEN system, an analysis of the formation of Eu(III) complexes with $HClO_4$ at 0.1 mol/L was not carried out.

5.4.2.3. Thermodynamic investigations on Eu(III)- and Cm(III)-TPAEN complexes using TRLFS

TRLFS experiments were carried out using a composition of Eu(III) or Cm(III) with TPAEN, respectively. The conditions for the experiments related to TPAEN and metal concentration were chosen to provide both, the solvent species and TPAEN complex species in significant amounts. Measurements at different temperatures were carried out in a temperature controlled TRLFS cell. To analyze the species distribution as a function of the temperature, spectra were collected after 90 minutes of equilibration at the individual temperature. A van t'Hoff plot can be derived using the resulting ln*K* for the individual temperatures. The slope derived from the ln*K* vs. 1/T plot is in direct connection to the thermodynamic values of the complex formation entropy (ΔS), the complex formation enthalpy (ΔH), and the Gibbs free energy (ΔG) following Equation 5 and Equation 6.

Equation 5: Simplified van t'Hoff equation

$$ln(K_{eq}) = -\frac{\Delta H}{RT} + \frac{\Delta S}{R}$$

With R=gas constant, T=temperature

Equation 6: Gibbs equation

$$\Delta G = \Delta H - T\Delta S$$

The influence of the temperature on the complex formation can be derived from the change of the spectra. Figure 93 shows the Cm(III) emission spectra of the Cm(III) solvent species and the [Cm(III)-TPAEN] complex at different temperatures.

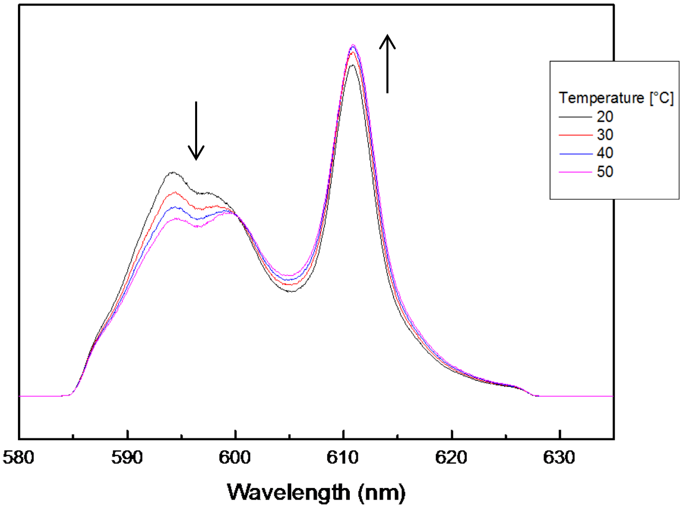

Figure 93: Normalized fluorescence emission spectra of Cm(III) solvent species and [Cm(III)-TPAEN] complex in 0.1 mol/L nitric acid at different temperatures. *[Cm(III)]* = 10^{-7} mol/L; *[TPAEN]* = $2.54 \cdot 10^{-5}$ mol/L.

A significant decrease of the solvent species in combination with an increase of the complex species with increasing temperature depicts an endothermic reaction for the formation of the [Cm(III)-TPAEN] complex.

The experiment was repeated using an Eu(III) sample. The spectra of the $^5D_0$ to $^7F_1$ and $^7F_2$ transition for the different temperatures are shown in Figure 94.

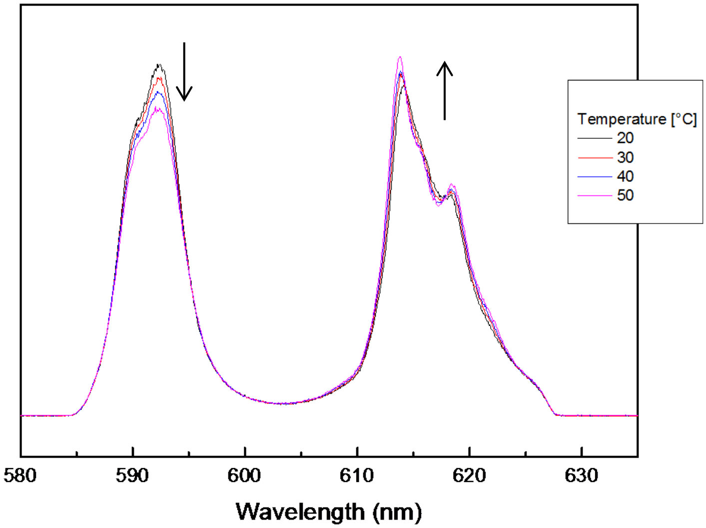

Figure 94: Normalized Eu(III) $^5D_0$ to $^7F_1$ and $^7F_2$ emission spectra of the Eu(III) solvent species and [Eu(III)TPAEN] complex in 0.1 mol/L nitric acid at different temperatures. *[Eu(III)]*= 10^{-5} mol/L; *[TPAEN]* =$4{\cdot}10^{-4}$ mol/L.

A peak de-convolution for the different spectra of the individual metals was carried out to obtain the species ratio at the different temperatures. The log*K* resulting from the species ratios were plotted as a function of 1/T in a van t'Hoff plot. Figure 95 shows the van t'Hoff plot for Eu(III) and Cm(III) TPAEN complexes.

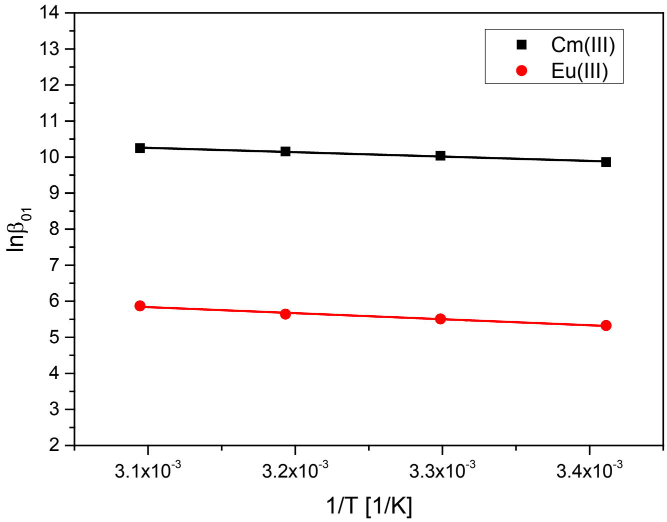

Figure 95: Van t'Hoff plot of the ln(β_{01}) values of the [Cm(III)TPAEN]- and [Eu(III)TPAEN]-complex calculated from the temperature experiments as a function of 1/T.

In the van t'Hoff plot in Figure 95 an endothermic formation reaction for both, Eu(III) and Cm(III) is visible. The stability constants of Eu(III) are significantly lower compared to the stability constants of Cm(III). Table 18 compares the thermodynamic data of Cm(III) and Eu(III) complexes obtained by TRLFS experiments. Additionally, the logK values for the thermodynamic experiments are compared to the logK of the titration experiments and found to be in excellent agreement.

Table 18: Thermodynamic data of the Eu(III) and Cm(III) TPAEN complex and comparison of the log(β) calculated from Thermodynamics and titration experiment.

M(III)	ΔH_{01}	ΔS_{01}	ΔG_{01}(293K)	log(K) Thermodynamics	log(K) Titration
Cm(III)	10 kJ/mol	116 J/(mol*K)	-24 kJ/mol	4.3	4.3
Eu(III)	13.9 kJ/mol	92 J/(mol*K)	-13 kJ/mol	2.3	2.4

The lifetime of the fluorescence of the Cm(III) or Eu(III) species is connected to the number of water molecules in the first coordination shell of the appropriate ion.[135] The absence of water molecules in the inner coordination sphere of the Cm(III)-TPAEN and Eu(III)-TPAEN complexes was analyzed by TRLFS-experiments and is evident from the fluorescence emission lifetimes (Cm(III)-TPAEN, ≈ 660 µs; Eu(III)-TPAEN, ≈ 1400 µs). This result depict a full complexation of the metal ions by a single TPAEN molecule resulting in the saturation of all coordination points of the metal ion by TPAEN. A 9-fold coordination of Cm(III) with water molecules is observed in aqueous solutions.[128] Assuming the 10-fold coordination to be the predominant coordination mode in aqueous solutions implies the coordination to nine free electron pairs of the TPAEN molecule. The Cm(III) needs therefore to be completely wrapped by the TPAEN molecule.

5.4.2.4. Biphasic Cm-TRLFS experiments

An extraction experiment with Cm(III) was carried out according to the description in the methods part using TODGA in Exxsol D80 + 5 vol.-% in the organic phase and 10 mmol/L H_4TPAEN with 10^{-7} mol/L Cm(III) in 0.1 mol/L nitric acid in the aqueous phase. After separation of the phases, Cm(III)-TRLFS measurements of the individual phases were carried out to analyze the speciation of Cm(III) in the individual phases. Figure 96 shows the fluorescence emission spectra of the extraction experiment in black. For comparison, emission spectra of the [Cm(III)-$TODGA_3$] complex from a single phase experiment using Cm(III) in TODGA EXXSOL D80 + 5 vol.-% 1 – octanol and the spectrum of the [Cm(III)-TPAEN]-complex from the titration experiment in 0.1 mol/L nitric acid are shown in red. Figure 96 confirms the formation of the [Cm(III)-TPAEN] complex in the aqueous phase as well as the formation of the [Cm(III)-$TODGA_3$]-complex in the organic phase at extraction conditions.

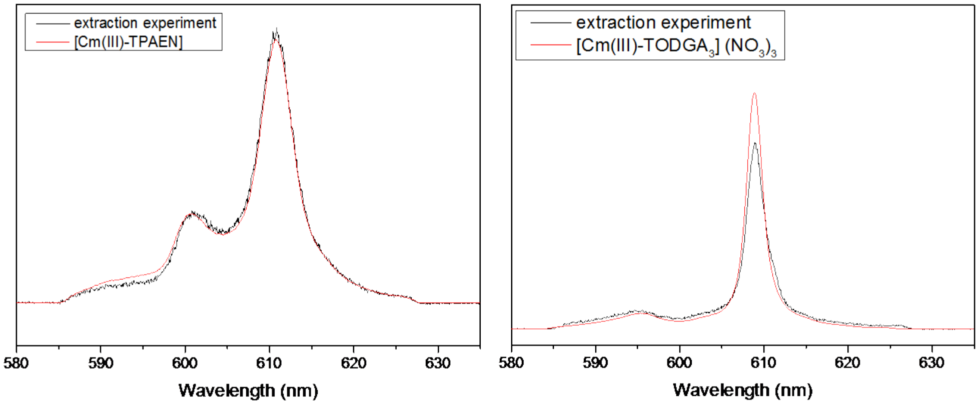

Figure 96: Cm(III) TRLFS-spectra of the aqueous phase (left side) and organic phase (right side) of the extraction experiment using TODGA in the organic phase and H_4TPAEN in the aqueous phase. Conditions: Org: 0.2 mol/L TODGA in Exxsol D80 + 5 vol.-% 1-octanol; Aq: 10^{-7} mol/L Cm(III) and 10 mmol/L H_4TPAEN in 0.1 mol/L nitric acid.

The formation of mixed complexes in either the aqueous or organic phase was not observed within the uncertainties of the TRLFS method.

5.4.3. Conclusions to H_4TPAEN

The polyaminocarboxylic acid H_4TPAEN showed high selectivity for Am(III) in combination with TODGA in the complexant screening. To obtain detailled information on the suitability of H_4TPAEN for the selective separation of americium, solvent extraction and laser spectrometric investigations were carried out. The influence of the nitric acid concentration was analyzed sowing a high sensitivity to changes of the acidity. A solvent extraction slope analysis gave a 1:1 metal to H_4TPAEN complex for trivalent actinides. Experiments on the behavior of the lanthanides in combination with H_4TPAEN showed an insufficient separation of the light lanthanides from americium. Additional solvent extraction experiments with high concentrations of trivalent actinides were carried out, showing high selectivity for americium even at high concentrations of americium and curium. Investigations on radiolysis stability and extraction kinetics of H_4TPAEN showed rather low radiation resistance but fast extraction kinetics in both, batch experiments and mixer cell kinetics. The effect of temperature was analyzed for the TODGA-H_4TPAEN system showing increased selectivity for americium at elevated temperatures. Time resolved laserfluorescence spectrometric investigations on europium and curium with H_4TPAEN confirmed the formation of a 1:1 metal to H_4TPAEN complex. Conditional stability constants in perchloric and nitric acid showed significantly higher stability for the complexes of the trivalent actinide curium. Biphasic TRLFS experiments show the formation of a 1:3 curium to TODGA complex in the organic, and a 1:1 H_4TPAEN to curium complex in the aqueous phase. The analysis of the inner coordination sphere of the curium-H_4TPAEN complex did not show any water, depicting a full complexation of curium by H_4TPAEN. Laser fluorescence based thermodynamic investigations on the TODGA-H_4TPAEN system showed endothermic thermodynamics for the complexation of europium and curium with H_4TPAEN.

6. Summary

The concept of co-extracting An(III) and Ln(III) using a TODGA based organic phase, followed by a selective An(III) stripping was successfully demonstrated in the innovative SANEX process in a laboratory scale counter-current process demonstration using a spiked simulated PUREX raffinate. The process showed excellent performance for the recovery of trivalent actinides. The use of SO_3-Ph-BTP prevents the need for a sensitive pH control and salting out agents as it was necessary in former processes. No hydrodynamic problems occurred during the process test. Ln(III) and An(III) were extracted by TODGA to more than 99.7 % within only four extraction stages and the An(III) were recovered >99.8 % in the An(III) product. Ln(III) were stripped by a buffered solution with a recovery of >99.5 %. The only issue to address is the behavior of Ru which was extracted in significant amounts but mainly stayed in the organic phase during the An(III) and Ln(III) stripping sections. A prevention of Ru-extraction or an effective solvent regeneration and recycling would therefore be important for an effective process application.

The extraction section of the i-SANEX process followed by an adapted selective stripping can be taken as a basis for the development of an Am(III) selective process. Novel americium selective complexing agents were necessary to enable for an adaption of the innovative SANEX process towards an americium selective process. Screening tests using the hydrophilic complexing agents Pytri-diol, TS-BTPhen and H_4TPAEN were carried out. H_4TPAEN and TS-BTPhen were found as promising complexing agents for a selective Am(III) separation in combination with TODGA for further investigation.

With TS-BTPhen separation factors of $SF_{Cm/Am} = 3.6$ were achieved in tracer based batch stripping experiments from a loaded TODGA phase at an acidity of 0.65 mol/L nitric acid. The possibility of a stripping at moderate nitric acid concentrations making the stripping step robust to pH changes. The lanthanides were separated from Am(III) with the lowest separation factor of $SF_{La/Am} = 20$ at 0.65 mol/L nitric acid. The application of the alternative ligand Me–TODGA allows a selective stripping of Am(III) even at acidities of > 1 mol/L nitric acid. The solvent extraction based slope analysis of TS-BTPhen indicated the formation of An(III)–TS-BTPhen 1:1 complexs which would be unusual for BTPhen type ligands, as lipophilic BTPhen ligands show the formation of 1:2 metal to ligand complexes. TRLFS experiments with Cm(III) and Eu(III) in perchloric acid and nitric acid showed the formation of 1:1 and 1:2 metal to TS-BTPhen complexes, with the 1:2 complex being the final, more stable complex present under solvent extraction conditions. Conditional stability constants of the complexes were determined for the individual media showing slightly higher complex stability compared to the cognate SO_3-Ph-BTBP used for development of the AmSel process. The promising results of selective Am(III) stripping using TS-BTPhen in combination with a TODGA or Me-TODGA based system are detracted by problems in the reproducible synthesis of the TS-BTPhen complexant. The synthesis of TS-BTPhen was developed and carried out by project partners, and was therefore out of the scope of this work. Samples from different TS-BTPhen batches showed a wide spread of distribution ratios and separation factors prohibiting further process development.

H_4TPAEN provided separation factors of $SF_{Cm/Am} = 4$ with an effective separation of Cm(III) over Am(III) at about pH 1. Slope analysis showed curves instead of lines which was related to its complex protonation chemistry. Experiments including lanthanides showed an insufficient separation of the light Ln from Am(III). Time dependent investigations of the stripping of An(III) in the presence of Ln(III) with H_4TPAEN showed faster kinetics for Ln(III) compared to An(III). Extensive investigations of Ln(III) loading were carried out to find the optimal conditions for the selective separation of Am(III) from Cm(III) and the Ln(III) and to provide basic data for numerical process development. The experiments indicated lanthanum and cerium to be the most problematic Ln(III) for the application of H_4TPAEN in combination with TODGA. An(III) loading experiments were carried out at the ATALANTE facility (CEA Marcoule) with up to 1.74 mmol/L Am(III) confirming the application of H_4TPAEN with high An(III) loadings. Thermodynamic solvent extraction investigations indicated an endothermic complexation of An(III) with H_4TPAEN. Furthermore, the separation factors of Ln(III) over Am(III) increased with elevated temperatures up to $SF_{La/Am} = 7$ while the $SF_{Cm/Am}$ stayed constant at about $SF_{Cm/Am} = 4$. TRLFS investigations with Eu(III) and Cm(III) in perchloric acid and nitric acid showed the formation of solely Metal(III) : TPAEN 1:1 complexes without the presence of water in the inner coordination sphere. Conditional stability constants of the complexes were determined from single- phase titration experiments using peak de-convolution method. The conditional stability constants were calculated for the individual media. Biphasic TRLFS experiments confirmed the formation of a Cm(III)-H_4TPAEN 1:1 complex under extraction conditions. Thermodynamic TRLFS studies with Eu(III) and Cm(III) confirmed an endothermic formation enthalpy for Cm(III) and Eu(III) as already indicated by the temperature variation in solvent extraction experiments.

Both hydrophilic complexing agents show similar selectivity for Am(III) over Cm(III) and allow an application in combination with TODGA. An innovative-SANEX-like extraction and scrubbing part can therefore be taken as a basis for a process for both tested hydrophilic complexants. Major disadvantages of TS-BTPhen are its non-CHON nature and its challenging synthesis. The Am/Cm separation factor is slightly lower compared to H_4TPAEN. However, TS-BTPhen provides a very stable system with respect to acidity changes in combination with TODGA and even more with Me-TODGA. TS-BTPhen provides good separation factors of Ln over Am.

H_4TPAEN was analyzed in more detail in this work. Its disadvantage is the very narrow region for a separation of Am(III) from Cm(III) and the Ln(III) concerning acidity and complexant solubility. An effective separation may require a process at elevated temperatures, being advantageous for an application in hot cells. However, a preliminary spiked, simulated laboratory scale test is necessary for concept approval. This work provides basic data to enable an advanced process design using the PAREX code to design an Am(III) selective flow-sheet even at different temperatures. Therefore, H_4TPAEN is recommended for the development of an Am(III) selective process.

7. Outlook

The selective separation of americium from PUREX raffinates depicts a further improvement to the options of spent fuel management. However, the separation of trivalent americium from curium is a challenging task. The two systems analyzed in this work focus on an americium selective adaption of the innovative SANEX process. The implementation of an americium selective stripping to the i-SANEX process would provide a sophisticated process option for americium recycling. Both hydrophilic complexing agents TS-BTPhen and H_4TPAEN show an increased selectivity for americium in the i-SANEX like TODGA based extraction system. A TS-BTPhen based process would provide an option to separate trivalent americum from curium and the lanthanides. The rather high acidity during the stripping step gives robustness to the process with respect to pH-changes. However, the synthesis of TS-BTPhen is a major drawback of the system, as the distribution ratios and separation factors vary between the different batches of TS-BTPhen. The implementation of a stable synthesis of TS-BTPhen would provide a basis to further develop an americium selective TS-BTPhen based version of the innovative SANEX process.

The hydrophilic complexing agent H_4TPAEN provides slightly higher selectivity for americium compared to TS-BTPhen. However, the implementation of an americium selective stripping in an innovative SANEX based process using H_4TPAEN would require for increased control of the acidity in the stripping section. Furthermore, the separation of americium from the light lanthanides lanthanum and cerium plays an additional role for the TODGA-H_4TPAEN system. The radiolysis stability of H_4TPAEN is rather low compared to e.g. TBP which is used in the PUREX-process. However, due to the process-related reduction of the dose received by H_4TPAEN to americium and curium, an application for an americium selective stripping requires less radiation stability compared to a process for handling spent nuclear fuel. A further development of a H_4TPAEN based americium selective adaption of the innovative SANEX process would enable for the separation of americium from PUREX raffinate and provide a simplified option with respect to existing americium selective processes.

8. References

1. OECD-IEA World Energy Outlook 2015 Factsheet; International Energy Agency; Paris; 2015.
2. OECD-NEA Annual Report 2015; OECD-Nuclear Energy Agency; Paris; 2016.
3. IAEA Nuclear Technology review 2015; International Atomic Energy Agency; Vienna; August 2015; 2016.
4. NEA Annual Report 2014; NEA No. 7238; OECD NEA; Paris; 2015.
5. Kelly, J.E. Generation IV International Forum: A decade of progress through international cooperation. Progress in Nuclear Energy **2014**, *77*, 240-246.
6. Haug, H.O. Calculations and Compilations of Composition, Radioactivity, Thermal Power, Gamma and Neutron Release Rates of Fission Products and Actinides of Spent Power Reactor Fuels and Their Reprocessing Wastes; KFK 1945, Gesellschaft für Kernforschung M.B.H; Karlsruhe; 1974.
7. Mortimer, C.E., *Chemie*. Georeg Thieme Verlag: Stuttgart, 1980; Vol. 3.
8. Sasahara, A.; Matsumura, T.; Nicolaou, G.; Papaioannou, D. Neutron and Gamma Ray Source Evaluation of LWR High Burn-up UO2and MOX Spent Fuels. J. Nucl. Sci. Technol. **2004**, *41* (4), 448-456.
9. Pfennig, G.K.-N., H.; Seemann-Eggebert, W., *Karlsruher Nuklidkarte*. 1998.
10. Taylor, R.; Bourg, S.; Glatz, J.-P.; Modolo, G. Development of actinide separation processes for future nuclear fuel cycles in Europe. Nucl. Future **2015**, *11* (4), 38-43.
11. Choppin, G.R.L., J-O; Rydberg, J., *Radiochemistry and nuclear chemistry*. 3 ed.; Butterworth-Heinemann: 2002.
12. Siebentes Gesetz zur Änderung des Atomgesetzes. Bundesanzeiger, Ed. Bundesanzeiger: Berlin, 1994; Vol. 46, p 1.
13. Gesetz zur Beendigung der Kernenergienutzung zur gewerblichen Erzeugung von Elektrizität. Bundesanzeiger: Berlin, 2002; p 9.
14. Euratom 70/2011. European Commission: 2011.
15. Abschlussbericht der Kommission Lagerung Hochradioaktive Abfallstoffe; Deutscher Bundestag; Berlin; 30.August 2016.
16. Programm für eine verantwortungsvolle und sichere Entsorgung bestrahlter Brennelemente und radioaktiver Abfälle; Bundesministerium für Umwelt, Naturschutz, Bau und Reaktorsicherheit; Berlin; August 2015.
17. Gesetz zur Suche und Auswahl eines Standortes für ein Endlager für Wärme entwickelnde radioaktive Abfälle (Standortauswahlgesetz - StandAG). Bundesanzeiger: Berlin, 2013; p 11.
18. The national programme for the management of radioactive waste and spent fuel. Ministry of Infrastructure and the Environment of the Kingdom of the Netherlands: 2016.
19. Renn, O. Partitionierung und Transmutation; acatech-Deutsche Akademie der Technikwissenschaften; Dezember 2013.
20. Poinssot, C.; Rostaing, C.; Baron, P.; Warin, D.; Boullis, B. Main Results of the French Program on Partitioning of Minor Actinides, a Significant Improvement Towards Nuclear Waste Reduction. Procedia Chem. **2012**, *7*, 358-366.

21. Magill, J.; Berthou, V.; Haas, D.; Galy, J.; Schenkel, R.; Wiese, H.-W.; Heusener, G.; Tommasi, J.; Youinou, G. Impact limits of partitioning and transmutation scenarios on the radiotoxicity of actinides in radioactive waste. Nucl. Energy **2003**, *42* (5), 263-277.
22. Lieser, K.H., *Einführung in die Kernchemie*. VCH: Weinheim, 1991; Vol. 3.
23. Sengler, G.; Forêt, F.; Schlosser, G.; Lisdat, R.; Stelletta, S. EPR core design. Nucl. Eng. Des. **1999**, *187* (1), 79-119.
24. IAEA High Burnup Fuels: Implications and Operation Experience; 1798, IAEA-TECDOC-CD-1798; International Atomic Energy Agency; Vienna; 2016; 2013.
25. McKibben, J.M. Chemistry of the PUREX process, Americal Chemical Society 135th National Meeting, Seattle, Washington, USA, 10 March 1983, 1983.
26. *Nuclear Fuel Cycle Science and Engineering*. Woodhead Publishing: Cambridge, 2012; Vol. 1, p 648.
27. Warin, D.; Poinssot, C.; Bourg, S. Future Nuclear Fuel Cycles: Meeting Sustainability through Actinide Recycling, Proceedings of GLOBAL 2011, Makuhari, Japan, 2011.
28. Gervaise, Y., Approche Analytique de la Detection des Fraudes. SGS Multilab: Rennes, France, 2014.
29. Pearson, R.G. Hard and Soft Acids and Bases. J. Am Chem Soc **1963**, *85* (22), 3533-3539.
30. Hill, C. Overview of Recent Advances in An(III)/Ln(III) Separation by Solvent Extraction. Chap. 3 in Ion Exchange and Solvent Extraction, A Series of Advances, Vol. 19, Moyer, B.A., CRC Taylor and Francis: pp 119-193, **2009**.
31. Stephan, H.G., K.; Beger, J.; Muhl, P. Liquid-Liquid-Extraction of Metal-Ions with Amido Podands. Solvent Extr. Ion Exch. **1991**, *9* (3), 459-469.
32. Ansari, S.A.; Pathak, P.; Mohapatra, P.K.; Manchanda, V.K. Chemistry of Diglycolamides: Promising Extractants for Actinide Partitioning. Chem. Rev. **2012**, *112* (3), 1751-1772.
33. Sasaki, Y.; Sugo, Y.; Suzuki, S.; Tachimori, S. The Novel Extractants, Diglycolamides, for the Extraction of Lanthanides and Actinides in HNO_3-n-dodecane System. Solvent Extr. Ion Exch. **2001**, *19* (1), 91-103.
34. Tachimori, S.; Sasaki, Y.; Suzuki, S. Modification of TODGA-n-dodecane solvent with a monoamide for high loading of lanthanides(III) and actinides(III). Solvent Extr. Ion Exch. **2002**, *20* (6), 687-699.
35. Modolo, G.; Asp, H.; Schreinemachers, C.; Vijgen, H. Development of a TODGA based Process for Partitioning of Actinides from a PUREX Raffinate Part I: Batch Extraction Optimization Studies and Stability Tests. Solvent Extr. Ion Exch. **2007**, *25* (6), 703-721.
36. Geist, A.; Modolo, G. TODGA Process Development: an Improved Solvent Formulation, Proceedings of GLOBAL (The Nuclear Fuel Cycle: Sustainable Options & Industrial Perspectives) 2009, Paris, 6-11 September, pp 1022-1026, paper 9193.
37. Iqbal, M.; Huskens, J.; Verboom, W.; Sypula, M.; Modolo, G. Synthesis and Am/Eu extraction of novel TODGA derivatives. Supramol. Chem. **2010**, *22* (11/12), 827-837.
38. Galán, H.Z., C.A.; Wilden, A.; Núñez, A.; Schmidt, H.; Egberink, R.J.M.; Leoncini, A.; Cobos, J.; Verboom, W.; Modolo, G.; Groenewold, G.S.; Mincher, B.J. Gamma-radiolytic stability of new methylated todga derivatives for minor actinide recycling. Dalton Trans. **2015**, *44* (41), 18049-18056.
39. Wilden, A.; Modolo, G.; Lange, S.; Sadowski, F.; Beele, B.B.; Skerencak-Frech, A.; Panak, P.J.; Iqbal, M.; Verboom, W.; Geist, A.; Bosbach, D. Modified Diglycolamides for the An(III) + Ln(III) co-separation: Evaluation by Solvent Extraction and Time-Resolved Laser Fluorescence Spectroscopy. Solvent Extr. Ion Exch. **2014**, *32* (2), 119-137.

40. Charbonnel, M.C.; Berthon, C.; Berthon, L.; Boubals, N.; Burdet, F.; Duchesne, M.T.; Guilbaud, P.; Mabille, N.; Petit, S.; Zorz, N. Complexation of Ln(III) and Am(III) with the hydrosoluble TEDGA: Speciation and Thermodynamics studies. Procedia Chem. **2012**, *7*, 20-26.
41. Modolo, G.; Asp, H.; Vijgen, H.; Malmbeck, R.; Magnusson, D.; Sorel, C. Demonstration of a TODGA-Based Continuous Counter-Current Extraction Process for the Partitioning of Actinides from a Simulated PUREX Raffinate, Part II: Centrifugal Contactor Runs. Solvent Extr. Ion Exch. **2008**, *26* (1), 62-76.
42. Modolo, G.; Wilden, A.; Daniels, H.; Geist, A.; Magnusson, D.; Malmbeck, R. Development and demonstration of a new SANEX Partitioning Process for selective actinide(III)/lanthanide(III) separation using a mixture of $CyMe_4BTBP$ and TODGA. Radiochim. Acta **2013**, *101* (3), 155-162.
43. Wilden, A.; Modolo, G.; Kaufholz, P.; Sadowski, F.; Lange, S.; Sypula, M.; Magnusson, D.; Müllich, U.; Geist, A.; Bosbach, D. Laboratory-Scale Counter-Current Centrifugal Contactor Demonstration of an Innovative-SANEX Process Using a Water Soluble BTP. Solvent Extr. Ion Exch. **2015**, *33* (2), 91-108.
44. Sasaki, Y.; Choppin, R. Solvent Extraction of Eu, Th, U, Np and Am with N, N'-Dimethyl-N, N'-dihexyl-3-oxapentanediamide and Its Analogous Compounds. Anal. Sci. **1996**, *12* (2), 225-230.
45. Serrano-Purroy, D.; Baron, P.; Christiansen, B.; Glatz, J.-P.; Madic, C.; Malmbeck, R.; Modolo, G. First demonstration of a centrifugal solvent extraction process for minor actinides from a concentrated spent fuel solution. Separation and Purification Technology **2005**, *45* (2), 157-162.
46. Manchanda, V.K.; Pathak, P.N. Amides and diamides as promising extractants in the back end of the nuclear fuel cycle: an overview. Separation and Purification Technology **2004**, *35* (2), 85-103.
47. Rostaing, C.; Poinssot, C.; Warin, D.; Baron, P.; Lorraina, B. Development and Validation of the EXAm Separation Process for Single Am Recycling. Procedia Chem. **2012**, *7*, 367-373.
48. Serrano-Purroy, D.; Baron, P.; Christiansen, B.; Malmbeck, R.; Sorel, C.; Glatz, J.P. Recovery of minor actinides from HLLW using the DIAMEX process. Radiochim. Acta **2005**, *93* (6), 351-355.
49. Miguirditchian, M.; Chareyre, L.; Heres, X.; Hill, C.; Baron, P.; Masson, M. GANEX: Adaptation of the DIAMEX-SANEX process for the group actinide separation, Proceedings of Global 2007: Advanced Nuclear Fuel Cycles and Systems 2007, Boise, ID, United States, 9-13 September 2007, pp 550-552.
50. Kolarik, Z. Complexation and Separation of Lanthanides(III) and Actinides(III) by Heterocyclic N-Donors in Solutions. Chem. Rev. **2008**, *108* (10), 4208-4252.
51. Kolarik, Z.; Müllich, U. Extraction of Am(lll) and Eu(lll) by 2-substituted benzimidazoles. Solvent Extr. Ion Exch. **1997**, *15* (3), 361-379.
52. Panak, P.J.; Geist, A. Complexation and Extraction of Trivalent Actinides and Lanthanides by Triazinylpyridine N-Donor Ligands. Chem. Rev. **2013**, *113* (2), 1199-1236.
53. Kolarik, Z.; Mullich, U.; Gassner, F. Selective extraction of Am(III) over Eu(III) by 2,6-ditriazolyl- and 2,6-ditriazinylpyridines. Solvent Extr. Ion Exch. **1999**, *17* (1), 23-32.
54. Hudson, M.J.; Harwood, L.M.; Laventine, D.M.; Lewis, F.W. Use of Soft Heterocyclic N ‑Donor Ligands To Separate Actinides and Lanthanides. J. Inorg. Chem. **2012**.

55. Hudson, M.J.; Boucher, C.E.; Braekers, D.; Desreux, J.F.; Drew, M.G.B.; Foreman, M.R.S.J.; Harwood, L.M.; Hill, C.; Madic, C.; Marken, F.; Youngs, T.G.A. New bis(triazinyl) pyridines for selective extraction of americium(III). New J. Chem. **2006**, *30* (8), 1171-1183.
56. Hudson, M.J.; Boucher, C.E. New bis(triazinyl) pyridines for selective extraction of americium(III). New J. Chem. **2006**, *30*, 1171-1183.
57. Foreman, M.R.S.J.; Hudson, M.J.; Geist, A.; Madic, C.; Weigl, M. An Investigation into the Extraction of Americium(III), Lanthanides and D-Block Metals by 6,6'-Bis-(5,6-dipentyl-[1,2,4]triazin-3-yl)-[2,2']bipyridinyl (C5-BTBP). Solvent Extr. Ion Exch. **2005**, *23* (5), 645-662.
58. Geist, A.; Hill, C.; Modolo, G.; Foreman, M.R.S.J.; Weigl, M.; Gompper, K.; Hudson, M.J.; Madic, C. 6,6'-Bis(5,5,8,8-tetramethyl-5,6,7,8-tetrahydro-benzo[1,2,4]triazin-3-yl)[2,2']bipyridine, an effective extracting agent for the separation of americium(III) and curium(III) from the lanthanides. Solvent Extr. Ion Exch. **2006**, *24* (4), 463-483.
59. Lewis, F.W.; Harwood, L.M.; Hudson, M.J.; Drew, M.G.B.; Wilden, A.; Sypula, M.; Modolo, G.; Vu, T.-H.; Simonin, J.-P.; Vidick, G.; Bouslimani, N.; Desreux, J.F. From BTBPs to BTPhens: The Effect of Ligand Pre-Organization on the Extraction Properties of Quadridentate Bis-Triazine Ligands. Proc. Chem. **2012**, *7*, 231-238.
60. Harwood, L.M.; Lewis, F.W.; Hudson, M.J.; John, J.; Distler, P. The Separation of Americium(III) from Europium(III) by Two New 6,6 '-Bistriazinyl-2,2 '-Bipyridines in Different Diluents. Solvent Extr Ion Exch **2011**, *29* (4), 551-576.
61. Lewis, F.W.; Harwood, L.M.; Hudson, M.J.; Drew, M.G.B.; Desreux, J.F.; Vidick, G.; Bouslimani, N.; Modolo, G.; Wilden, A.; Sypula, M.; Vu, T.-H.; Simonin, J.-P. Highly Efficient Separation of Actinides from Lanthanides by a Phenanthroline-Derived Bis-triazine Ligand. J. Am. Chem. Soc. **2011**, *133* (33), 13093-13102.
62. Geist, A.; Müllich, U.; Magnusson, D.; Kaden, P.; Modolo, G.; Wilden, A.; Zevaco, T. Actinide(III)/Lanthanide(III) Separation Via Selective Aqueous Complexation of Actinides(III) Using a Hydrophilic 2,6-Bis(1,2,4-Triazin-3-yl)-Pyridine in Nitric Acid. Solvent Extr. Ion Exch. **2012**, *30* (5), 433-444.
63. Wagner, C.; Müllich, U.; Geist, A.P., Petra J. Selective Extraction of Am(III) from PUREX raffinate: The AmSel system. Solvent Extr. Ion Exch. **2016**, *34* (2), 103-113.
64. Sypula, M.W., A.; Schreinemachers, C.; Malmbeck, R.; Geist, A.; Taylor, R.; Modolo, G. Use of polyaminocarboxylic acids as hydrophilic masking agents for fission products in actinide partitioning processes. Solvent Extr. Ion Exch. **2012**, *30* (7), 748-764.
65. Magnusson, D.C., B.; Glatz, J-P.; Malmbeck, R.; Modolo, G.; Serrano-Purroy, D.; Sorel, C. Demonstration of a TODGA based extraction process for the partitioning of minor actinides from a PUREX raffinate Part III: Centrifugal contactor run using genuine fuel solution. Solvent Extr. Ion Exch. **2009**, *27* (1), 26-35.
66. Sypula, M.; Wilden, A.; Schreinemachers, C.; Malmbeck, R.; Geist, A.; Taylor, R.; Modolo, G. Use of polyaminocarboxylic acids as hydrophilic masking agents for fission products in actinide partitioning processes. Solvent Extr. Ion Exch. **2012**, *30* (7), 748-764.
67. Nash, K.L. Introduction to Reprocessing and Recycling of Spent Nuclear Fuel. in Reprocessing and Recycling of Spent Nuclear Fuel, Taylor, R., Elsevier, **2015**.
68. Taylor, R.J.; Gregson, C.R.; Carrott, M.J.; Mason, C.; Sarsfield, M.J. Progress towards the Full Recovery of Neptunium in an Advanced PUREX Process. Solvent Extr. Ion Exch. **2013**, *31* (4), 442-462.
69. Moyer, B.A.; Lumetta, G.J.; Mincher, B.J. Minor actinide separation in the reprocessing of spent nuclear fuels: recent advances in the United States. Chap. 11 in Reprocessing and

Recycling of Spent Nuclear Fuel, Taylor, R., Woodhead Publishing: Oxford, pp 289-312, **2015**.

70. Todd, T.A.; Moyer, B.A. Novel Approaches to the Separation of Trivalent Actinides from Used Nuclear Fuel, Nuclear Fuel Cycle Conference, Machester, UK, 23-25 April 2012, 2012.
71. OECD-NEA, Curium Management Studies in France, Japan and USA. OECD-NEA: Paris, 2012; Vol. 2, p 39.
72. Modolo, G.; Wilden, A.; Kaufholz, P.; Bosbach, D.; Geist, A. Development and demonstration of innovative partitioning processes (i-SANEX and 1-cycle SANEX) for actinide partitioning. Prog. Nucl. Energy **2014**, *72*, 107-114.
73. Adnet, J.-M.; Miguirditchian, M.; Hill, C.; Heres, X.; Lecomte, M.; Masson, M.; Brossard, P.; Baron, P. Development of New Hydrometallurgical Processes for Actinide Recovery: GANEX concept., Proceedings of GLOBAL 2005, Tsukuba, Japan, 9.-13.10.2005.
74. Carrott, M.; Geist, A.; Heres, X.; Lange, S.; Malmbeck, R.; Miguirditchian, M.; Modolo, G.; Wilden, A.; Taylor, R. Distribution of plutonium, americium and interfering fission products between nitric acid and a mixed organic phase of TODGA and DMDOHEMA in kerosene, and implications for the design of the "EURO-GANEX" process. Hydrometallurgy **2015**, *152*, 139-148.
75. Carrott, M.B., K.; Brown, J.; Geist, A.; Gregson, C.; Hères, X.; Maher, C.; Malmbeck, R.; Mason, C.; Modolo, G.; Müllich, U.; Sarsfield, M.;Wilden, A.; Taylor, R. Development of a new flowsheet for co-separating the transuranic actinides: The “EURO-GANEX” process. Solvent. Solvent Extr. Ion Exch. **2014**, *32* (5), 447-467.
76. Taylor, R.C., M.; Galan, H.; Geist, A.; Hères, X.; Maher, C.; Mason, C.; Malmbeck, R.; Miguirditchian, M.; Modolo, G.; Rhodes, C.; Sarsfield, M.; Wilden, A. The EURO-GANEX Process: Current Status of Flowsheet Development and Process Safety Studies. Procedia Chem. **2016**, *21*, 524-529.
77. Carrott, M.; Bell, K.; Brown, J.; Geist, A.; Gregson, C.; Hères, X.; Maher, C.; Malmbeck, R.; Mason, C.; Modolo, G.; Müllich, U.; Sarsfield, M.; Wilden, A.; Taylor, R. Development of a New Flowsheet for Co-Separating the Transuranic Actinides: The “EURO-GANEX” Process. Solvent Extr. Ion Exch. **2014**, *32* (5), 447-467.
78. Carrott, M.; Geist, A.; Hères, X.; Lange, S.; Malmbeck, R.; Miguirditchian, M.; Modolo, G.; Wilden, A.; Taylor, R. Distribution of plutonium, americium and interfering fission products between nitric acid and a mixed organic phase of TODGA and DMDOHEMA in kerosene, and implications for the design of the “EURO-GANEX” process. Hydrometallurgy **2015**, *152*, 139-148.
79. Sarsfield, M.J. The coprecipitation and conversion of mixed actinide oxalates for aqueous-based reprocessing of spent nuclear fuels. Chap. 13 in Reprocessing and recycling of spent nuclear fuel, Taylor, R., Elsevier: pp 325-351, **2015**.
80. Madic, C.; Hudson, M.J.; Liljenzin, J.-O.; Glatz, J.-P.; Nannicini, R.; Facchini, A.; Kolarik, Z.; Odoj, R. Recent achievements in the development of partitioning processes of minor actinides from nuclear wastes obtained in the frame of the NEWPART European programme (1996–1999). Progr. in Nucl. Energy **2002**, *40* (3–4), 523-526.
81. Courson, O.; Lebrun, M.; Malmbeck, R.; Pagliosa, G.; Romer, K.; Satmark, B.; Glatz, J.P. Partitioning of minor actinides from HLLW using the DIAMEX process. Part 1 - Demonstration of extraction performances and hydraulic behaviour of the solvent in a continuous process. Radiochim. Acta **2000**, *88* (12), 857-863.

82. Malmbeck, R.; Courson, O.; Pagliosa, G.; Romer, K.; Satmark, B.; Glatz, J.P.; Baron, P. Partitioning of minor actinides from HLLW using the DIAMEX process. Part 2 - "Hot" continuous counter-current experiment. Radiochim. Acta **2000**, *88* (12), 865-871.
83. Magnusson, D.; Christiansen, B.; Foreman, M.R.S.; Geist, A.; Glatz, J.P.; Malmbeck, R.; Modolo, G.; Serrano-Purroy, D.; Sorel, C. Demonstration of a SANEX Process in Centrifugal Contactors using the CyMe$_4$-BTBP Molecule on a Genuine Fuel Solution. Solvent Extr. Ion Exch. **2009**, *27* (2), 97-106.
84. Warin, D.; Boullis, B. Future nuclear fuel cycles: Prospects and challenges, Proceedings of Tenth Information Exchange Meeting 2008, Mito, Japan, 6-10 October 2008, Vol. 6420, pp 221-225.
85. Modolo, G.; Wilden, A.; Geist, A.; Magnusson, D.; Malmbeck, R. A review of the demonstration of innovative solvent extraction processes for the recovery of trivalent minor actinides from PUREX raffinate. Radiochim. Acta **2012**, *100* (8-9, Plutonium Futures), 715-725.
86. Chen, J.; He, X.; Wang, J. Nuclear fuel cycle-oriented actinides separation in China. Radiochim. Acta **2014**, *102* (1-2), 41.
87. Modolo, G.; Odoj, R. Synergistic selective extraction of Actinides (III) over Lathanides from nitric acid using new aromatic Diorganyldithiophosphinic acids and neutral Organophosphorus compounds. Solvent Extr. Ion Exch. **1999**, *17* (1), 33-53.
88. Modolo, G.; Seekamp, S. Hydrolysis and radiation stability of the ALINA solvent for actinide(III)/lanthanide(III) separation during the partitioning of minor actinides. Solvent Extr. Ion Exch. **2002**, *20* (2), 195-210.
89. Modolo, G.; Kluxen, P.; Geist, A. Demonstration of the LUCA process for the separation of americium(III) from curium(III), californium(III), and lanthanides(III) in acidic solution using a synergistic mixture of bis(chlorophenyl)dithiophosphinic acid and tris(2-ethylhexyl)phosphate. Radiochim. Acta **2010**, *98* (4), 193-201.
90. Modolo, G.; Nabet, S. Thermodynamic study on the synergistic mixture of bis(chlorophenyl) dithiophosphinic acid and tris(2-ethylhexyl) phosphate for separation of actinides(III) from lanthanides(III). Solvent Extr. Ion Exch. **2005**, *23* (3), 359-373.
91. Wilden, A.; Schreinemachers, C.; Sypula, M.; Modolo, G. Direct Selective Extraction of Actinides (III) from PUREX Raffinate using a Mixture of CyMe$_4$BTBP and TODGA as 1-cycle SANEX Solvent. Solvent Extr. Ion Exch. **2011**, *29* (2), 190-212.
92. Magnusson, D.; Geist, A.; Wilden, A.; Modolo, G. Direct selective extraction of actinides (III) from PUREX-Raffinate using a mixture of Cy-Me4-BTBP and TODGA as 1-cycle Sanex part II: Flowsheet design for a counter current centrifugal contactor demonstration process. Solvent Extr. Ion Exch. **2013**, *31*, 11.
93. Wilden, A.; Modolo, G.; Schreinemachers, C.; Sadowski, F.; Lange, S.; Sypula, M.; Magnusson, D.; Geist, A.; Lewis, F.W.; Harwood, L.M.; Hudson, M.J. Direct Selective Extraction of Actinides (III) from PUREX Raffinate using a Mixture of CyMe$_4$BTBP and TODGA as 1-cycle SANEX Solvent Part III: Demonstration of a Laboratory-scale Counter-Current Centrifugal Contactor Process. Solvent Extr. Ion Exch. **2013**, *31* (5), 519-537.
94. Wilden, A.; Modolo, G.; Sypula, M.; Geist, A.; Magnusson, D. The Recovery of An(III) in an Innovative-SANEX Process using a TODGA-based Solvent and Selective Stripping with a Hydrophilic BTP. Procedia Chem. **2012**, *7*, 418-424.
95. Magnusson, D.; Geist, A.; Malmbeck, R.; Modolo, G.; Wilden, A. Flow-sheet design for an innovative SANEX process using TODGA and SO$_3$-Ph-BTP. Procedia Chem. **2012**, *7*, 245-250.

96. Geist, A.; Modolo, G.; Wilden, A.; Kaufholz, P. Minor Actinide Separation: Simplification of the DIAMEX-SANEX Strategy by Means of Novel SANEX Processes, Proceedings of GLOBAL 2013 "Nuclear Energy at a Crossroad" 2013, Salt Lake City, UT, USA, 29 September - 03 October 2013, pp 1054-1059.
97. Bollesteros, M.-J.; Calor, J.-N.; Costenoble, S.; Montuir, M.; Pacary, V.; Sorel, C.; Burdet, F.; Espinoux, D.; Hérès, X.; Eysseric, C. Implementation of Americium Separation from a PUREX Raffinate. Procedia Chem. **2012**, *7*, 178-183.
98. Wagner, C.; Müllich, U.; Panak, P.J.; Geist, A. AmSel, a New System for Extracting Only Americium from PUREX Raffinate, Sustainable Nuclear Energy Conference, Manchester, UK, 9-11 April 2014, 2014.
99. Mincher, B.J.; Schmitt, N.C.; Schuetz, B.K.; Shehee, T.C.; Hobbs, D.T. Recent advances in f-element separations based on a new method for the production of pentavalent americium in acidic solution. RSC Adv. **2015**, *5* (34), 27205-27210.
100. Donnet, L.; Adnet, J.-M.; Faure, N.; Bros, P.; Brossard, P.; Josso, F. Development of the SESAME Process, Proceedings of 5th Information Exchange Meeting on Actinide and Fission Product Partitioning and Transmutation 1998, Mol, Belgium, pp 161-168.
101. Jensen, M.P.; Chiarizia, R.; Shkrob, I.A.; Ulicki, J.S.; Spindler, B.D.; Murphy, D.J.; Hossain, M.; Roca-Sabio, A.; Platas-Iglesias, C.; de Blas, A.; Rodriguez-Blas, T. Aqueous Complexes for Efficient Size-based Separation of Americium from Curium. Inorg. Chem. **2014**, *53* (12), 6003-6012.
102. P. Lindqvist-Reis, C.W., R. Klenze, A. Eichhöfer and T. Fanghänel Large Ground-State and Excited-State Crystal Field Splitting of 8-fold-Coordinate Cm3+ in [Y(H2O)8]Cl3·15-crown-5. The Journal of Physical Chemistry B **2006**, *110*, 5279-5285.
103. Rajnak, W.T.C.a.K. Electronic energy level and intensity correlations in the spectra of the trivalent actinide aquo ions. II. Cm3 +. The Journal of Chemical Physics **1975**, *63*, 3510-3514.
104. G. Plancque, V.M., P. Toulhoat and C. Moulin Europium speciation by time-resolved laser-induced fluorescence. Analytica Chimica Acta **2003**, *478*, 11-22.
105. Choppin, J.C.G.B.G.R., *Lanthanide probes in life, chemical and earth sciences: Theory and practice,*. Elsevier Science Ltd.: Amsterdam, 1989.
106. Ruff, C.M. Spetroskopische und thermodynamische Untersuchung der Komplexierung von Cm(III) und Eu(III) mit hydrophilen Bis-Triazinylpyridinen. Ruprecht-Karls-Universität Heidelberg, 2013.
107. Davidenko, K.B.Y.N.K. Absorption spectra and structure of lanthanide coordination compounds in solution. Coordination Chemistry Reviews **1979**, *27*, 223-273.
108. Jr, S.T.F.a.W.D.H. On correlating the frequency of the 7F0 -> 5D0 transition in Eu3+ complexes with the sum of ‘nephelauxetic parameters’ for all of the coordinating atoms,. Inorganica Chimica Acta, **1995**, *229*, 383-390.
109. Heits Zusammensetzung und Herstellung von HAW/HAWC-Simulaten gemäß den Planungsgrundlagen der DWK und den Erfahrungen der WAK; Deutsche Gesellschaft für Wiederaufarbeitung von Kernbrennstoffen mbH; Karlsruhe; 1982.
110. Lewis, F.W.; Harwood, L.M.; Hudson, M.J.; Geist, A.; Kozhevnikov, V.N.; Distler, P.; John, J. Hydrophilic sulfonated bis-1,2,4-triazine ligands are highly effective reagents for separating actinides(III) from lanthanides(III) via selective formation of aqueous actinide complexes. Chem. Sci. **2015**, *6* (8), 4812-4821.
111. Borrini, J.; Favre-Reguillon, A.; Lemaire, M.; Gracia, S.; Arrachart, G.; Bernier, G.; Pellet-Rostaing, S. Water Soluble PDCA Derivatives for Selective Ln(III)/An(III) and Am(III)/Cm(III) Separation. Solvent Extr. Ion Exch. **2015**, *33* (3), 224-235.

112. Manual of 10 mm annular centrifugal contactors. INET Tsinghua University: Beijing, China.

113. Bremer, A.; Whittaker, D.M.; Sharrad, C.A.; Geist, A.; Panak, P.J. Complexation of Cm(III) and Eu(III) with CyMe$_4$-BTPhen and CyMe$_4$-BTBP studied by time resolved laser fluorescence spectroscopy. Dalton Trans. **2014**, *43* (6), 2684-2694.

114. Magnusson, D.G., A.;Wilden, A.; Modolo, G.; Malmbeck, R. Computer Code Development for Flow-Sheet Design and Modeling with Verification Towards a Novel Partitioning Process,, Proceedings of Proceedings of GLOBAL 2011 2011, Makuhari, Japan, 11-16 December,, p 355757 (Paper No.).

115. Magnusson, D.C., B.; Glatz, J.-P.; Malmbeck, R.; Modolo, G.; Serrano-Purroy, D.; Sorel, C. Towards an optimized flow-sheet for a SANEX demonstration process using centrifugal contactors. Radiochim. Acta **2009**, *97* (3), 155-159.

116. Magnusson, D.M., R. Development of a solvent extraction model for process tests in short residence time centrifugal contactors. Solvent Extr. Ion Exch. **2012**, *30* (2), 115-126.

117. Magnusson, D.G., A.; Malmbeck, R. SX process-A code for solvent extraction processes in centrifugal contactors simulation. Chem. Eng. Sci **2013**, *99*, 292-297.

118. Sasaki, Y.T., Y.; Kitatsuji, Y.; Sugo, Y.; Shirasu, N.; Morita, Y.; Kimura, T. Extraction behavior of metal ions by TODGA, DOODA, MIDOA, and NTAamide extractants from HNO3 to n-dodecane. Solvent Extr. Ion Exch. **2013**, *31* (4), 401-415.

119. Macerata, E.M., E.; Scaravaggi, S.; Mariani, M.; Mele, A.; Panzeri, W.; Boubals, N.; Berthon, L.; Charbonnel, M.-C.; Sansone, F.; Arduini, A.; Casnati, A. Hydrophilic Clicked 2,6-Bis-triazolyl-pyridines Endowed with High Actinide Selectivity and Radiochemical Stability: Toward a Closed Nuclear Fuel Cycle. J. Am. Chem. Soc. **2016**, *138* (23), 7232-7235.

120. Chatterton, N.; Bretonniere, Y.; Pecaut, J.; Mazzanti, M. An efficient design for the rigid assembly of four bidentate chromophores in water-stable highly luminescent lanthanide complexes. Angew. Chem., Int. Ed. **2005**, *44* (46), 7595-7598.

121. Gracia, S.; Arrachart, G.; Marie, C.; Chapron, S.; Miguirditchian, M.; Pellet-Rostaing, S. Separation of Am (III) by solvent extraction using water-soluble H4tpaen derivatives. Tetrahedron **2015**, *71* (33), 5321-5336.

122. Šť'astná, K.; John, J.; Šebesta, F.; Vlk, M. Separation of curium from americium using composite sorbents and complexing agent solutions. J. Radioanal. Nucl. Chem. **2015**, *304* (1), 349-355.

123. Mazzanti, M. Method for obtaining highly luminescent lanthanide complexes with chromophoric decadentate ligands for use in medical imaging and bioassays and in materials for nanotechnology. FR2890657A1.

124. Marie, C.; Duchesne, M.-T.; Russello, E.; Kaufholz, P.; Wilden, A.; Modolo, G.; Casnati, A.; Miguirditchian, M. Development of a selective americium separation process using TPAEN as a water-soluble stripping agent, Proceedings of GLOBAL 2015 Nuclear Fuel Cycle for a Low-carbon Future 2015, Paris, France, 20-24 September, p Paper 5101.

125. Nash, K.L.; Madic, C.; Mathur, J.N.; Lacquement, J. Actinide Separation Science and Technology. Chap. 24 in The Chemistry of Actinide and Transactinide Elements, 3rd ed.; Morss, L.R.; Edelstein, N.M.; Fuger, J.; Katz, J.J., Springer: Dordrecht, The Netherlands, pp 2622-2798, **2006**.

126. Trumm, S.; Lieser, G.; Foreman, M.; Panak, P.J.; Geist, A.; Fanghanel, T. A TRLFS study on the complexation of Cm(III) and Eu(III) with 4-*t*-butyl-6,6 '-bis-(5,6-diethyl-1,2,4-triazin-3-yl)-2,2 '-bipyridine in a water/2-propanol mixture. Dalton Trans. **2010**, *39* (3), 923-929.

127. Wagner, C.; Mullich, U.; Geist, A.; Panak, P.J. TRLFS study on the complexation of Cm(III) and Eu(III) with SO3-Ph-BTBP. Dalton Trans. **2015**, *44* (39), 17143-17151.
128. Edelstein, N.M.; Klenze, R.; Fanghänel, T.; Hubert, S. Optical properties of Cm(III) in crystals and solutions and their application to Cm(III) speciation. Coord. Chem. Rev. **2006**, *250*, 948-973.
129. Weissman, S.I. Intramolecular Energy Transfer The Fluorescence of Complexes of Europium. J. Chem. Phys. **1942**, *10*, 214-217.
130. Skerencak, A.; Panak, P.J.; Hauser, W.; Neck, V.; Klenze, R.; Lindqvist-Reis, P.; Fanghanel, T. TRLFS study on the complexation of Cm(III) with nitrate in the temperature range from 5 to 200 degrees C. Radiochim. Acta **2009**, *97* (8), 385-393.
131. Sugo, Y.S., Y.; Tachimori, S. Studies on hydrolysis and radiolysis of N,N,N',N'-tetraoctyl-3-oxapentane-1,5-diamide. Radiochim. Acta **2002**, *90* (3), 161-165.
132. Zarzana, C.A.G., G.S.; Mincher, B.J.; Mezyk, S.P.; Wilden, A.; Schmidt, H.; Modolo, G.; Wishart, J.F.; Cook, A.R. A Comparison of the γ-Radiolysis of TODGA and T(EH)DGA Using UHPLC-ESI-MS Analysis. Solvent Extr. Ion Exch. **2015**, *33* (5), 431-447.
133. Mincher, B.J.M., G.; Mezyk, S.P. The effects of radiation chemistry on solvent extraction: 1. Conditions in acidic solution and a review of TBP radiolysis. Solvent Extr. Ion Exch. **2009**, *27* (1), 1-25.
134. Arisaka, M.; Kimura, T. Thermodynamic and Spectroscopic Studies on Am(III) and Eu(III) in the Extraction System of N,N,N',N'-Tetraoctyl-3-Oxapentane-1,5-Diamide in n-Dodecane/Nitric Acid. Solvent Extr. Ion Exch. **2011**, *29* (1), 72-85.
135. Kimura, T.; Choppin, G.R.; Kato, Y.; Yoshida, Z. Determination of the Hydration Number of Cm(III) in Various Aqueous Solutions. Radiochim. Acta **1996**, *72* (2), 61-64.

Acknoledgements

First I would like to thank the head of IEK-6 Professor Dr. Dirk Bosbach and my Supervisor Professor Dr. Giuseppe Modolo for the opportunity to prepare my PhD-thesis at the IEK-6 of Forschungszentrum Jülich. This includes the numerous experiments carried out at the lab of IEK-6, but also the community I was allowed to work in. The combination of the excellent supervision in combination with the cooperations with research groups all over Europe was a major premise for this work. Furthermore, the staff at IEK-6 offered an open and friendly atmosphere which supports a comfortable and motivating style of work. In particular, there were Dr. Andreas Wilden, Dr. Elena Mühr-Ebert, Dr. Sanela Hadic, Christian Schreinemachers, Holger Schmidt, Larissa Klass, Fabian Sadowski and Steve Lange, who were always open for a talk or discussion. Many thanks to the trainees Rainer Engelmann and Markus Gerdes and the master student Benjamin Kraus who supported my lab work in the frame of their education. Leaving IEK-6 was not easy due to leaving a lot of colleagues and friends.

During the preparation of this thesis I was allowed to gather experiences at facilities of different project partners all over Europe. During my first stay I went to KIT Karlsruhe to analyze the complexation of Eu(III) and Cm(III) by laserfluorescence methods which was carried out in cooperation with University of Heidelberg. For the interesting time in Karlsruhe I would like to thank Dr. Andreas Geist from KIT and Professor Dr. Petra J. Panak from the University of Heidelberg for welcoming me at their labs and for numerous discussions. Another important person in Karlsruhe was Christoph Wagner. We spent a lot of time together in the lab and at conferences.

My second stay brought me to the CEA Marcoule in the south of France where I was allowed to stay for three month. There were a number of people I have to thank for the warm welcome in France and for the nice stay: First of all, there are Dr. Marie-Christine Charbonnel, Dr. Cécile Marie, Dr. Philippe Guilbaud and Dr. Manuel Miguirditchian who helped with the organization of the stay and hosted me in their labs. Additionally I have to say thank you to Emilie Russello and Marie-Therese Duchesne for their support and the good atmosphere in the lab. Eros Mossini and Jessica Drader, who were my house mates in Avignon and also exchange students at the CEA helped to overcome the language issue in the everyday life and we developed to be friends.

The hydrophilic complexing agents used in this work were synthesized by different European project partners. TS-BTPhen was syntheized by Dr. Frank W. Lewis and Dr Andrew W. Smith in the group of Professor Dr. Laurence M. Harwood from the University of Reading, UK. Pytri-diol was synthesized in the Group of Professor Dr. Alessandro Casnati at the University of Milan, Italy. The radiolysis experiments were carried out in the group of Professor Dr. Christian Ekberg at the University of Gothenburgh in Sweden. Many thanks for the fruitful and inspiring co-operation to all the project partners, especially the ones mentioned above.

Financial support for the PhD-thesis work, the stays abroad, and the project meetings was provided by the European Commission in the frame of the SACSESS project. I would like to thank the project manager Dr. Stephane Bourg and the whole SACSESS community for the opportunity to work in this open and friendly atmosphere within an important international project as SACSESS was.

Last but not least there always have to be people helping to put the focus on the work life balance. They support the work in a different but very important way, helping to forget about the PhD thesis for a while or supporting a three month stay in France as friends and family. Therfore, one of the most important parts during this time and in my entire life are my Parents, my Brother and the rest of my family who always supported me or brought me to back down when my ideas got to strange. I also would like to say thank you to my friends, organized in the Jugendheim Süggerath with its head Peter Holz. We are all look back to more than 15 years of friendship, supporting each other in our carreers since school times.

List of Publications

Publications in international reviewed Journals:

Modolo, G.; Wilden, A.; **Kaufholz, P.**; Bosbach, D.; Geist, A.

Development and demonstration of innovative partitioning processes (i-SANEX and 1-cycle SANEX) for actinide partitioning.
Progress in Nuclear Energy 2014, 72, pp. 107-114.

Wilden, A.; Modolo, G.; **Kaufholz, P**.; Sadowski, F.; Lange, S.; Sypula, M.; Magnusson, D.; Müllich, U.; Geist, A.; Bosbach, D.

Laboratory-Scale Counter-Current Centrifugal Contactor Demonstration of an Innovative-SANEX Process Using a Water Soluble BTP.
Solvent Extraction and Ion Exchange 2015, 33 (2), pp. 91-108.

Wilden, A.; Modolo, G.; **Kaufholz, P**.; Sadowski, F.; Lange, S.; Munzel, D.; Geist, A.

Process Development and Laboratory-scale Demonstration of a regular-SANEX Process Using C5-BPP.
Separation Science and Technology 2015, 50 (16), pp. 2467-2475.

Kaufholz, P.; Wilden, A.; Modolo, G.; Sadowski, F.; Lewis, F.W.; Smith, A.W.; Harwood, L.M.

TS-BTPhen as a Promising Hydrophilic Complexing Agent for Selective Am(III) Separation by Solvent Extraction.
Nukleonika 2015, 60 (4), pp. 815-820.

Kaufholz, P.; Modolo, G.; Wilden, A.; Sadowski, F.; Bosbach, D.; Wagner, C.; Geist, A.; Panak, P.J.; Lewis, F.W.; Harwood, L.M.

Solvent extraction and fluorescence spectroscopic investigation of the selective Am(III) complexation with TS-BTPhen.
Solvent Extraction and Ion Exchange 2016, 34 (2), pp. 126-140.

Boubals, N.; Wagner, C.; Dumas, T.; Chanèac, L.; Manie, G.; Marie, C.; Panak, P. J.; **Kaufholz, P**.; Wilden, A.; Modolo, G.; Geist, A.; Guilbaud, P.

Selective Separation of Americium Using the H_4TPAEN Water-soluble stripping agent: determination of the complexation constants. Inorganic Chemistry 2017, (submitted March, 07th 2017)

Publications in conference proceedings Journals:

Geist, A.; Modolo, G.; Wilden, A.; **Kaufholz, P**.

Minor Actinide Separation: Simplification of the DIAMEX-SANEX Strategy by Means of Novel SANEX Processes,
Proceedings of GLOBAL 2013 "Nuclear Energy at a Crossroad" 2013, Salt Lake City, UT, USA, 29 September - 03 October 2013, pp. 1054-1059.

Marie, C.; Duchesne, M.-T.; Russello, E.; **Kaufholz, P**.; Wilden, A.; Modolo, G.; Casnati, A.; Miguirditchian, M.

Development of a selective americium separation process using TPAEN as a water-soluble stripping agent,
Proceedings of GLOBAL 2015 Nuclear Fuel Cycle for a Low-carbon Future 2015, Paris, France, 20-24 September, Paper 5101.

Vanel, V.; Marie, C.; **Kaufholz, P**.; Montuir, M.; Boubals, N.; Wilden, A.; Modolo, G.; Geist, A.; Sorel, C.

Modeling and Flowsheet Design of an Am Separation Process Using TODGA and H_4TPAEN. Procedia Chemistry 2016, 21, pp. 223-230.

Oral Presentations:

P. Kaufholz, A. Wilden, G. Modolo, L.M. Harwood, F. Lewis, C. Wagner, P. Panak, A. Geist

Selective Separation of Am(III) using the Hydrophilic Complexing Agent SO3Ph-BTPhen.

SACSESS 1st International Workshop, 22.-24. April 2015, Wasrsaw, Poland

Poster Presentation:

Kaufholz, P. Wilden, A. Modolo, G. Sadowski, F. Bosbach, D. Harwood, L. M. Lewis, F. Wagner, C. Geist, A. Panak, P.

Development of a TODGA based Liquid-liquid extraction system for the separation of Am(III) using Hydrophilic complexing agents.

International Solvent Extraction Conference 2014, 07th to 11th September 2014.

Kaufholz, P. Wilden, A. Modolo, G. Sadowski, F. Harwood, L.M. Lewis, F. Wagner, C. Geist, A. Panak, P.

Investigations on a TODGA-based Liquid-Liquid Extraction System using SO_3PhBTPhen for the Separation of Americium(III) from a Simulated PUREX Raffinate.

First SACSESS International Workshop, 22th to 25th April 2015.

Mossini, E.; **Kaufholz, P.;** Wilden, A.; Modolo, G.; Maccerata, E.; Mariani, M.; Arduini, A.; Iotti, N.; Casnati, A.

i-SANEX single-stage centrifugal contactor experiment with a novel hydrophilic complexing agent

ATALANTE 2016 5 to 10 June 2016, Montpellier, France

Band / Volume 389
Modelling of High Temperature Polymer Electrolyte Fuel Cells
Q. Cao (2017), 173 pp
ISBN: 978-3-95806-263-4

Band / Volume 390
Potential use of nitrification inhibitors for mitigating N_2O emission from soils
D. Wu (2017), 206 pp
ISBN: 978-3-95806-264-1

Band / Volume 391
Mechanical Characterization of Solid Oxide Fuel Cells and Sealants
J. Wei (2017), II, 151 pp
ISBN: 978-3-95806-266-5

Band / Volume 392
Microcrystalline Silicon Carbide for Silicon Heterojunction Solar Cells
M. B. Pomaska (2017), 150 pp
ISBN: 978-3-95806-267-2

Band / Volume 393
Einfluss der Kristallisation auf das Fließverhalten oxidischer Schmelzen
S. Seebold (2017), 168 pp
ISBN: 978-3-95806-268-9

Band / Volume 394
Water vapour in the UTLS – Climatologies and Transport
P. R. Neis (2017), x, 124 pp
ISBN: 978-3-95806-269-6

Band / Volume 395
Neutronenaktivierungsanalyse mit gepulsten 14 MeV Neutronen zur Charakterisierung heterogener radioaktiver Abfälle
F. Mildenberger (2017), vi, 128 pp
ISBN: 978-3-95806-271-9

Band / Volume 396
Coupled biotic-abiotic mechanisms of nitrous oxide production in soils during nitrification involving the reactive intermediates hydroxylamine and nitrite
S. Liu (2017), xvii, 148 pp
ISBN: 978-3-95806-272-6

Band / Volume 397
Mixed-phase and ice cloud observations with NIXE-CAPS
A. Costa (2017), xviii, 117 pp
ISBN: 978-3-95806-273-3

Band / Volume 398
Deposition Mechanisms of Thermal Barrier Coatings (TBCs) Manufactured by Plasma Spray-Physical Vapor Deposition (PS-PVD)
W. He (2017), ix, 162 pp
ISBN: 978-3-95806-275-7

Band / Volume 399
Carbonyl Sulfide in the Stratosphere: airborne instrument development and satellite based data analysis
C. Kloss (2017), vi, 84, 1-14 pp
ISBN: 978-3-95806-276-4

Band / Volume 400
Lagrangian transport of trace gases in the upper troposphere and lower stratosphere (UTLS)
P. Konopka (2017), ii, 70 pp
ISBN: 978-3-95806-279-5

Band / Volume 401
Numerical Simulation of Plasma Spray-Physical Vapor Deposition
P. Wang (2017), IX, 127 pp
ISBN: 978-3-95806-282-5

Band / Volume 402
The Selective Separation of Am(III) from Highly Radioactive PUREX Raffinate
P. Kaufholz (2017), IV, 173 pp
ISBN: 978-3-95806-284-9

Weitere ***Schriften des Verlags im Forschungszentrum Jülich*** unter
http://wwwzb1.fz-juelich.de/verlagextern1/index.asp

Energie & Umwelt / Energy & Environment
Band / Volume 402
ISBN 978-3-95806-284-9

JÜLICH
Forschungszentrum